Characterising pH response in phase separated hydrogels using Small Angle X-ray Scattering

University of Sheffield
Department of Chemistry

by Joshua Michael George Swann

Submitted to the University of Sheffield
In fulfillment of the requirements for the award of
Doctor of Philosophy

January 2010

ABSTRACT

A range of (methyl methacrylate)-*block*-poly(2-(diethylamino)ethyl methacrylate)-*block*-poly(methyl methacrylate) [PMMA-*block*-PDEA-*block*-PMMA] and poly(methyl methacrylate)-*block*-poly(methacrylic acid)-*block*-poly(methyl methacrylate) [PMMA-*block*-PMAA-*block*-PMMA] triblock copolymers have been prepared via group transfer and anionic polymerisation respectively. These hydrophilic-hydrophobic block copolymers were characterized with respect to their chemical composition and molecular weights by ^{1}H and by gel permeation chromatography respectively. Morphological development in solvent cast films were followed using SAXS by monitoring changes in the structure peak. [PMMA-*block*-PMAA-*block*-PMMA] triblocks were found to be mechanically weak and therefore not suitable as chemical actuators.

Using SAXS the "static" equilibrium molecular response of phase separated films of [PMMA-*block*-PDEA-*block*-PMMA] triblock copolymers to changes in pH, ionic strength and salt identity was evaluated. Changes in pH were effected using a controlled set of buffers, namely citric acid, sodium phosphate and ethanol amine. The ionic strength of the buffers was fixed using a series of salts from the Hofmeister series, namely NaAce, NaCl, NaBr, NaI, $NaNO_3$ and NaSCN.

At a fixed pH and ionic strength the equilibrium expansion ratio of the polymer was found to be highly dependent on the identity of the salt. The extent of swelling was correlated with the surface charge density of the anionic component of the salt. Hydrogels swollen in solution containing more polar anions were found to have a larger expansion ratio. This was explained in terms of the water perturbing effect of the ion. The swelling of the polymer was also monitored as a function of pH. A drastic collapse of the polymer was observed at a specific pH corresponding to the apparent pK_a of the PDEA block. The apparent pK_a of [PMMA-*block*-PDEA-*block*-PMMA] copolymers was found to be dependent on the overall molecular weight, where higher molecular weight material had a lower apparent pK_a. Below the apparent pK_a the extent of swelling in solutions prepared at 0.1M ionic strength was found to be dependent on the pH. This has been attributed to the complex interplay of citrate species in the buffer. The effect of ionic strength on the swelling was also investigated at fixed pH and salt identity using buffer and simple mineral acid. A modified Donnan theory has been used to interpret the results. SAXS was found to be a highly sensitive technique for measuring the "static response" of the hydrogels.

The use of SAXS was also investigated as a technique for measuring the swelling "kinetics" of [PMMA-*block*-PDEA-*block*-PMMA] hydrogels. Thin annealed films of hydrogel were swollen in a range of control buffered solutions. The *in-situ* nature of the technique afforded high resolution data. The kinetics of swelling was monitored by following the change in the structure peak position and its half height peak width, which gave the expansion ratio and diffusive behavior respectively. Swelling stresses induced in the samples made measuring the kinetics problematic and this limited the technique.

Finally, to avoid the expense and limited availability of SAXS beam lines a new technique was used to monitor the response of the hydrogels. A diffraction grating was imprinted onto the surface of the hydrogel, and "static" and "kinetic" response was measured by monitoring the change in the diffraction pattern. This technique was found to offer similar accuracy as SAXS, at a significantly reduced cost.

ACKNOWLEDGMENTS

I would like to thank my supervisor, Professor Tony Ryan for all his help and encouragement throughout this project. Further, I would also like to say a big thank you to Dr Paul Topham (Tops) for his help throughout the project, and especially for letting me use his precious "J1" polymer sample. Not forgetting, Dr Jon Howse, for all his help in Grenoble at the ESRF. I will never forget the hours of long discussions we have had over dinner in the ESRF canteen. I would also like to thank Jon for his assistance with liquid cell designs and Lab view programming.

None of the polymers in this project would have been synthesised without the help of Dr Christine Fernyhough back at the start of my PhD. Thank you for teaching me the intricate techniques of anionic polymerisation. I would also like to thank Dr Andrew Pryke for his helpful mountain bike advice, but most of all for sharing his wealth of experience in polymer synthesis. I would like to thank Dr O. Mykhaylyk, Dr Nadia Tzokova and Dr Patrick Fairclough for their very useful advice whenever I have needed it. I must not forget to mention Dr Pierre Chambon, and soon to be Dr Adam Blanazs for constantly keeping me amused in the lab. Many thanks also to Dr Rob McKean for his support in Grenoble, especially at keeping me awake during the long and tiring night shifts. I would also like to thank Claire Wilshaw for helping me with AFM.

Thanks also to Richard Wilkinson for machining the much needed liquid cell, and Dan Jackson for assistance with glass blowing.

I also wish to thank all the people I have worked with in the Lab, past and present including Colin, Carme, Mel, Dave, Chris, Oscar and Lorena.

CONTENTS

SYMBOLS AND ABBREVIATIONS

Å	Angstrom
α	Degree of ionisation
σ	Grating density of polymer chains (chapter 4)
$\triangle\sigma$	Change in peak width (chapter 6)
σ_0	Peak width of the initially unswollen gel (chapter 6)
σ_t	Peak width at a given time of swelling (chapter 6)
σ_{ref}	Dry length (chapter 7)
σ_{eq}	Equilibrium length (chapter 7)
C_H	Concentration of H^+
C_{AH}	Concentration of un-dissociated buffer
C_{AT}	Total concentration of buffer
d	Equilibrium domain spacing (chapter 6)
d_0	Dry domain spacing (chapter 6)
d	Scattering vector (chapter 7)
D	Distance between the sample and the detector (chapter 7)
ER	Expansion ratio
K_a	Acid dissociation constant
I	Ionic strength
$[\eta]_c$	Intrinsic viscosity
m	Diffraction order
M_s	Mass of the swollen gel
M_d	Mass of the dry gel
N	Number of monomers
p	Path difference
$P(q)$	Form factor
$S(q)$	Structure factor
R_w	Swelling ratio
s	Repeat length of the diffraction grating (chapter 7)
T_m	Temperature at maximum heat capacity

V_r	Retention volume
χ	Flory-Huggins interaction parameter
ADP	Adenosine diphosphate
$AlEt_3$	Triethylaluminium
AFM	Atomic Force Microscopy
ATP	Adenosine-5'-triphosphate
bpy	*Bipyridine*
BCC	Body centred cubic
BMMC	4-Bis (methoxytrimethylsiloxymethylene) cyclohexane
BuLi	Butyl Lithium
BZ	*Belozov*–Zhabotinsky
DEA	Diethylaminoethyl methacrylate
DMAEMA	Dimethylaminoethyl methacrylate
FT-IR	Fourier transform infrared spectroscopy
GPC	Gel Permeation Chromatography
GTP	Group Transfer Polymerisation
HPMC	Hydroxy propyl methyl cellulose
HPC	Hydroxy propyl cellulose
LiCl	Lithium Chloride
Mn	Number Average Molecular Weight
Mw	Weight Average Molecular Weight
NaAce	Sodium Acetate
NaBr	Sodium Bromide
NaCl	Sodium Chloride
NaI	Sodium Iodide
$NaNO_3$	Sodium Nitrate
NaSCN	Sodium Thiocyanate
NIPAM	Poly (N-isopropylacrylamide)
Pa	Pascal
PDEA	Poly (diethylaminoethyl methacrylate)
PDI	Polydispersity index
PMAA	Poly (methacrylic acid)

PMMA	Poly (methyl methacrylate)
Ru	Ruthenium
SAXS	Small Angle X-ray Scattering
TBABB	Tetrabutylammonium Hydrogen Bisbenzoate
THF	Tetrahydrofuran

Chapter 1

Introduction: chemical actuation in hydrogels

1.1 INTRODUCTION

Chemically actuated hydrogels share a unique feature with living systems; they are both driven by their ability to convert chemical energy into a mechanical response. However, macroscopic applications of hydrogels are limited due to the slow response rate of the material. This problem has been overcome by developing materials at micrometer length scales, as the diffusion kinetics are related to the square of the size of smallest dimension of the gel. In this introduction, the progress in the field of chemical actuation in hydrogel systems will be discussed, putting emphasis on ways in which new devices have been designed.

Polyelectrolyte hydrogels are water insoluble polymer networks capable of accommodating large amounts of water. The volume of water absorbed is a balance between the thermodynamic forces of mixing and the elastic restoring force of the polymer. In a non-ionic hydrogel the thermodynamic force is controlled by the enthalpic interactions between the solvent molecules and polymer (largely controlled by the Flory-Huggins interaction parameter, χ [2]). However in ionic gels, osmotic pressure which results from a build up of counter-ions in the network is the dominating force, largely outweighing any effect from mixing [3]. The elastic restoring force in both cases is provided by the entropic stretching of the polymer between cross-links. As well as countering the expansion of the network, the cross-links provide structural integrity to the hydrogel network; without them the polymer would simply dissolve when immersed in a good solvent. Hydrogels can either be physically or chemically cross-linked. In a chemically cross-linked gel the polymer chains are connected together with permanent covalent bonds.

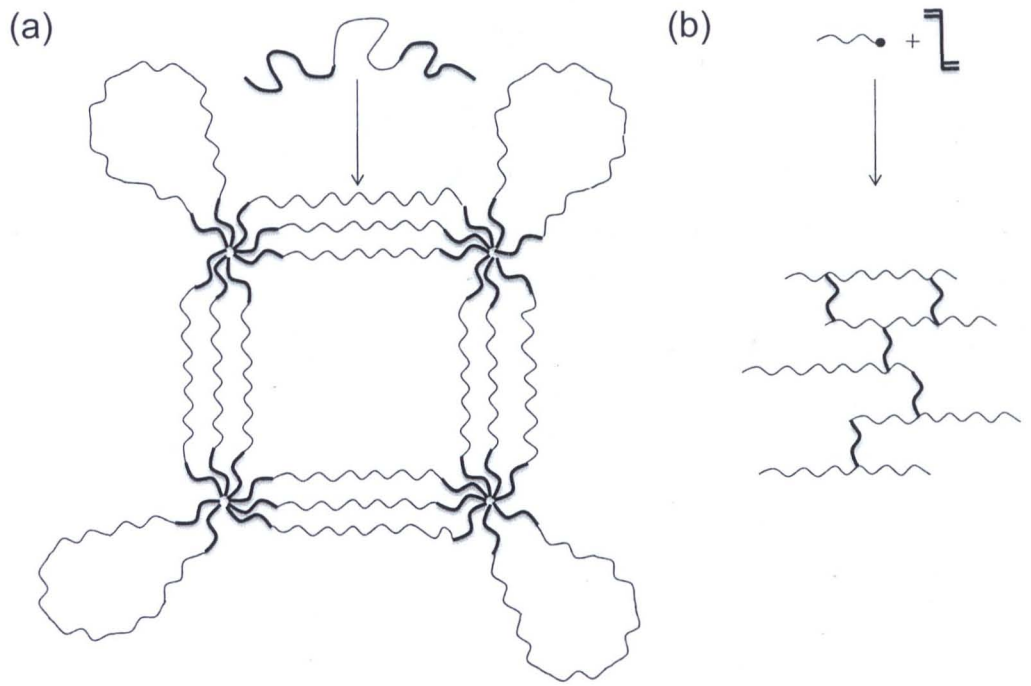

Figure 1.1: Examples of cross-linking present in hydrogels. (a): Phase separation of an ABA triblock copolymer creates inter-micelle physical cross-links above a critical polymer concentration. (b): Random chemical cross-links.

In physically cross-linked gels the chains can be connected together in a variety of different ways including microphase separated domains [4] [5], electrostatic hydrogen bonding [6] and ionic clusters [7], as shown in figure 1.1. The type and amount of cross-linking present in hydrogels has a strong influence on both the mechanical and swelling characteristics [8].

Many hydrogels exhibit large changes in their swelling ratio in response to external conditions, such as pH [9], temperature [9], ionic strength [10] and electric field [11]. This macroscopically observed swelling is a consequence of the conformational change of the individual molecules within the polymer gel.

Hydrogels are frequently referred to as *smart materials,* being able to detect a stimulus as a signal (sensing function), and then amending their function as a result of this (response function) [12]. Stimuli responsive hydrogels have been developed for use in a plethora of fields including their use as drug delivery systems [13] and artificial muscle actuators [12]. However, the number of macroscopic applications is limited, a consequence of the slow rate of solvent diffusion into the gel during swelling [14]. To avoid the inherent diffusion problems associated with macroscopic gels researchers

have taken inspiration from nature, and synthesised hydrogels at micrometer length scales. In the micrometer range the primary drawback of long diffusion times can be avoided (diffusion is related to the square of the shortest dimension of the gel [15]). Using this concept researchers have used photolithography techniques to fabricate micron sized pH responsive hydrogel valves inside microfluidic cells [16]. These gels act as tiny switches, which open and close in response to the pH of their environment. The reduction in gel dimensions was found to drastically improve the response times.

1.2 DISCUSSION: MOTILITY IN HYDROGELS

The ability of hydrogels to harness the chemical composition of their environment into a mechanical response is a common mode of operation found throughout nature. Probably the best known example of this is biological muscle actuation. An illustration describing the analogies between "synthetic" and "mammalian" muscle is given in figure 1.2. In both processes, transduction of chemical energy causes a conformational change, which causes motion or a so-called "power stroke". In muscle contraction, motion is driven by a conformational change in the myosin head group, a process fuelled by ATP [17]. In the hydrogel the macroscopic response is an assemble of the conformational response of the individual molecules making up the network, in this example driven by ions in solution.

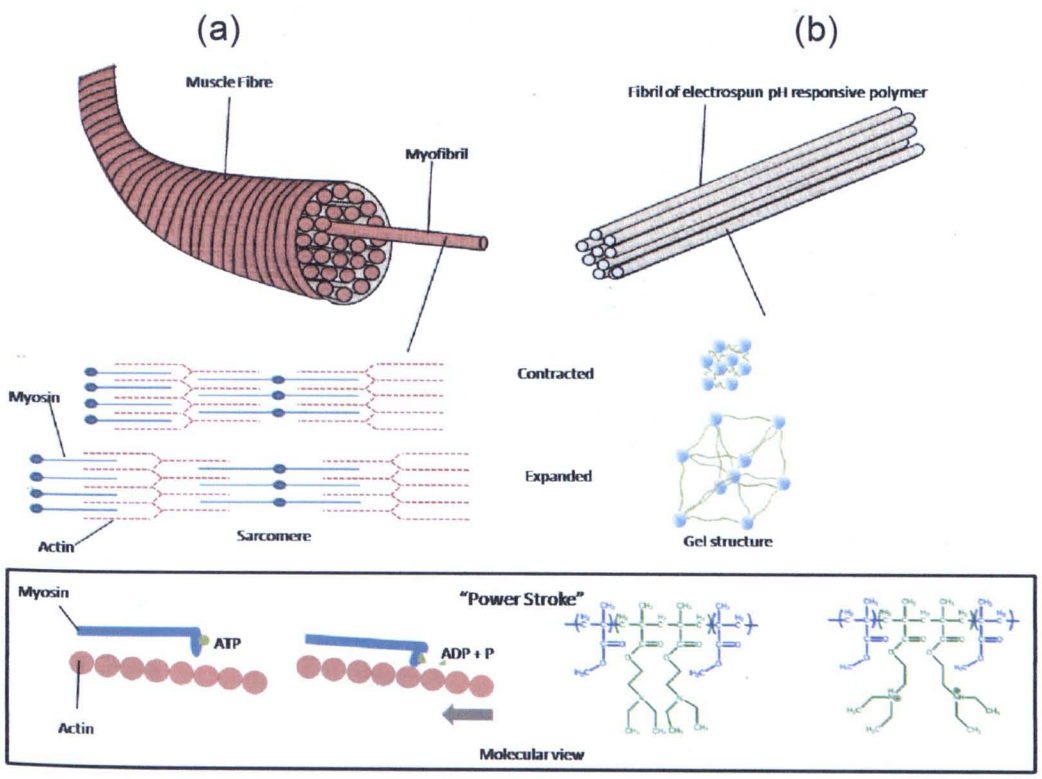

Figure 1.2: Generating the "power stroke". (a) (Mammalian muscle): ATP drives a conformational change in the myosin head group, which produces a 10 nm motion. (b) (pH responsive electrospun nanofibres): osmotic pressure causes a conformation change in the polymer chains driving expansion of the network.

Kuhn [18] and Katchalsky [19] in 1949 recognised that the coupling of a chemically cross-linked poly(acrylic acid) hydrogel with a change in ionization state would induce a macroscopic shape change similar to that observed in biological muscle. They demonstrated one of the first examples of a mechanochemical coupling. More recent examples of mechanochemical actuation can be found in work reported by Yoshida [20]. They coupled a non-linear chemical oscillator, namely the Belousov-Zhabotinsky (BZ) reaction [21] with a temperature responsive poly(NIPAM-*co*-$Ru(bpy)_3^{2+}$) gel.

During the course of the BZ reaction there is a periodic change in the oxidation state of the polymer-bound metal ion catalyst. This change in oxidation state alters the transition temperature of the poly(NIPAM) chains, which results in mechanical oscillations in the gel when held at isothermal temperature. An illustration depicting the hierarchical synchronization in BZ coupled self-oscillated gels is given in figure 1.3, along with an image showing the diffusion coupled chemical wave propagation in a rectangular gel. This system, in contrast to the early work reported by Kuhn, requires

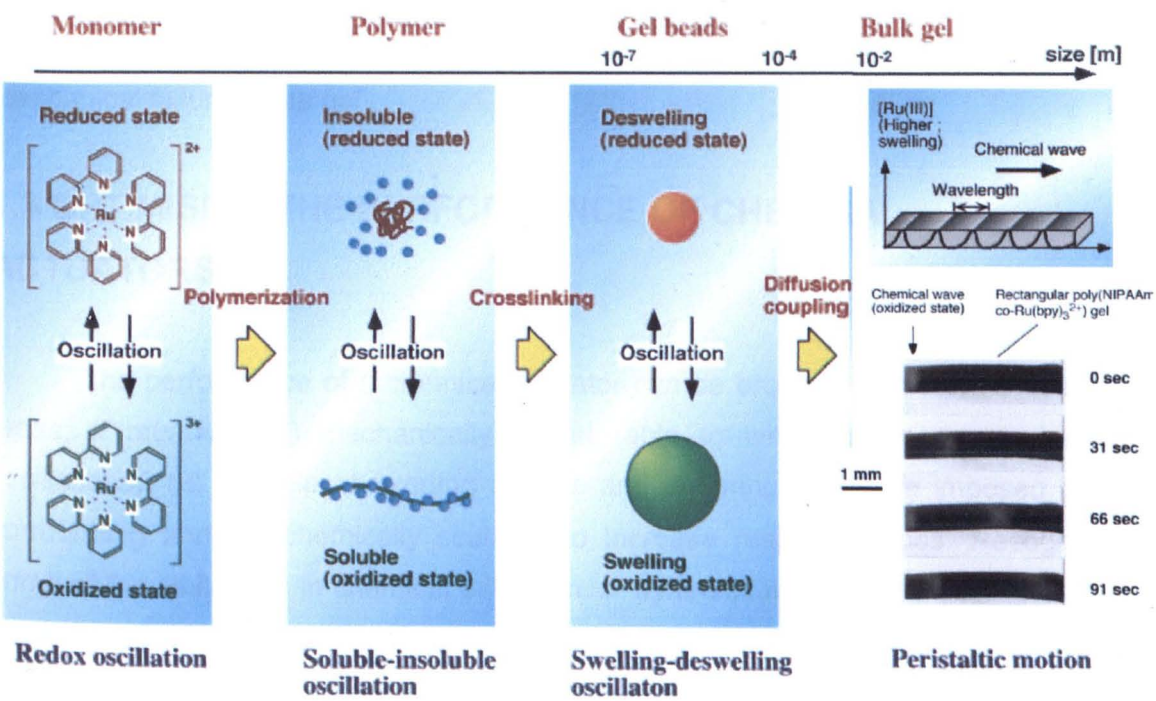

Figure 1.3: Illustration representing the hierarchical synchronisation in self-oscillating gels which utilise the Belousov-Zhabotinsky (BZ) reaction. Lower right: picture of the propagating chemical wave in a rectangular polymer gel [1].

no external on-off switching to drive the actuation. The system is autonomous and mechanical cycles continue for several hours without intervention as long as substrate remains. However, the actuator is limited by the small amplitude of the gel oscillation. Early examples reported by Yoshida oscillated by only 20 % of the dry length of the polymer, though later work improved upon this, exploiting other driving reactions such as [Ca^{2+}] and even ATP to ADP [22]. Utilization of ATP was achieved using an anionically prepared polymer with phosphoric groups attached, to which creatine kinase was immobilised. When this gel was immersed in a solution of ATP an enzymatic reaction occurred which caused reversible fluctuations in the concentration of Ca^{2+}. The calcium ion was able to act as a physical crosslinking point between the phosphoric acid groups resulting in reversible expansion and collapse of the polymer.

All of the actuator designs discussed so far have been based on chemically cross-linked polymers. It has clearly been demonstrated that the anisotropic nature of chemical cross-links reduce the mechanical strength of hydrogels [23] [24] [25] such that they make weak muscles. This is a result of the random nature of the distribution of cross-links that hold the gel together. During expansion of the network non-isotropic expansion leads to localised stresses, ultimately resulting in fracture and, therefore, mechanical failure of the gel.

1.3 OPTIMISING THE PERFORMANCE OF CHEMICAL ACTUATORS

The performance of a chemical actuator can be broken down into several key areas; it must be (1) mechanically robust (able to withstand many mechanical oscillations), (2) capable of exerting a force and enduring any force imposed by its surrounding and (3) chemically scalable to increase response times. Recognising some of the limitations in chemical actuation, a "synthetic muscle" has been designed based on nanostructured block co-polymer self-assembly. It is well known that block copolymers "microphase separate" to form periodical nanostructures [26]. In early efforts Howse *et al.* [27] synthesised an A-B-A type polyacid triblock copolymer comprising of glassy self-assembled domains of poly(methyl methacrylate) [PMMA], each separated by a series of single chains of poly(methacrylic acid) [PMAA] that

spanned between the PMMA domains. These domains, whilst providing physical cross-links to give the gel its structural integrity, additionally acted as "*markers*" allowing the molecular response of the polymer to be followed by small angle x-ray scattering (SAXS). In contrast to chemically cross-linked systems the physical entanglements are homogenously distributed throughout the network, a factor which should help alleviate network stresses during expansion. The cross-links are evenly distributed due to thermodynamic equilibrium achieved during self-assembly, and as the polymer chains are near-monodisperse the length scales between domains are very similar. To create a free running "synthetic muscle" the polyacid was coupled with a Landolt chemical oscillator [28]. This complex chemical reaction oscillates in pH value between 3 and 7, with a period of 20 minutes. When immersed in the solution the polyacid produced rhythmical mechanical oscillations with a maximum specific power output of 20 mW kg^{-1}. Building on the success of this system, Topham *et al.* [29] synthesised a similar phase separated triblock, replacing the polyacid midblock with a polybasic material, namely poly(2-(diethylamino)ethyl methacrylate) that had opposite polarity. The material produced similar mechanical oscillation when placed in an oscillating chemical reaction [30]. In more recent work from the same group the polyacid and polybase triblock discussed above was "solvent welded" together to produce a "*bi-polymeric strip*" [31], as shown in figure 1.4.

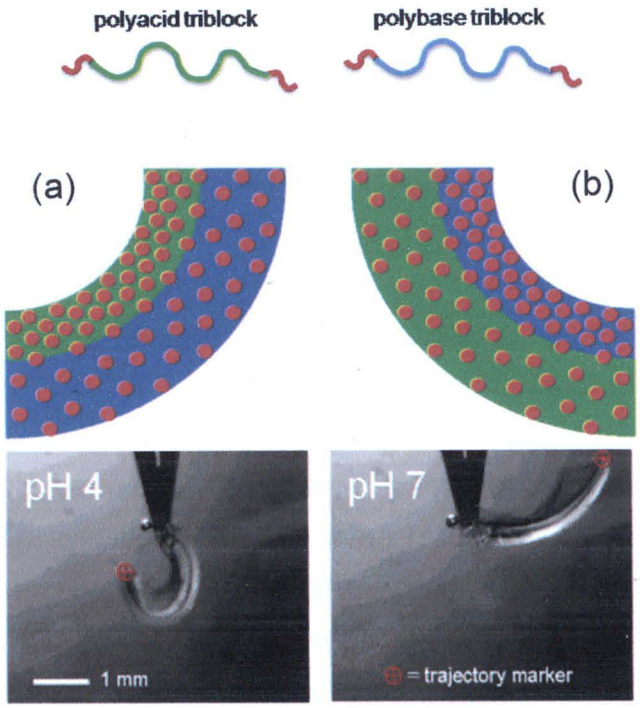

Figure 1.4: (a) systematic diagram representing the change in shape of the "*bi-polymeric strip*" when placed in acidic and neutral conditions. (b) microscopy images taken under the same conditions [31].

At low pH (pH4) the polyacid is in its collapsed form and the polybase is expanded causing the strip to bend in the direction of the polyacid. At high pH (pH7) the strip bends in the direction of the polybase material. The antagonistic coupling of the two materials benefitted the macroscopic actuation of the material, when compared to the actuation of the separate polymers under the same conditions.

Actuator design based on microphase separated structures allows material properties to be optimised from the nanoscale up. The molecular structure of the material can be optimised for a particular purpose, for example a lamellar structure can be targeted where a particular application requires actuation in one direction only.

Another advantage over chemically cross-linked systems is that the material can be processed much faster into a variety of shapes and sizes, complex patterning techniques such as photolithography are not required. However, presently these materials are limited by their relatively small power output. Compared to biological systems such as myosin, the actuators synthesised by Howse *et al.* [27] were found to be over 1 million times weaker in specific power [32]. The power output is a function of

both the force the material can generate and the time scale of the actuation, as power is equal to the force multiplied by the velocity. Altering either of these two variables should have a measured effect on the power output and several possibilities exist to improve this value. Processing the material into nanofibres is one option [33], this has been demonstrated to increase the response rate of the material, a result of the increased surface area. Another more challenging option is to increase the inherent stiffness (and strength) of the material. One candidate to optimise the strength is to increase the molecular weight of the material. This would increase the number of chain entanglements and improve the mechanical properties.

A relationship between entanglement molecular weight and tensile strength has previously been identified by Tong *et al.* [34]. They synthesised a series of (PMMA)-*block*-poly(alkylacrylate)-*block*-(PMMA) copolymers and found that the tensile strength was dependent on the molecular weight between chain entanglements in the midblock. However, increasing the molecular weight comes at a price. Synthesis of monodisperse triblock copolymers with high molecular weight (> 100,000 g mol^{-1}) often requires specialist techniques such as group transfer (GTP) [35] and anionic polymerisation [36]. In the limit of high molecular weight such techniques require strict control on the purity of reagents. As the amount of initiator must remain small it becomes increasingly difficult to produce monodisperse materials. Polydispersity and the presence of diblock/ homopolymer contamination in these systems have a strong influence on the mechanical properties. Guice *et al.* [37] recently investigated the pH response of self-assembled lamellar forming polystyrene-poly(2-hydroxyethyl methacrylate-*co*-2-(dimethylamino) ethyl methacrylate (PHD) diblock and triblock copolymers with varying amount of 2-(dimethylamino)ethyl methacrylate (DMAEMA). They found that the polymer architecture played a critical role in the robustness of the material. In PHD triblock copolymers the PS domains helped to serve as effective physical cross-linking points, but this was not the case in diblock material. In PHD diblock with high DMAEMA content the material simply broke into pieces when protonated. SAXS data taken from broken fragments indicated that the polymer still retained a lamellar morphology, which suggests that grain boundaries may also be a factor leading to early polymer fracture.

When designing any new chemically actuated system the mechanical properties are one of the key performance indicators. To design new materials it is

important to be able to understand how to increase mechanical properties through material design and ultimately, one needs to be able to accurately measure the property itself. When hydrogels are used as chemical actuators it is important not just to know the solid state mechanical properties of the material themselves, but more so to know how these properties change when the material is used in a particular environment. As a specific example of this, Johnson *et al.* [8] recognised that the design of new microfluidic devices required fundamental knowledge of the mechanical properties of the hydrogel components under varying conditions. They investigated, along with other variables, how the ultimate tensile strength of a pH-sensitive hydrogel changed when in its swollen and un-swollen states. They found that the swelling of hydrogels had a significant effect on the tensile strength, changing from 300 kPa when dry to 60 kPa when in the swollen state.

When actuation is been driven by chemical fuel (such as changes in pH) it is also important to consider how this is supplied. As the specific power output is related to the velocity of the actuation step then changing the chemistry of the fuel provides a route to increasing this value, i.e. by altering the rate of the swelling/ collapse transition. In a pH responsive polymer the swelling kinetics are controlled by several factors. Careful consideration must be paid not only to the pH but more importantly the specific species in solution. Firestone and Siegel [38] performed a systematic study looking at such effects on the swelling kinetics and equilibrium swelling ratio of methacrylate/ (2-dimethylamino ethyl methacrylate) chemically cross-linked hydrogels. They concluded that swelling rates in the gels were much faster in the presence of buffer when compared to simple mineral acid solutions at the same pH. This study implies that when evaluating the overall performance of any new chemical actuator it is important to consider not only the properties of the material but also the solution chemistry controlling the pH which drives the actuation.

We now sit on the brink of chemically actuated gels being the working materials of a range of nanotechnologies. These include self-actuated valves for delivery devices and the propulsive mechanism in flagella for synthetic biology. An understanding of the fundamental science has been developed and rudimentary design rules are in place.

REFERENCES

1. Yoshida, R., *Bulletin of the Chemical Society of Japan*, 2008, **81**, 676.
2. Flory, P. J., *Journal of Chemical Physics*, 1942, **10**, 51.
3. De, S. K., Aluru, N. R., Johnson, B., Crone, W. C., Beebe, D. J., and Moore, J., *Journal of Microelectromechanical Systems*, 2002, **11**, 544.
4. Serero, Y., Aznar, R., Porte, G., Berret, J. F., Calvet, D., Collet, A., and Viguier, M., *Physical Review Letters*, 1998, **81**, 5584.
5. Gotzamanis, G. T., Tsitsilianis, C., Hadjiyannakou, S. C., Patrickios, C. S., Lupitskyy, R., and Minko, S., *Macromolecules*, 2006, **39**, 678.
6. Bromberg, L. E. and Ron, E. S., *Advanced Drug Delivery Reviews*, 1998, **31**, 197.
7. Percec, V., *Biomacromolecules*, 2002, **3**, 272.
8. Johnson, B. D., Beebe, D. J., and Crone, W. C., *Materials Science and Engineering C*, 2004, **24**, 575.
9. Chen, G. and Hoffman, A. S., *Nature*, 1995, **373**, 49.
10. Zhang, K., Luo, Y., and Li, Z., *Soft Matter*, 2007, **5**, 183.
11. Bar-Cohen, Y., Electroactive Polymer (EAP) Actuators as Artificial Muscles Reality, Potential and Challenges, SPIE Press 21, (2001).
12. Okano, T., Biorelated polymer and Gels, Academic press, San Diego 1, (1998).
13. Hoare, T. R. and Kohane, D. S., *Polymer*, 2008, **49**, 1993.
14. Ryan, A. J., Crook, C. J., Howse, J. R., Topham, P., Jones, R. A. L., Geoghegan, M., Parnell, A. J., Ruiz-Perez, L., Martin, S. J., Cadby, A., Menelle, A., Webster, J. R. P., Gleeson, A. J., and Bras, W., *Faraday Discussions*, 2004, **128**, 55.
15. Tanaka, T., Sato, E., Hirokawa, Y., Hirotsu, S., and Peetermans, J., *Physical Review Letters*, 1985, **55**, 2455.
16. Beebe, D. J., Moore, J. S., Bauer, J. M., Yu, Q., Liu, R. H., Devadoss, C., and Jo, B.-H., *Nature*, 2000, **404**, 588.
17. Vale, R. D. and Milligan, R. A., *Science*, 2000, **288**, 88.
18. Kuhn, W., *Experientia*, 1949, **5**, 318.
19. Katchalsky, A., *Experientia*, 1949, **5**, 319.
20. Yoshida, R., Takahashi, T., Yamaguchi, T., and Ichijo, H., *Journal of the American Chemical Society*, 1996, **118**, 5134.
21. Zaikin, A. N. and Zhabotinskii, A. M., *Nature*, 1970, **225**, 535.
22. Uesusuki, R. Y. a. Y., *Biomacromolecules*, 2005, **6**, 2923.
23. Tanaka, Y., Gong, J. P., and Osada, Y., *Progress in Polymer Science*, 2005, **30**, 1.
24. Kurua, E. A., Orakdogena, N., and Okay, O., *European Polymer Journal*, 2007, **43**, 2913.
25. Shibayama, M., *Macromol. Chem. Phys*, 1998, **199**, 1.
26. Bates, F. S. and Fredrickson, G. H., *Annual Review of Physical Chemistry*, 1990, **41**, 525.
27. Howse, J. R., Topham, P., Crook, C. J., Gleeson, A. J., Bras, W., Jones, R. A. L., and Ryan, A. J., *Nano Letters*, 2006, **6**, 73.
28. Edblom, E. C., Orban, M., and Epstein, I. R., *Journal of the American Chemical Society*, 1986, **108**, 2826.

29. Topham, P. D., Howse, J. R., Mykhaylyk, O. O., Armes, S. P., Jones, R. A. L., and Ryan, A. J., *Macromolecules*, 2006, **39**, 5573.
30. Topham, P. D., Howse, J. R., Crook, C. J., Gleeson, A. J., Wim Bras, Armes, S. P., Jones, R. A. L., and Ryan, A. J., *Macromolecular Symposia: Polymer Networks*, 2007, **256**, 95.
31. Topham, P. D., Howse, J. R., Crook, C. J., Armes, S. P., Jones, R. A. L., and Ryan, A. J., *Macromolecules*, 2007, **40**, 4393.
32. Mahadevan, L. and Matsudaira, P., *Science*, 2000, **288**, 95.
33. Wang, L., Topham, P. D., Mykhaylyk, O. O., Howse, J. R., Bras, W., Jones, R. A. L., and Ryan, A. J., *Advanced Materials*, 2007, **19**, 3544
34. Tong, J. D., Leclere, P., Doneux, C., Bredas, J. L., Lazzaroni, R., and Jerome, R., *Polymer*, 2001, **42**, 3503.
35. 0. W. Webster, W. R. H., D. Y. Sogah, W. B. Farnham, and T. V. RajanBabu, *Journal of the American Chemical Society*, 1983, **105**, 5706.
36. Szwarc, M., *Nature*, 1956, **178**, 1168.
37. Guice, K. B., Marrou, S. R., Gondi, S. R., Sumerlin, B. S., and Loo, Y.-L., *Macromolecules*, 2008, **41**, 4390.
38. Firestone, B. A. and Siegel, R. A., *Journal of Biomaterials Science, Polymer Edition* 1994, **5**, 433.

PUBLICATIONS

1. Swann, J. M. and Ryan, A. J., *Polymer International*, 2009, **58**, 285.

Chapter 2
Aims

2.1 AIMS

pH responsive hydrogels show great promise for applications in the field of chemical actuation. The potential of these materials as discussed in the introduction, was first recognized in the 1950's by Kuhn and Katchalsky [1, 2], where they noted their "muscle like" behavior. Since this time there has been an explosion in the use of stimuli responsive materials, which in part can be attributed to the work of Tanaka in the 1980's, who was responsible for the development of responsive gels sensitive to a wide range of stimuli including light, solvent, pH, and temperature. It was not until the year 2000 when the basic fundamentals for technological applications were developed, which commenced with the creation of microsized gels using photolithography for use inside microfluidic devices [3].

In recent years there has been a huge interest in the area of block copolymers for use in the field of nano-science and technology. This is mainly attributed to their promise of being easily manipulated at molecular length scales. The materials can be tailored atom-by-atom, and molecule-by-molecule, to create devices which are orders of magnitude better in terms of their functionally and performance [4].

Preparation of nano-materials is usually achieved by one of two routes, known as *top-down* or *bottom-up*. In the *top-down* approach a macroscopic pre-existent material is "sculpted", to create the final device with the required, shape, properties and dimensions. However, the final device is usually not atom or energy –efficient and is typically limited to dimensions greater than 100nm. In the quest for ultimate miniaturization and control the nanotechnology community has strived to develop materials with sizes between 10 -100nm. This has been achieved by chemists using the *bottom-up* approach. This technique involves creating hierarchical structures from the assembly (physical or chemical) of a finite number of simple building blocks

(atoms, molecules and macromolecules) [5]. This is a much simpler route requiring fewer steps.

Self-organization in block copolymers has recently been used to create nanostructured materials which have switching (responsive) properties based on their phase transitions. The work of Howse et al [6] is one of the most interesting developments in the field of chemically actuated gels, they constructed a scalable, pH-responsive gel from a robust, self-assembled block copolymer comprising of glassy domains of poly(methyl methacrylate) [PMMA], each separated by a series of single chains of poly(methacrylic acid) [PMAA] that spanned between the PMMA domains. These domains, whilst providing physical cross-links to provide structural integrity, additionally acted as "markers" allowing the molecular response of the polymer to be followed by small angle x-ray scattering (SAXS). The group was also responsible for the creation of other pH responsive self-assembled structures. The reader is directed to the introduction for further details.

This novel material offered two key developments to the community. Unlike conventional chemically cross-linked hydrogels, their network linkage was a result of physical entanglement. A feature made possible by the *bottom-up* approach. In addition the self-assembled structure afforded the unique opportunity to measure their chemical response at the molecular level using SAXS.

This thesis will be split into two parts. The first will be concerned with the synthesis of a series of well-defined PMMA-*block*-PMAA-*block* PMMA and PMMA-*block*-PDEA-*block*-PMMA triblock copolymers. Annealing studies will then be performed on the raw polymer to determine and fine tune the necessary conditions for microphase separation. This will be evaluated using SAXS and AFM. These studies can be found in chapter 3.

The second part of the thesis will be concerned with using SAXS to evaluate the static and dynamic response of the polymer to changes in pH, ionic strength and salt identity putting the earlier work [6-10] in a sound thermodynamic framework. The use of SAXS in itself for this purpose will be evaluated. Chapters 4 - 6 are devoted to these studies. In chapter 7 a novel diffraction grating method, which takes advantage of the *bottom-up* approach is used to compare the results of the static and kinetic SAXS studies.

REFERENCES

1. Katchalsky, A., *Experientia*, 1949, **5**, 319.
2. Kuhn, W., *Experientia*, 1949, **5**, 318.
3. Beebe, D. J., Moore, J. S., Bauer, J. M., Yu, Q., Liu, R. H., Devadoss, C., and Jo, B.-H., *Nature* 2000, **404**, 588.
4. Borsali, R. and Pecora, R., Soft-Matter Characterization, 1 ed, Springer 160, (2008).
5. Ikkala, O. and Brinke, G. t., *Chemical Communication*, 2004, 2131.
6. Howse, J. R., Topham, P. D., Crook, C. J., Gleeson, A. J., Bras, W., Jones, R. A. L., and Ryan, A. J., *Nano Letters*, 2006, **6**, 73.
7. Topham, P. D., Howse, J. R., Crook, C. J., Armes, S. P., Jones, R. A. L., and Ryan, A. J., *Macromolecules*, 2007, **40**, 4393.
8. Topham, P. D., Howse, J. R., Crook, C. J., Gleeson, A. J., Bras, W., Armes, S. P., Jones, R. A. L., and Ryan, A. J., *Macromolecular Symposia*, 2007, **256**, 95
9. Ryan, A. J., Crook, C. J., Howse, J. R., Topham, P., Jones, R. A. L., Geoghegan, M., Parnell, A. J., Ruiz-Perez, L., Martin, S. J., Cadby, A., Menelle, A., Webster, J. R. P., Gleeson, A. J., and Bras, W., *Faraday Discussions*, 2004, **128**, 55.
10. Topham, P. D., Howse, J. R., Mykhaylyk, O. O., Armes, S. P., Jones, R. A. L., and Ryan, A. J., *Macromolecules*, 2006, **39**, 5573.

Chapter 3
Synthesis and processing of pH-responsive self-assembled triblocks

3.1 INTRODUCTION

Fundamental work by a number of researchers has demonstrated how phase separated triblock copolymers can be successfully harnessed to create temperature [1] [2], and pH [3, 4] responsive materials. One of the greatest advantages of using this methodology is the way in which the polymer properties can be easily tuned [3].

Block copolymers are extremely well suited to the *bottom-up* approach of design [5]. The materials can be synthesised in a controlled way to ensure they have the desired final properties. For example, Guice *et al* synthesised a self-assembled pH sensitive triblock copolymer composed of polystyrene, PS, and poly(2-hydroxyethyl methacrylate-*co*-2-(dimethylamino)ethyl methacrylate), PHD, with varying 2-(dimethylamino)ethyl methacrylate (DMAEMA) content. By varying the length of the DMAEMA block they were able to change the expansion ratio in a controlled way [3].

One of the other advantages of phase separated materials is that it minimizes heterogeneities in the cross-link distribution. Topham *et al* [6] have demonstrated the usefulness of this feature, creating robust chemical actuators from self-assembled pH responsive PMMA-*block*-PDEA-*block*-PMMA (polybasic) and PMMA-*block*-PMAA-*block*-PMMA (polyacid) triblock copolymers [4, 7]. The robustness of these materials, and those reported by Guice *et al* is a result of physical cross-links. In the latter case the glassy hydrophobic PMMA blocks serve as physical cross-linking points.

The materials synthesised by Topham *et al* and Guice *et al* were also particularly unique, in that their pH response could be measured at the molecular level using SAXS. In both cases this was achieved by measuring the long order microdomain spacing between the hydrophobic end groups. See the introduction, section 1.3 for further details.

In this chapter, a number of similar PMMA-*block*-PDEA-*block*-PMMA (polybasic) and PMMA-*block*-PMAA-*block*-PMMA (polyacid) triblock copolymers will be synthesised. The specially designed materials will be processed to create microphase separated structures. This will be achieved using either thermal or solvent annealing. The specific conditions to achieve this will be evaluated and the final equilibrium molecular structures will be evaluated using SAXS.

A number of these polymers will then be further evaluated using SAXS to monitor how their "static" equilibrium molecular response changes as a function of pH, ionic strength and salt identity. These studies are reported in chapter 4 and 5. In later chapters SAXS will be used to investigate the kinetics of expansion.

An introduction into block copolymer phase separation, with an emphasis on triblock copolymer processing is given in the following section.

3.1.1 Microphase separation in block copolymers

A block copolymer is a macromolecule which contains sequences or blocks of chemically different repeat units covalently linked together [8]. A linear diblock is one of the simplest forms of a block copolymer where two distinct polymers are joined together in sequence (i.e. —A_nB_m—). A variety of higher order block copolymer architectures can be synthesised, such as linear triblock copolymers which contain two distinct polymer chains (—$A_nB_mA_o$—), or three distinct polymer chains in sequence (—$A_nB_mC_o$—). Structures may not necessarily be linear, for example, star copolymers can be synthesised when more than two distinct block copolymers are attached at a common branch point [9].

In many blends of block copolymer the component blocks are usually incompatible [10]. This is a consequence of repulsion between individual monomers in the different blocks, the effect being magnified due to the large number of repeats.

It is now well established that block copolymers self-assemble into various structures with well-defined spacing and size on the tens of nanometre length scale [11, 12]. The local segregation or formation of distinct phases in block copolymers is known as *microphase separation*, where domains rich in A and B are formed the morphology of which is dominated by the internal interfacial energy [13].

Microphase separation is driven by the enthalpy of demixing of the component blocks, whilst macrophase phase separation is not possible due to the chemical connectively of the blocks [14]. This enthalpy is proportional to the Flory-Huggins segment-segment interaction parameter, χ, which is found to be inversely proportional to the temperature according to equation 3.1,

$$\chi = \frac{A}{T} + B \tag{3.1}$$

The values A and B are system dependent constants and T is the temperature. At high temperatures the component blocks mix homogenously resulting in the disordered phase (DIS), but as the temperature is lowered (the Flory-Huggins segment-segment interaction parameter increases) the blocks separate into ordered microstructures. There is also an entropic penalty associated with phase separation which is related to chain stretching. The magnitude of which is related to degree of polymerisation, N.

The particular structure adopted by a block copolymer depends on the following controllable parameters, i) the Flory-Huggins interaction parameter χ, ii) the overall degree of polymerisation, N, iii) the volume fraction of the component blocks f and finally the particular polymer architecture. In the case of an A-B-C triblock for example, one must consider three interaction parameters and two composition variables, compared to one interaction parameter and one composition variable in a diblock. This complicates the phase behaviour somewhat but also increases the number of observed phases [15].

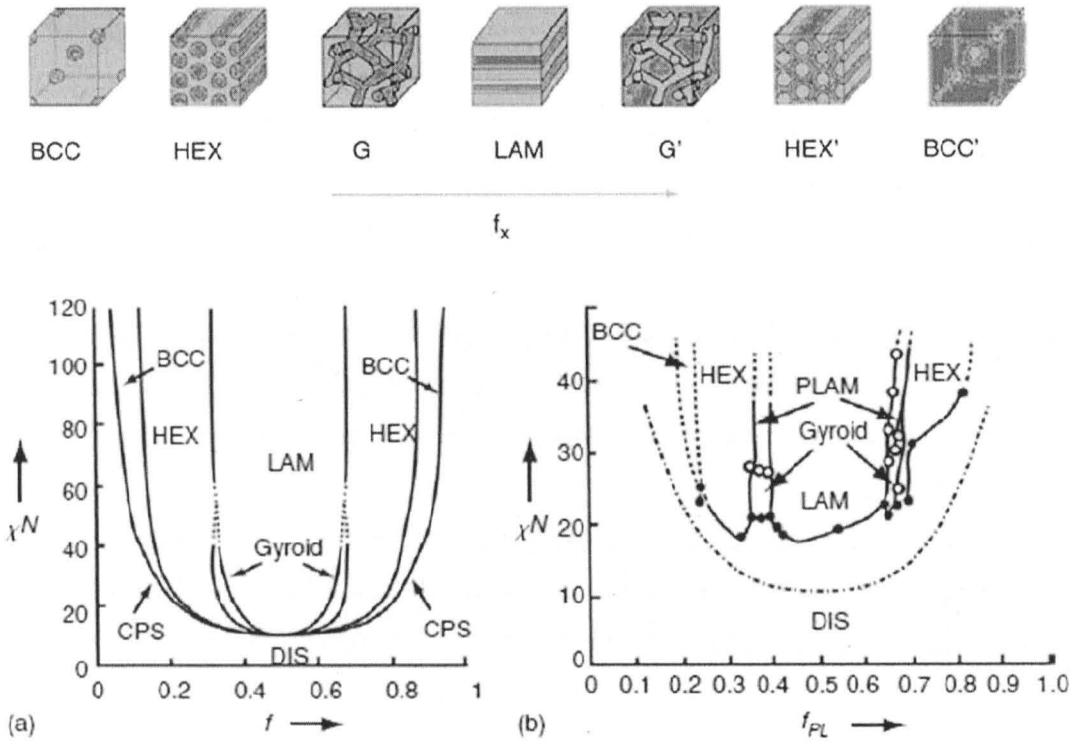

Figure 3.1: (a) Theoretical and (b) experimental phase diagram and corresponding morphologies for block copolymers. The phases are as follows: close packed spheres (CPC), body centred cubic (BCC), hexagonal (HEX), gyroid (G), lamellar (LAM). Adapted from reference [16] and [5].

The theoretically derived phase diagram for linear AB diblock melts is shown in figure 3.1a. An experimentally observed phase diagram for a typical PS-PI diblock copolymer is also included for comparison. Each diagram encompasses the controllable parameters previously discussed. The simplest microphase morphology is the lamellar (L) phase which consists of A and B monomers separated into *A*-rich and *B*-rich lamellae. Other commonly observed phases include gyroid (G), hexagonal-packed cylinders (HEX) and body centred cubic spheres (BCC).

3.1.2 Block copolymer processing

Processing of block copolymer nanostructures in the bulk can be achieved using a number of strategies. Of the routes available, solvent [17] and thermal annealing [18] are some of the more commonly reported.

The solvent annealing method involves preparing a solution of the block copolymer at a concentration ranging from 1 to 50% w/w. The solvent is then slowly evaporated. Several other factors must be controlled to ensure the formation of well-ordered films. This includes the temperature, evaporation rate and the chemical atmosphere.

The type of solvent used to anneal the polymer has a direct influence on the microstructure [17]. In an A-B-A triblock copolymer for example, one can choose to use a *selective* solvent which is a good solvent for both blocks. Or alternatively, a *solvent* can be chosen which is a good solvent for one block and a neutral solvent for the other. When a polymer is dissolved in *a solvent* which is selective for both blocks all of the chains are freely mobile. This is a due to the solvent depressing the glass transition temperature of the chains. The addition of a selective solvent for both blocks is analogous to increasing the temperature or reducing the segment-segment interaction parameter, χ.

During the annealing process evaporation of solvent increases the concentration of the polymer solution. Chain mobility is progressively reduced and at a certain concentration the polymer begins to microphase separate. This is energetically favoured as it reduces the interchain interaction between the incompatible blocks.

With the use of a *solvent which is selective* for only one of the blocks it is possible to alter, or tailor the morphology of a block copolymer. This affect happens because the self-assembly process is initiated from a pre-organised state.

In a polymer in the melt state, solvents with different degrees of selectivity can be used to move the system to smaller or larger degrees of segregation. This corresponds to a vertical trajectory along the phase diagram in figure 3.1. This effect has been exploited to change the microphase morphology of self-assembled styrene-isoprene (SI) diblock copolymers in the melt [17].

Thermal annealing is another method to achieve phase separation. In some respects it is analogous to solvent annealing. The block copolymer is first heated above its glass transition temperate. This is equivalent to dissolving the polymer in a dilute solution of non-selective solvent, i.e. the polymer chains become mobile. The polymer is then slowly cooled, and as the chain mobility is reduced the polymer phase separates to reduce unfavourable interchain interactions.

3.13 Physical cross-links in amphiphilic block-copolymer networks

In self-assembled triblock copolymers the mechanical robustness is in part a result of physical cross-links [19]. This effect has recently been illustrated by Guice *et al* [3]. They synthesised a series of diblock and triblock pH responsive copolymers of polystyrene, PS, and poly(2-hydroxyethyl methacrylate-*co*-2-(dimethylamino)ethyl methacrylate), PHD. They found that the presence of PS physical cross-links in the triblock to be critical for structural stability. Diblock copolymers protonated under identical conditions simply fell to pieces.

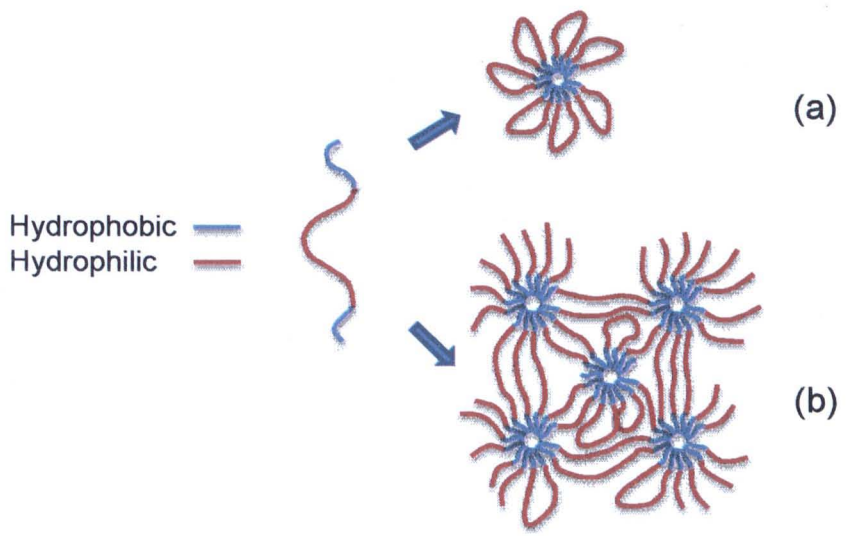

Figure 3.2: Schematic representation of (a) flower micelles and (b) physical cross links.

An example of physical entanglements in a triblock copolymer is shown in figure 3.2. The illustration also shows an example of a flower micelle. Flower micelles are created when there is a difference in the Flory Huggins interaction parameter

between the component polymer blocks, and the blocks with similar values tend to aggregate together [20]. The presence of flower micelles is undesirable as they impart no rigidity to the polymer network. To avoid flower micelles it is important to prepare the polymers at high concentration. This brings the aggregates closer together, and the midblock is forced to span two neighboring microdomains to form a bridge.

3.14 Effect of microphase structure on polymer properties.

It is also important to consider how the microphase structure changes the polymer properties. Nykaenen *et al* [2] have demonstrated this effect. They synthesised a number of temperature responsive polystyrene-*block*-poly(N-isopropylacrylamide)-*block*-polystyrene triblock copolymers. They compared the swelling ratio of the hydrogel as a function of microphase morphology. They identified that the morphology had a drastic effect on swelling. Hydrogels with a spherical morphology were found to have the largest swelling ratio, and lamellar the smallest. This was a result of the lamellae domains hindering the diffusion of water compared to the spherical morphology which did not restrict expansion in any direction.

3.2 SYNTHESIS OF PMMA-*block*-PMAA-*block*-PMMA BLOCK COPOLYMERS

3.2.1 Introduction

A series of pH responsive, PMMA-*block*-PMAA-*block*-PMMA triblock copolymers with a range of molecular weights were targeted. This polymer is amphiphilic, having water insoluble hydrophobic PMMA end groups and a polar pH responsive midblock. When the polymer is placed in a solution above the pK_a of the midblock it is known to expand [21]. An introduction into polyelectrolyte hydrogels can be found in the introduction, section 1.1.

To maximise the magnitude of expansion the PMMA-*block*-PMAA-*block*-PMMA polymers were designed to phase separate with a spherical morphology. As previously discussed in section 3.13 this allows the material to expand unimpeded in three dimensions.

As the phase behaviour of a symmetric triblock is very similar to a linear AB diblock one can use the phase diagram in figure 3.1 to estimate the required volume fraction of PMMA for a BCC morphology [19]. Based on this diagram, and previous results on a similar polymer [21], the triblock was targeted to have a PMMA volume fraction of approximately 15 percent, which corresponds to 7.5 percent on each end as it will be a symmetrical.

There are several synthetic techniques available to achieve this which include anionic and atom transfer radical polymerisation (ATRP) [22]. However to produce a triblock which will successfully phase separate with well defined ordering at the molecular level, it is desirable to synthesise a polymer with a low molecular weight distribution, ideally less than 1.1. Additionally, reducing the length distribution of the PMMA end blocks in thermoplastic elastomers has been demonstrated to increase mechanical properties as more of the chains can be involved in network formation [23].

Living anionic polymerisation is the technique most suited to producing well defined methacrylate based triblock copolymers with low molecular weight distribution (less than 1.2) [24]. An introduction into anionic polymerisation can be found in the appendix, section 9.1.1.

3.2.2 PMMA-*block*-PMAA-*block*-PMMA block copolymers via anionic polymerisation

Synthesis of PMMA-*block*-PMAA-*block*-PMMA copolymers was accomplished anionically using the bifunctional initiator, 1,3-bis (1-phenylethenyl) benzene, as shown in figure 3.3. (note: this synthetic route produces the PMMA-*block*-P(*ter*-BuMA)-*block*-PMMA precursor which must be hydrolysed to give the desired polymer).

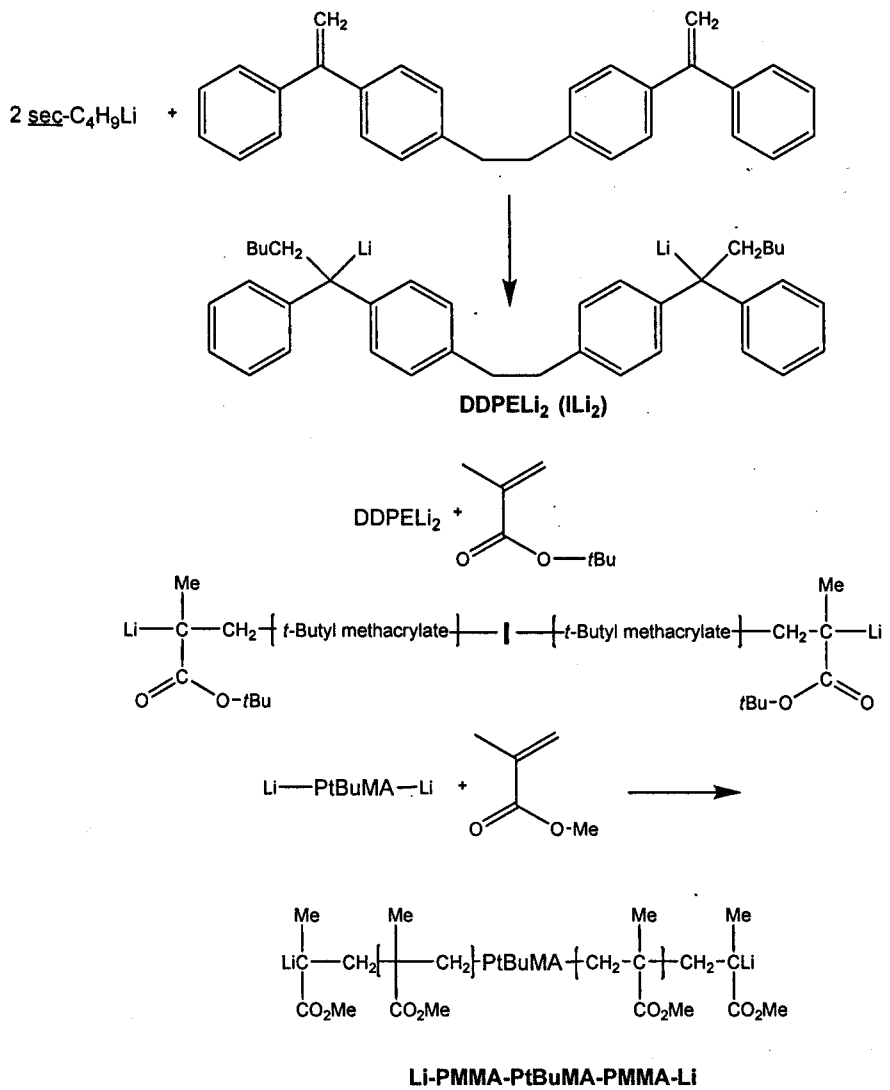

Figure 3.3: Synthesis of PMMA-*block*-P(*ter*-BuMA)-*block*-PMMA triblock copolymer via living anionic polymerisation. I represents the initiator, 1,3-bis (1-phenylethenyl) benzene (BMMC).

Using a bifunctional initiator simplifies the reaction by reducing the number of monomer addition steps from three to two (as compared to sequential monomer addition using a monofunctional initiator). A reduction in the number of steps is advantageous as it reduces the chance of introducing unwanted terminating species at each monomer addition. GPC traces of PMMA-*block*-P(*ter*-BuMA)-*block*-PMMA precursor synthesised using the bifunctional initiator are shown in figure 3.4.

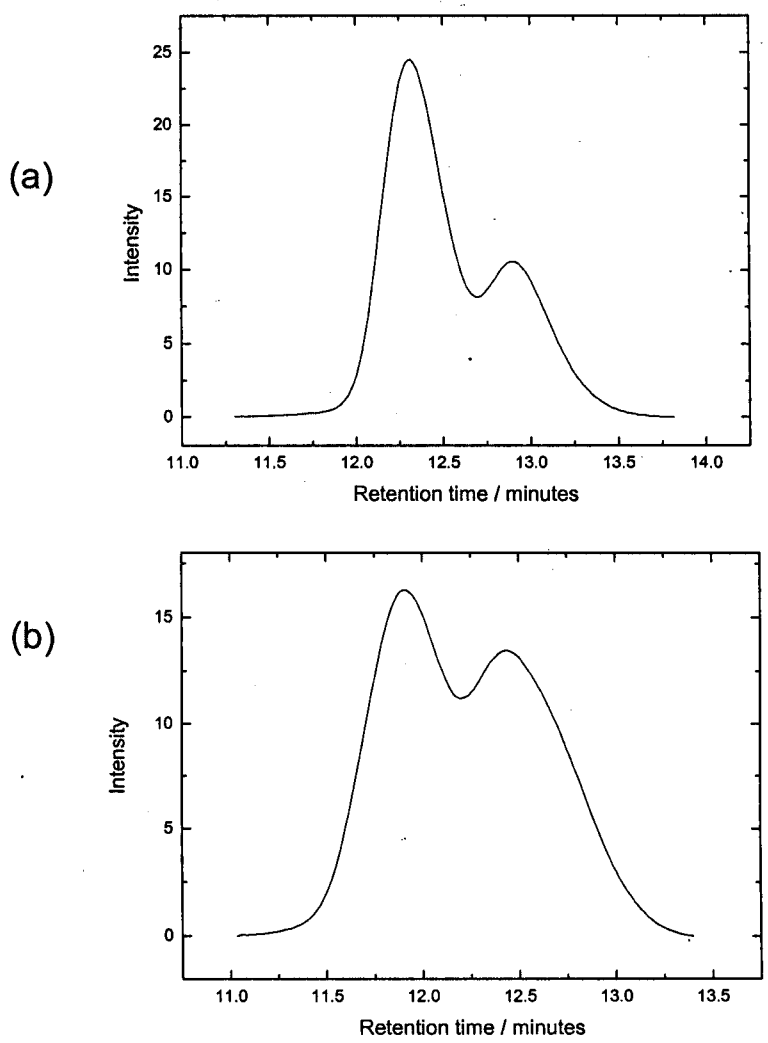

Figure 3.4: GPC chromatogram of (a) PMMA-*block*-P(*ter*-BuMA)-*block*-PMMA triblock (JSTB02) (65% triblock, 35% diblock) and (b) PMMA-*block*-P(*ter*-BuMA)-*block*-PMMA triblock (JSTB04) (42% triblock, 58% diblock) synthesised using the bifunctional initiator 1,3-bis (1-phenylethenyl) benzene (BMMC).

A summary detailing the molecular weight, volume fraction and M_w/ M_n of polymers synthesised using this method is given below in table 3.1.

Table 3.1: A summary of copolymer compositions, molecular weight and polydispersities of various PMMA-*block*-PMAA-*block*-PMMA triblock copolymers.

Sample I.D.	Theoretical MAA volume fraction	Experimental MAA volume fraction[a]	Theoretical M_n	Experimental M_n[b]	M_w/ M_n	Percentage of triblock
JSTB02	0.85	0.76	79362	45700	1.14	65
JSTB04	0.85	0.84	80108	72744	1.14	42

a: As determined by ^{1}H NMR (section 3.2.3)

b: Molecular weight determined by triple detector GPC from the PMMA-*block*-P(*ter*-BuMA)-*block*-PMMA precursor assuming 100% hydrolysis of the *ter*-BuMA group (confirmed using ^{1}H NMR by loss of the *ter*-BuMA signal at 1.6ppm).

3.2.3 Calculating the composition of PMMA-*block*-PMAA-*block*-PMMA block copolymers by ^{1}H NMR

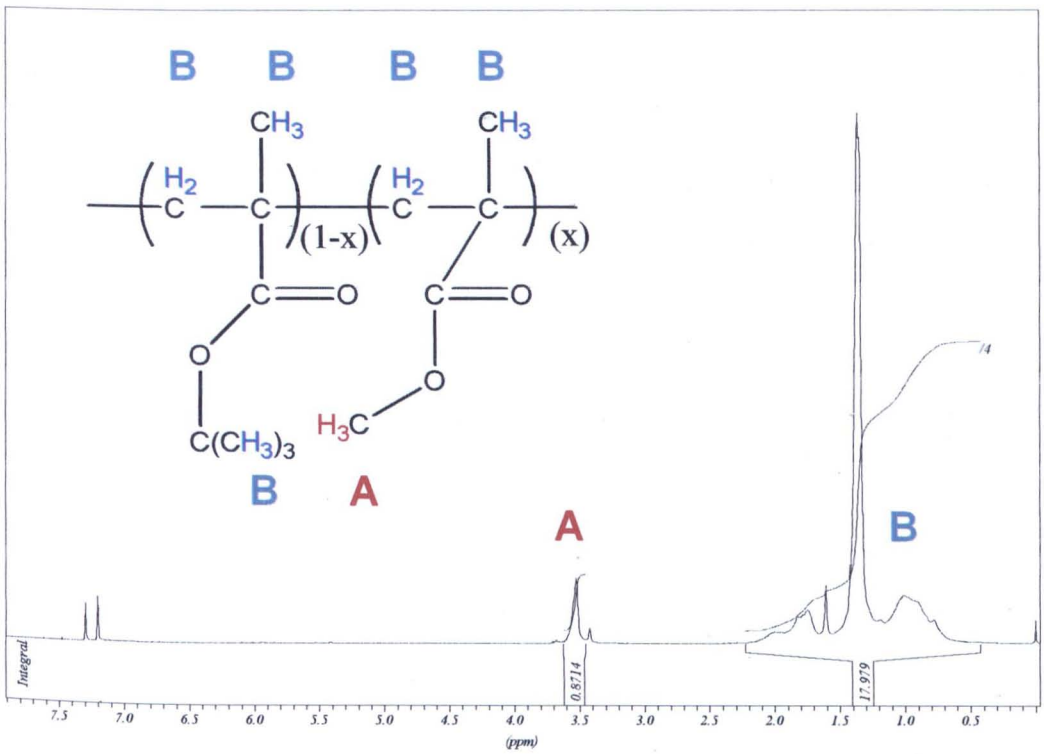

Figure 3.5: ^{1}H NMR Spectrum of PMMA-*block*-P(*ter*-BuMA)-*block*-PMMA (JSTB02).

For each PMMA-*block*-PMAA-*block*-PMMA polymer the volume fraction of methacrylic acid was calculated using the following procedure. ^{1}H NMR was used to determine the mole fraction of *ter*-BuMA in the precursor polymer. Using this value (assuming an identical volume fraction in PMMA-*block*-PMAA-*block*-PMMA) and previously reported densities [6] for the corresponding component homopolymers, the mole fraction was converted to a volume fraction. A sample calculation is detailed below.

As illustrated in the NMR spectrum given above in figure 3.5,

Mole fraction of *ter*-BuMA = (1-x)
Mole fraction of MMA = x

To calculate x, the mole fraction of MMA, it is necessary to find the ratio between the O-CH_3 protons (A) on the MMA repeat unit and the remaining protons of the MMA (B) and *ter*-BuMA (B) unit as a function of x. For every repeat unit of MMA there are three equivalent O-CH_3 (A) protons. Therefore, A = 3x. The remaining signal which corresponds to B is due to the 5 remaining protons on the MMA subunit and 14 protons on the *ter*-BuMA subunit. Therefore B = 5x + 14 (1-x) = 5x + 14 - 14x. The ratio of B to A is therefore:

$$\frac{B}{A} = \frac{5x + 14 - 14x}{3x} \tag{3.2}$$

$$x = \frac{14}{3(B/A) + 9} \tag{3.3}$$

From the ^1H NMR spectrum given in figure 3.5 the ratio (B/A) is 20.63. Substituting this value into equation 3.3 gives a value for the MMA mole fraction of 0.20. Therefore the triblock has the molar composition 0.10-0.80-0.10. The corresponding volume fraction of each subunit is calculated by first multiplying the mole fraction by the molar mass to give a mass fraction, and then dividing this value by its density to give a volume. The volume of each component in the block copolymer is then divided by the total volume to give the volume fraction. An example is given below,

$$\text{Volume of MAA} = \frac{0.8 \times 86.09}{1.285} = 53.60 \text{ cm}^3 \tag{3.4}$$

$$\text{Volume of MMA} = \frac{0.2 \times 100.12}{1.185} = 16.90 \text{ cm}^3 \tag{3.5}$$

$$\text{MMA volume fraction} = \frac{53.60}{53.60 + 16.90} = 0.76 \tag{3.6}$$

The PMMA-*block*-PMAA-*block*-PMMA triblock therefore has the following volume composition, 0.12:0.76:0.12.

As can be seen from table 3.1 this method allows good control of the target molecular weight and produces polymers with polydispersity indices (PDI's) less than 1.2. In all cases, however it was not possible to produce a monodisperse sample. Figure 3.4 shows GPC traces of polymers synthesised using this method. All polymerisations have a clear bimodal distribution. In figure 3.4a the peak at lower retention time, corresponding to 65% of the sample is believed to be triblock, and the second peak corresponds to diblock. A bimodal distribution from a bifunctional initiator suggests partial deactivation of a number of the active chain ends. This is a known complication arising from the use of bifunctional initiators especially in high molecular weight polymers as there are relatively few initiating species. To avoid active chain end deactivation the monomers used in this polymerisation were thoroughly dried with CaH_2 and subsequently washed with living polystyrene [25], making this mechanism of termination less plausible. Alternatively the bimodal distribution may be a result of the initiator chain end functionality. The active bifunctional initiator is produced from the reaction between *sec*-BuLi and 1,3-bis (1-phenylethenyl) benzene. For the initiator, 1,3-bis (1-phenylethenyl) benzene to be truly bifunctional both double bonds must react with *sec*-BuLi. However it is possible that during this reaction some of the initiator species may have only reacted on one end of the molecule. This will give rise to a mixture of both bifunctional and monofunctional initiator. To circumvent this from happening, in all polymerisations the initiator solution was added titrimetrically to the *sec*-BuLi solution [26]. This ensured that the *sec*-BuLi solution always remained in excess compared to the initiator.

It is also known that not all difunctional initiators behave in an ideal manner in all solvents and monomers. It may be simply that in this combination of solvent, initiator and monomer the system cannot generate a pure difunctional polymer. In this case it will simply not be possible to synthesise a monodisperse sample. Due to the high level of complexity and time required for anionic polymerisations they were not further optimized.

3.3 ANNEALING OF PMMA-*block*-PMAA-*block*-PMMA TRIBLOCK COPOLYMERS

3.3.1 Network formation

As discussed in section 3.1.3, the PMMA-*block*-PMAA-*block*-PMMA triblock copolymers need to be suitably processed and annealed. Annealing produces the desired self-assembled physically cross-linked network, as without this the polymer would have no structural integrity, and would simply fall to pieces when placed into an aqueous environment [3].

3.3.2 Annealing Conditions for PMMA-*block*-PMAA-*block*-PMMA triblock copolymers

In its unprocessed raw state the PMMA-*block*-PMAA-*block*-PMMA triblock copolymer consists of amorphous chains which have no molecular long range order. This has been confirmed by SAXS as shown in figure 3.6. There is clearly no structure peak which is expected for a phase separated polymer.

To induce microphase separation the block copolymer must be either thermally or solvent annealed. Thermal annealing requires the triblock to be heated above the glass transition temperature of the two component blocks. The alternative method, solvent annealing, functions by reducing the glass transition temperature of the component blocks. Both cases correspond to a vertical trajectory across the block copolymer phase diagram (see section 3.1.1).

As the glass transition temperatures (T_g) for poly (methyl methacrylate) and poly (methacrylic acid) homopolymer are 120°C and 228°C respectively [27], the use of thermal annealing is less attractive. Therefore the block copolymers were processed using solvent annealing.

To process and solvent anneal thin films of PMMA-*block*-PMAA-*block*-PMMA it is essential to find a good common solvent, or combination of selective solvents for the component blocks. Several solvents are recognised in the literature [27]. Dioxane and methanol are good solvents for poly (methacrylic acid) and dioxane and acetone are good solvents for poly (methyl methacrylate).

3.3.3 Selectivity of solvent on the self assembly of PMMA-*block*-PMAA-*block*-PMMA triblock copolymer thin films

The effect of the thermodynamic selectivity of dioxane and 85:15 v/v methanol/acetone solvent on the self assembly of PMMA-*block*-PMAA-*block*-PMMA triblock copolymers, JSTB02 and JSTB04, was investigated using SAXS. Thin films of each polymer were solution cast from a forty weight percent solution, and subsequently solvent annealed for a period of one month (see appendix, section 9.5). The SAXS profiles obtained for each polymer after annealing is illustrated in figure 3.6 and 3.7.

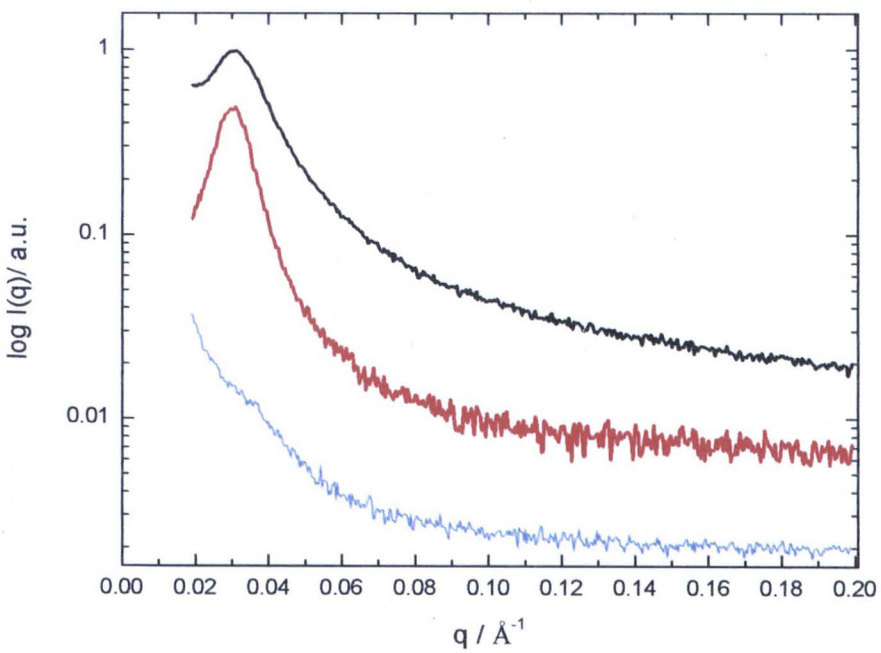

Figure 3.6: Plot of relative scattering intensity versus wave vector q for a PMMA-*block*-PMAA-*block*-PMMA (JSTB02) triblock (——) which was annealed in 85/15 methanol/acetone (——) and dioxane (——) for 1 month at 20°C.

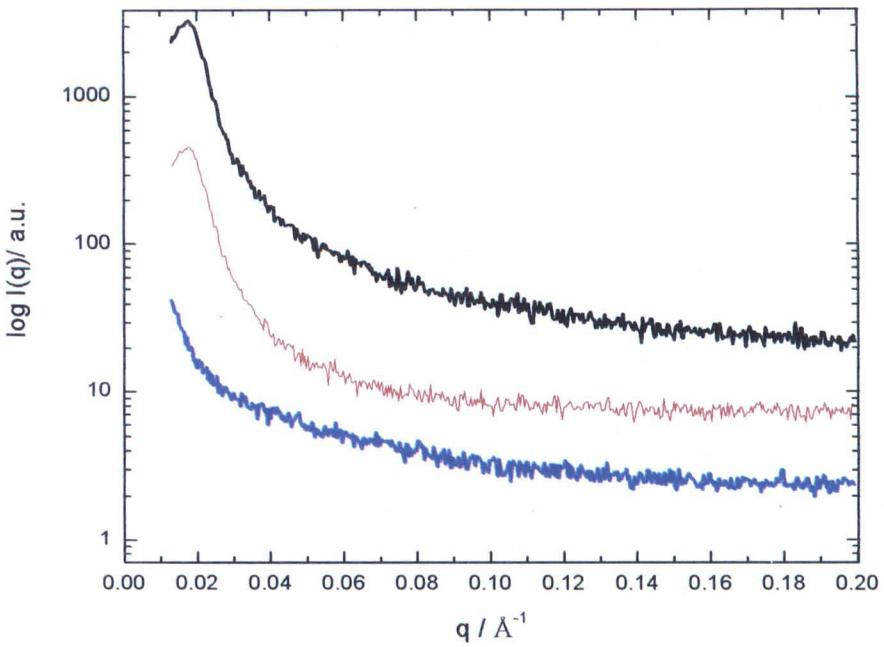

Figure 3.7: Plot of relative scattering intensity versus wave vector q for a PMMA-*block*-PMAA-*block*-PMMA (JSTB04) triblock (——) which was annealed in 85:15 v/v methanol/acetone (——) and dioxane (——) for 1 month at 20°C.

The selective co-solvent system was prepared at a ratio of 85:15 (v/v) to try and steer the polymer into a body centred cubic morphology.

Both polymers have no structure peak in the raw material. This is thermodynamically expected due to the high glass transition temperature of the component blocks, which are significantly higher than the temperature used in the annealing experiments.

The scattering profile of JSTB02 in figure 3.6 indicates that solvent annealing in dioxane produces a more defined structure peak than the same polymer annealed in 85:15 (v/v) methanol / acetone. This implies that the polymer chains annealed in dioxane are more ordered. This observation may be a result of the vapour pressure difference in the co-solvent system. Acetone has a vapour pressure of approximately 200mmHg at 20°C, compared to methanol which is 100mmHg at the same temperature. During the course of one month, it would not be unreasonable to assume

that the concentration of acetone in the co-solvent atmosphere will decrease at a faster rate than methanol. Therefore the co-solvent behaves more like a single solvent over time, and selectivity towards PMMA is lost. This will ultimately decrease the mobility of the PMMA chains reducing the ability for the polymer to reach its true equilibrium structure.

It is difficult to compare the effect of the two solvents on JSTB04 due to the structure peak being very close to the beam stop of the instrument which masks the required structural information.

The domain spacing of the two polymers was also determined by SAXS. The results are listed in table 3.2 which indicate that JSTB04 has a larger domain spacing compared to JSTB02. This observation is expected as the triblock has a higher molecular weight which will increase the distance between the PMMA domains.

Table 3.2: Summary of domain spacing for PMMA-*block*-PMAA-*block*-PMMA triblock copolymers determined by SAXS.

Copolymer I.D.	Domain Spacing q/ $Å^{-1}$	Domain Spacing nm
JSTB02	0.0304	20.6
JSTB04	0.0170	36.7

3.4 SYNTHESIS OF PMMA-*block*-PDEA-*block*-PMMA BLOCK COPOLYMERS

3.4.1 PMMA-*block*-PDEA-*block*-PMMA block copolymers via group transfer polymerisation

A series of PMMA-*block*-PDEA-*block*-PMMA triblock copolymers with a range of molecular weights were also targeted as discussed in section 3.1. The polymers were made by group transfer polymerisation (GTP) following a modified method described in the literature [4]. This technique is living and is known to produce polymers with controlled architectures and narrow PDI's. An introduction into GTP can be found in the appendix, section 9.1.2.

Synthesis of PMMA-*block*-PDEA-*block*-PMMA copolymers was accomplished using the bifunctional initiator 1,4-Bis (methoxytrimethylsiloxymethylene) cyclohexane (BMMC), as shown in figure 3.8.

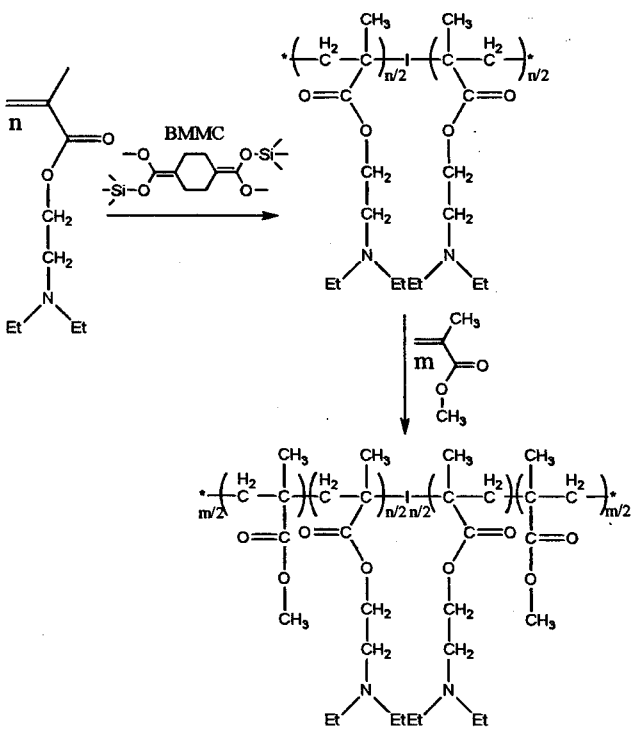

Figure 3.8: Synthesis of PMMA-*block*-PDEA-*block*-PMMA triblock copolymer via group transfer polymerisation. I represents the bifunctional initiator 1,4-Bis (methoxytrimethylsiloxymethylene) cyclohexane.

GPC traces of a number of PMMA-*block*-PDEA-*block*-PMMA copolymers synthesised using the bifunctional initiator are given below in figure 3.9.

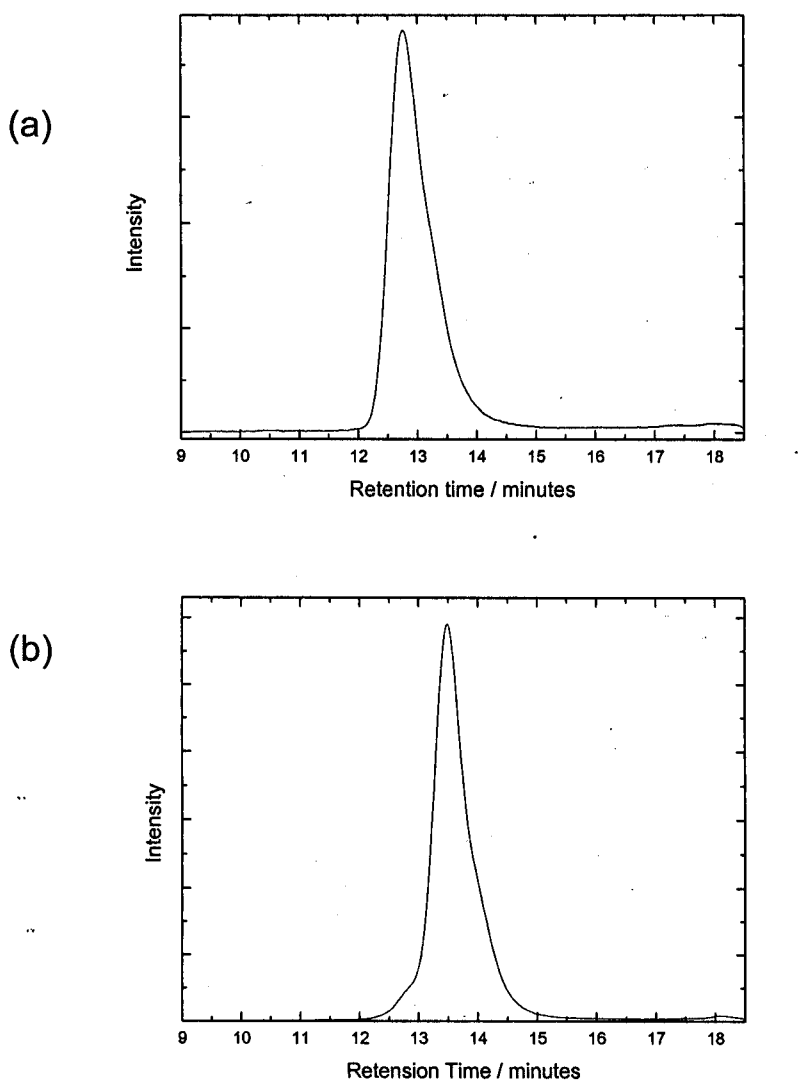

Figure 3.9: GPC chromatograms of (a) PMMA-*block*-PDEA-*block*-PMMA (JSPB05) and (b) PMMA-*block*-PDEA-*block*-PMMA (JSPB06) triblocks synthesised using the bifunctional initiator 1,4-Bis (methoxytrimethylsiloxymethylene) cyclohexane.

A summary detailing the molecular weight, volume fraction and M_w/ M_n of polymers synthesised using this method is given below in table 3.3.

Table 3.3: A summary of copolymer compositions, molecular weight and polydispersities of various PMMA-*block*-PDEA-*block*-PMMA triblock copolymers.

Copolymer I.D.	Theoretical MMA volume fraction	Experimental MMA volume fraction[a]	Theoretical M_n	Experimental M_n[b]	M_w/M_n
JSPB01	0.17	0.17	48242	226863 (triblock) 103552 (diblock)	1.05 (triblock) 1.19 (diblock)
JSPB03	0.17	0.17	48242	58941	1.38
JSPB04	0.17	0.17	69714	91941	1.41
JSPB05	0.17	0.17	71084	79582	1.22
JSPB06	0.17	0.17	96485	156394	1.22
JSPB07	0.16	0.16	48242	66796	1.30
JSPB08	0.12	0.12	48242	58400	1.22

a: As determined by ^{1}H NMR

b: As determined by GPC analysis (molecular weights calibrated against methyl methacrylate standards)

3.4.2 Calculating the composition of PMMA-*block*-PDEA-*block*-PMMA block copolymers by ^{1}H NMR

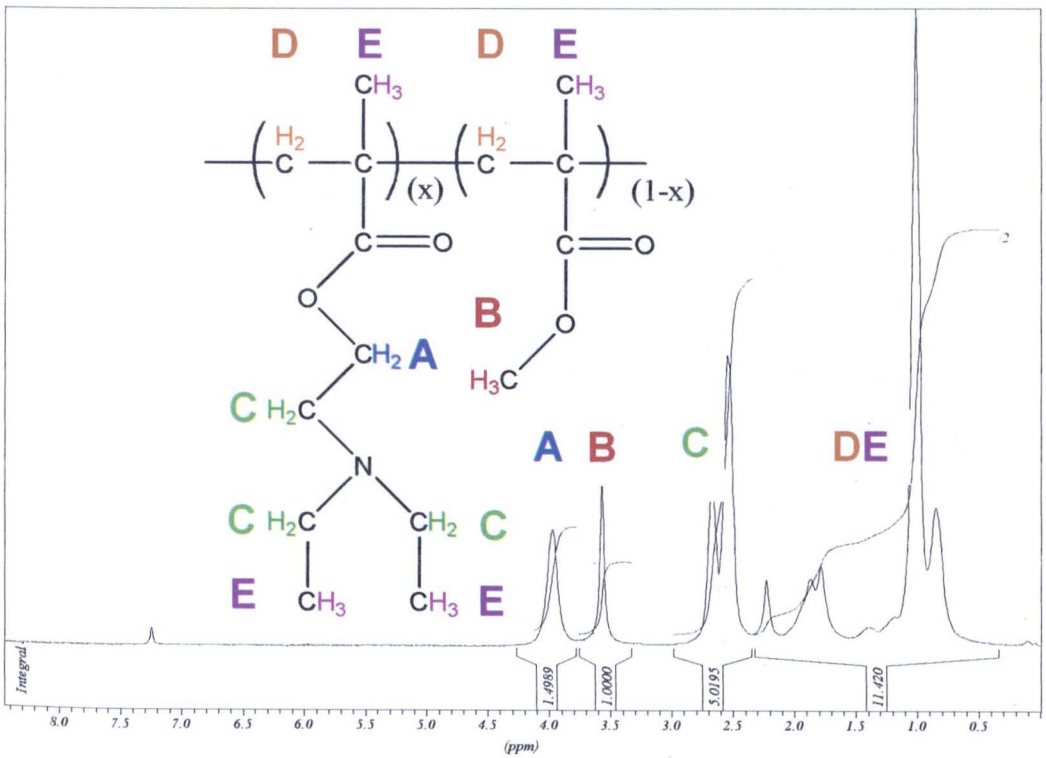

Figure 3.10: ^{1}H NMR Spectrum of PMMA-*block*-PDEA-*block*-PMMA.

For each PMMA-*block*-PDEA-*block*-PMMA polymer the volume fraction of DEA was calculated in the following way. ^{1}H NMR was used to determine the mole fraction of PDEA in the polymer. Using this value and previously reported densities [6] for the corresponding component homopolymers, the mole fraction was converted to a volume fraction. A sample calculation is detailed below.

As illustrated in the NMR spectrum given above in figure 3.10,

Mole fraction of DEA = x

Mole fraction of MMA = (1-x)

To calculate x, the mole fraction of DEA, it is necessary to find the ratio between the O-CH_2 protons (A) on the DEA repeat unit and the O-CH_3 (B) protons on

the methyl methacrylate repeat unit, as a function of x. For every repeat unit of DEA there are two equivalent O-CH_2 (A) protons. Therefore, A = 2x. For every repeat unit of MMA there are three O-CH_3 (B) protons. Therefore B = 3(1-x) = 3 -3x. The ratio of B to A is therefore:

$$\frac{B}{A} = \frac{3-3x}{2x} \tag{3.7}$$

$$x = \frac{3}{2(B/A)+3} \tag{3.8}$$

From the ^{1}H NMR spectrum given in figure 3.10 the ratio (B/A) is 0.667. Substituting this value into equation 3.8 gives a value for the DEA mole fraction of 0.70. Therefore the triblock has the molar composition 0.15-0.70-0.15. The corresponding volume fraction of each subunit is calculated by first multiplying the mole fraction by the molar mass to give a mass fraction, and then dividing this value by its density to give a volume. The volume of each component in the block copolymer is then divided by the total volume to give the volume fraction. An example is given below,

$$\text{Volume of DEA} = \frac{0.7 \times 185.26}{1.035} = 125.30 \text{ cm}^3 \tag{3.9}$$

$$\text{Volume of MMA} = \frac{0.3 \times 100.12}{1.185} = 25.35 \text{ cm}^3 \tag{3.10}$$

$$\text{MMA volume fraction} = \frac{125.30}{25.35 + 125.30} = 0.83 \tag{3.11}$$

The PMMA-*block*-PDEA-*block*-PMMA triblock therefore has the following composition, 0.085:0.83:0.085.

3.4.3 Optimizing conditions for the synthesis of PMMA-*block*-PDEA-*block*-PMMA block copolymers

Early attempts to synthesise PMMA-*block*-PDEA-*block*-PMMA polymers (see table 3.3, JSPB01 as an example) following the published method [4] resulted in the formation of triblock copolymers with diblock contamination. An investigation to determine the origin of this indicated that monomer impurity was the cause.

In the published procedure the monomers were dried over CaH_2 without any further purification. It was found that an additional step was required to clean the monomers. In addition to drying over CaH_2 the monomers were passed through a basic alumina column. It was found that polymers synthesised using this modified method were monodisperse in all cases.

Due to the group transfer polymerisation reaction being exothermic its progress can easily be monitored. During the course of all GTP polymerisations the reaction temperature was recorded, as illustrated in figure 3.11.

During polymerisation of the first monomer there was a gradual increase in the temperature of the reaction mixture. Once the initial exotherm abated (marked by a reduction in the reaction temperature), the second monomer was introduced immediately. Following the reaction in this manner allowed one to determine precisely when to add the second monomer, thus reducing the chances of unwanted secondary chain coupling reactions.

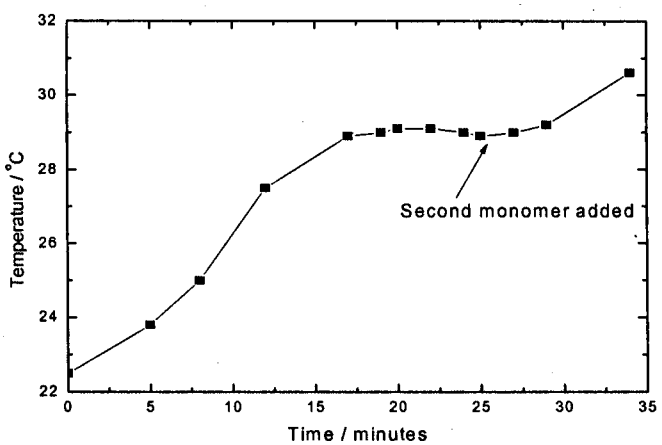

Figure 3.11: Typical reaction exotherm recorded during the synthesis of PMMA-*block*-PDEA-*block*-PMMA triblock copolymers. Time at which the second monomer was introduced into the reaction is indicated on the figure.

3.5 ANNEALING OF PMMA-*block*-PDEA-*block*-PMMA TRIBLOCK COPOLYMERS

3.5.1 Network formation

As previously discussed in section 3.1.3 and 3.3.1 the specially designed PMMA-*block*-PDEA-*block*-PMMA triblock copolymers need to be suitably processed and annealed.

3.5.2 Annealing Conditions

Annealing of PMMA-*block*-PDEA-*block*-PMMA triblock copolymers can be achieved thermally or by using a solvent system as discussed in section 3.1.3. The glass transition temperatures of the PDEA and PMMA blocks are 16°C and 120°C respectively [27]. Due to the low glass transition temperature of the PDEA block annealing is accessible using both methods. However, in provisional thermal annealing studies it was found that elevated temperatures caused a distinct colour change in the polymer films. The film changed from being initially transparent to yellow/green. The same colour change also occurred when polymer dissolved in annealing solvent was left for extended periods. These polymers were no longer soluble suggesting cross linking had occurred. As a result of this all PMMA-*block*-PDEA-*block*-PMMA polymers used for annealing experiments were solvent annealed. This was achieved using THF, which is a good solvent for both PMMA and PDEA homopolymer [27].

3.5.3 Selectivity of THF solvent on the self assembly of PMMA-*block*-PMAA-*block*-PMMA triblock copolymer thin films

The effect of the thermodynamic selectivity of THF on the self assembly of a range of PMMA-*block*-PDEA-*block*-PMMA triblock copolymers was investigated using SAXS. Thin films of each polymer were solution cast from a 40 wt % solution in THF, and subsequently solvent annealed for various amounts of time (see appendix, section

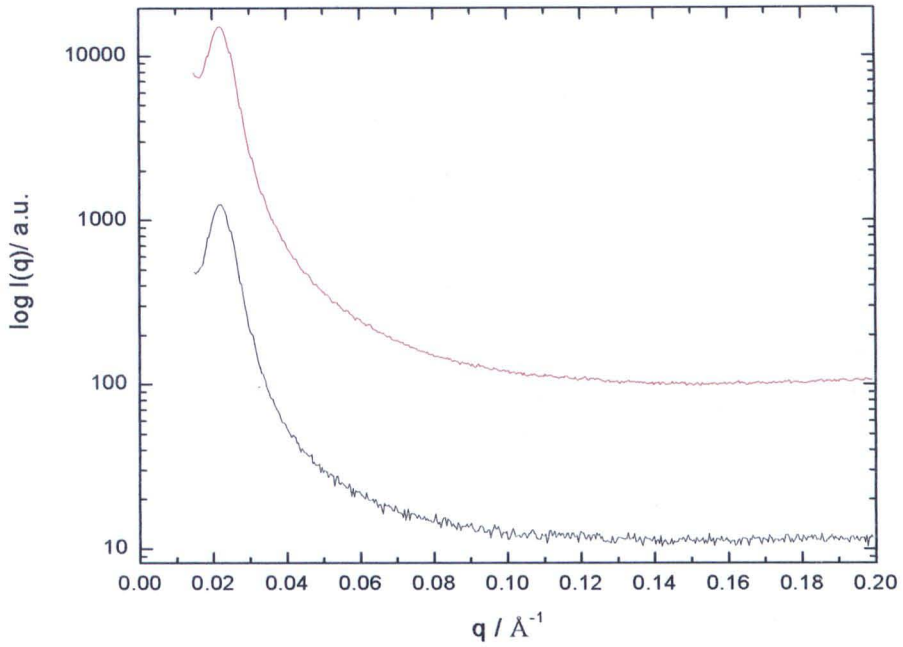

Figure 3.12: Plot of scattering intensity versus wave vector q for an unannealed PMMA-*block*-PDEA-*block*-PMMA (JSPB01) triblock (——) and the same polymer annealed in THF for 1 week (——) at 20°C.

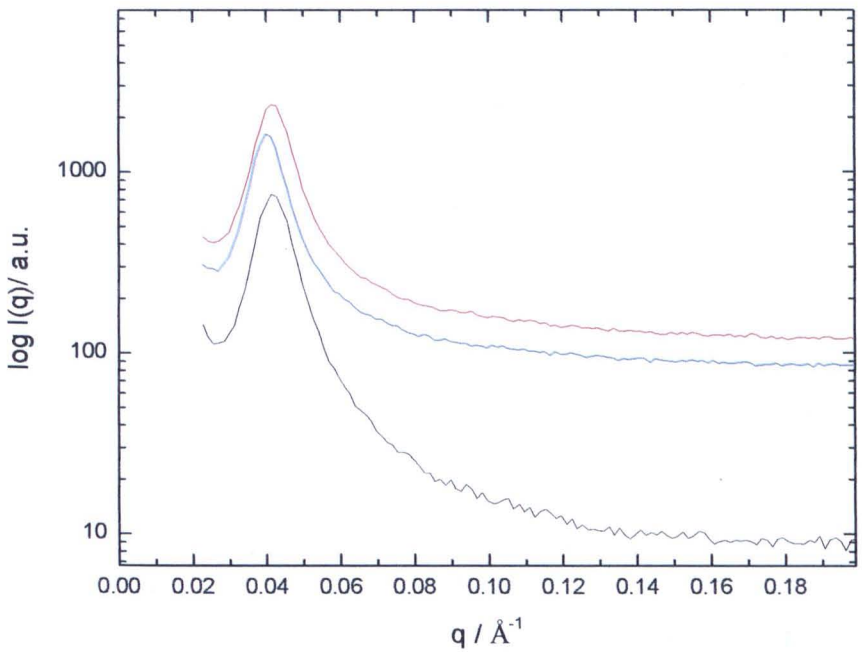

Figure 3.13: Plot of scattering intensity versus wave vector q for an unannealed PMMA-*block*-PDEA-*block*-PMMA (JSPB03) triblock (——) and the same polymer annealed in THF for 4 weeks (——), and 8 weeks (——) at 20°C.

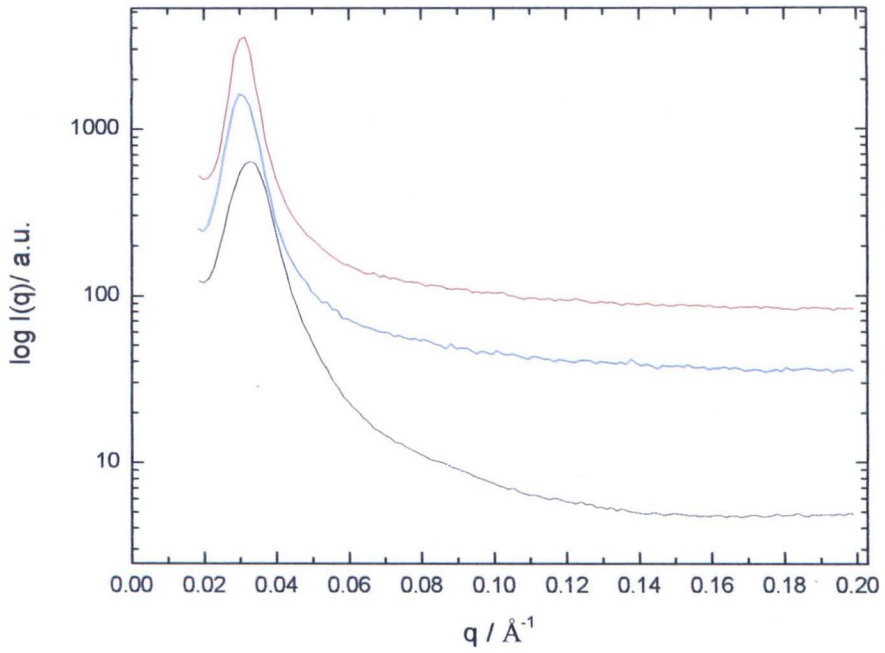

Figure 3.14: Plot of scattering intensity versus wave vector q for an unannealed PMMA-*block*-PDEA-*block*-PMMA (JSPB05) triblock (——) and the same polymer annealed in THF for 4 weeks (——), and 8 weeks (——) at 20°C.

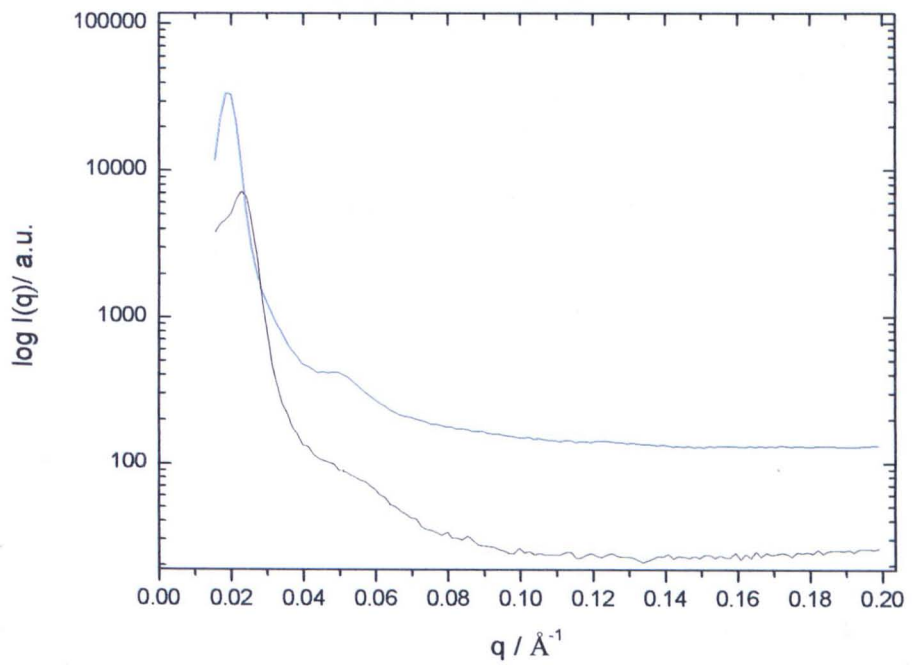

Figure 3.15: Plot of scattering intensity versus wave vector q for an unannealed PMMA-*block*-PDEA-*block*-PMMA (JSPB06) triblock (——) and the same polymer annealed in THF for 1 week (——) at 20°C.

9.5). The SAXS profiles obtained for a selection of the polymers after annealing are illustrated in figures 3.12-3.15.

The SAXS profiles of the neat un-annealed copolymers illustrated in figures 3.12-3.15 all show a pronounced structure peak. This initial ordering which is present without specific annealing is likely a result of the way in which the polymers are prepared. Polymer synthesis was carried out in THF solvent, and after the polymerisation reached completion the material was recovered by rotary evaporation of solvent. It is therefore possible that the slow removal of solvent by rotary evaporation induced microphase separation in the polymers.

For several of the annealed polymers the peak width at half height of the structure factor was measured during the course of solvent annealing. The results are shown in table 3.4. Using the peak width of the raw polymer as a reference, the percentage change in the peak width was determined for each annealing time, as shown in figure 3.16. All of the polymers in table 3.4 show a reduction in peak width with time, the only exception to this is JSPB03 which appears to increase after 4 weeks. However, if one compares the raw peak width to the peak width at 8 weeks, all polymers show a narrowing. This general reduction is anticipated as polymers which have had longer periods of solvent annealing have had more time to reach their lowest energy equilibrium structure. The reduction in peak width becomes less pronounced with longer annealing times, an indication the polymer is beginning to reach its final equilibrium structure. The greatest reduction in peak width is observed for JSPB05, which has reduced by forty percent as compared to the raw polymer.

Table 3.4: Peak width half maximum characteristics for PMMA-*b*-PDEA-*b*-PMMA triblock copolymers.

Copolymer I.D.	PDI	Peak width at half maximum / q $Å^{-1}$		
		0 Weeks	**4 weeks**	**8 weeks**
JSPB03	1.38	0.0105	0.0114	0.0099
JSPB05	1.22	0.0119	0.0090	0.0071
JSPB07	1.30	0.0156	n/a	0.0107
JSPB08	1.22	0.0250	0.0206	0.0185

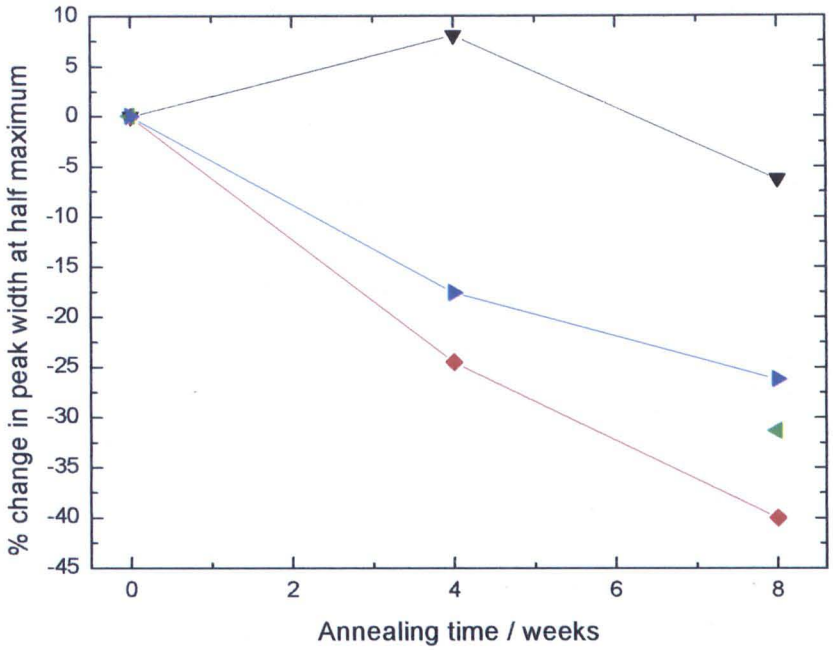

Figure 3.16: Percentage change in the peak width at half height for B JSPB03 Λ JSPB05 Ω JSPB07 and β JSPB08 PMMA-*block*-PDEA-*block*-PMMA triblock copolymers annealed in THF for varying amounts of time.

Table 3.4 also lists the polydispersity index (PDI) for each polymer. It may be expected that polymers with a narrower PDI have a smaller width at half height, given that more of the polymer chains have a similar length. However no correlation was found. Additionally, none of the plots in figure 3.16 have a zero gradient suggesting that the equilibrium structure was not reached even after 8 weeks of annealing.

SAXS spectra of the majority of annealed PMMA-*block*-PDEA-*block*-PMMA polymers exhibited the first order Bragg peak only, which prevents a proper identification of the phases by stand crystallographic arguments. Only JSPB06 had indication of any further ordering beyond a structure factor. In the diffuse part of scattering data where the main contribution of scattering comes from the form factor component (see section 9.4.1), there is a small anomaly present at 0.05 $Å^{-1}$. Even if this peak was attributed to a form factor, the lack of any further oscillations make it unfeasible to accurately comment further on the molecular structure of this polymer.

It is also worth emphasising that the structure peak in annealed JSPB06 has shifted from 0.0230 $Å^{-1}$ in the unprocessed material to 0.0192 $Å^{-1}$ after one week of

annealing, an increase of approximately 5nm or 18.5 percent. In addition the shoulder at higher q is much more defined in the annealed material.

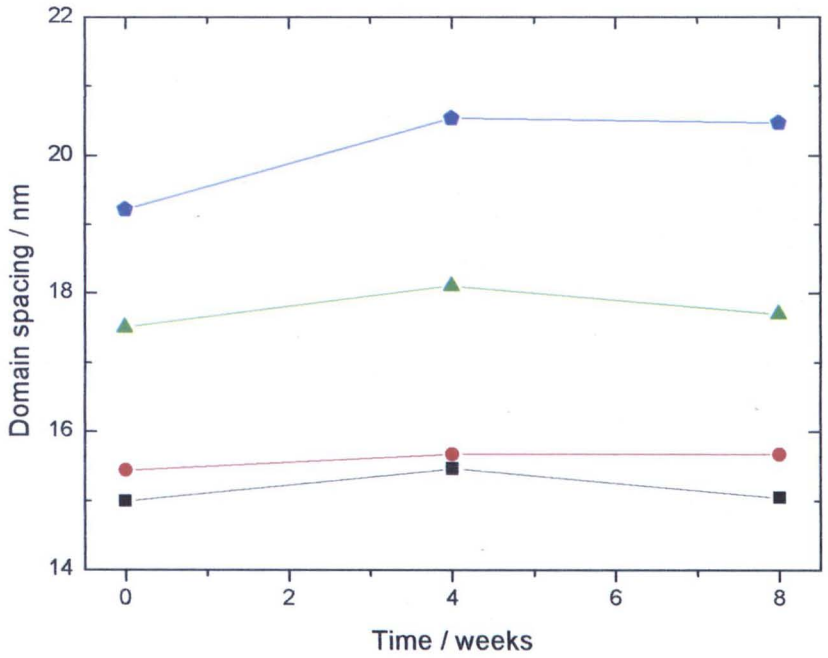

Figure 3.17: Change in the domain spacing for ■ JSPB03 ● JSPB05 ▲ JSPB07 and ⬟ JSPB08 PMMA-*block*-PDEA-*block*-PMMA triblock copolymers annealed in THF for varying amounts of time.

The change in domain spacing with annealing time was also evaluated for the other PMMA-*block*-PDEA-*block*-PMMA block copolymers, as illustrated in figure 3.17.

After 4 weeks of solvent annealing all of the polymers investigated showed an increase in domain spacing. The largest increase of 6.8% was observed for JSPB08. This is, however, almost a factor of three times smaller when compared to JSPB06.

One possible explanation for the large change in domain spacing of JSPB06 relates to the molecular weight of the material. JSPB06 has a molecular weight over twice that of the other polymers (156k vs 58-80k). As a result of this the polymer has a larger number of chain entanglements.

It would appear from figure 3.17 that the lower molecular weight polymers were already close to equilibrium in their raw state, therefore only showing a small change in domain spacing upon further annealing. The low glass transition temperature of PDEA,

and fewer entanglements in lower molecular weight polymers would support this conclusion. However, JSPB06 being a higher molecular weight polymer has a greater thermodynamic barrier for phase separation. The results indicate that JSPB06 was not phase separated as fully compared to the other polymers in the raw state. As a result when JSPB06 was further annealed the polymer chains stretched to reach their optimum configuration which explains the large increase in domain spacing not seen in the other polymers. Libera and Kim have also reported an increase in the domain spacing of a Polystyrene–Polybutadiene–Polystyrene (SBS) triblock copolymer during the course of solvent annealing [28], as have Shibayama *et al* [29] on a solvated lamellar forming diblock. It is also evident that in several of the polymers there is a decrease in the domain spacing after 8 weeks of annealing. Hashimoto *et al* have observed a similar trend [30]. During solvent annealing of PS-PI block copolymers they found the domain increased, this is explained in terms of a thermodynamic argument (i.e domains increase to lower surface to volume ratio). With further evaporation of solvent they observed a decrease in the expansion ratio, and this was observed due to kinetic constrains. At a critical concentration the polymer mobility is too low to enable adjustments to the bulk morphology, and the domain decreases due to deswelling.

3.6 DOMAIN SPACING VS MOLECULAR WEIGHT

Table 3.5 lists the domain spacing calculated by SAXS for a selection of the PMMA-*block*-PDEA-*block*-PMMA triblock copolymers. It is evident that the domain spacing of the polymers increases with increasing molecular weight. Figure 3.18 shows a double-logarithmic plot of the experimental domain spacing vs the number-averaged molecular weights, *Mn* of the triblock copolymers.

In a similar plot assuming an unperturbed (Gaussian) polymer chain one would expect to have an exponent of 0.5, however a slightly higher value is observed in block copolymers. This is due to chain constraint, as the polymer chains must minimise both interfacial and chain deformation. To achieve this the polymer chains stretch in the direction normal to the intermaterial dividing surface, thus the domain size would be expected to scale as $N^{2/3}$ [31].

It is obvious from figure 3.18 that the domain spacing systematically increases with total molecular weight. The best fit line in Figure 3.18 has a slope of 0.73. This systematic increase in domain spacing with molecular weight is consistent with previous findings [32]. Hashimoto and Kawai were one of the first groups to use SAXS to investigate the relationship between domain spacing and molecular weight [33]. They investigated the relationship using a series of symmetric lamellar polystyrene/ polyisoprene (PS-PI) copolymers. In a double logarithmic plot similar to figure 3.18 they recorded a slope of 2/3 to 4/5 [34]. Our findings are consistent with this result, and scale as Domain spacing $\propto Mn^{0.73}$.

Table 3.5: Domain spacing and molecular weight characteristics for PMMA-*block*-PDEA-*block*-PMMA triblock copolymers.

Copolymer I.D.	Domain Spacing $Å^{-1}$	Domain Spacing nm	Molecular weight $gmol^{-1}$
JSPB03	0.0418	15.0	58941
JSPB05	0.0328	19.2	79582
JSPB06	0.0192	32.7	159394
JSPB07	0.0357	17.5	66796
JSPB08	0.0401	15.6	58400
J1[a]	0.0237	26.4	119869

a: donated by Dr Paul Topham

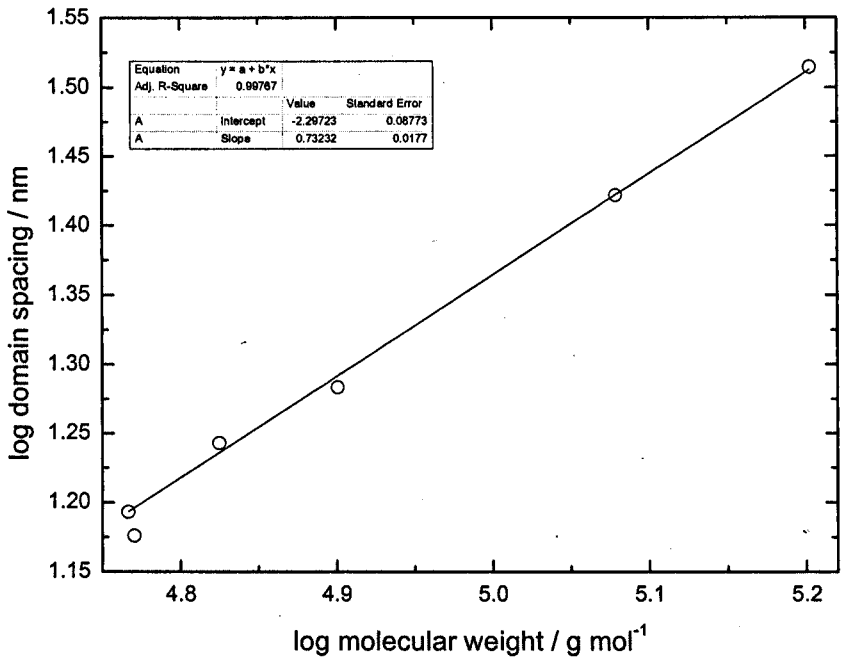

Figure 3.18 – log-log plot of molecular weight vs domain spacing for a series of PMMA-*block*-PDEA-*block*-PMMA copolymers. The following polymers were used in order of increasing molecular weight, JSPB08, JSPB03, JSPB07, JSPB05, J1*, JSPB06. *donated by Dr Paul Topham.

3.7 SURFACE MORPHOLOGY OF PMMA-*block*-PDEA-*block*-PMMA BLOCK COPOLYMER FILMS

All of the SAXS profiles presented in section 3.5.3 (with the possible exception of JSPB06) show no evidence of a form factor or further order scattering peaks. AFM was used to further investigate the microphase morphology of the block copolymers. Thin films (~100 nm) of PMMA-*block*-PDEA-*block*-PMMA triblock copolymer were spin coated (2000rpm) onto silicon wafers from a THF solution (~5.0% w/w). The triblock copolymer films were subsequently solvent annealed using THF for one week.

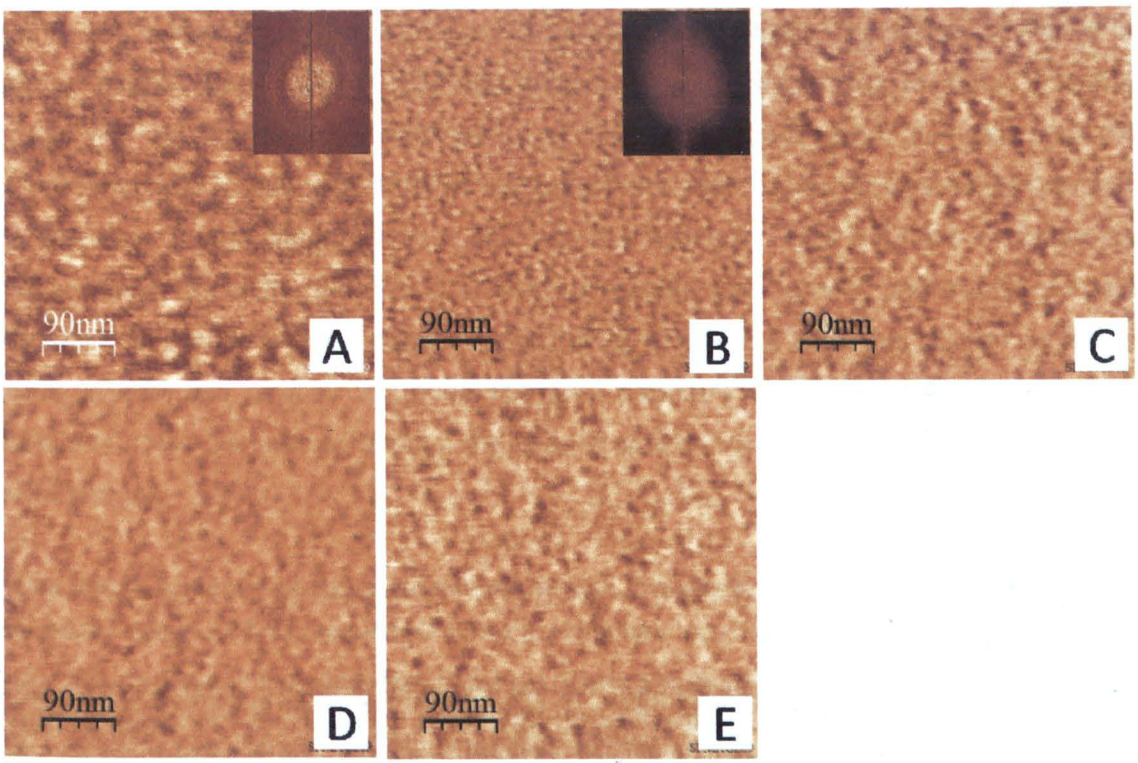

Figure 3.19: AFM phase images of PMMA-*block*-PDEA-*block*-PMMA triblock copolymer, (A) JSPB03, (B) JSPB05, (C) JSPB06, (D) JSPB07, (E) JSPB08.

The composition of each polymer is listed in table 3.6. Based on the 17 percent volume fraction of PMMA in JSPB03, JSPB05 and JSPB06 it was anticipated these polymers would phase separate with a spherical morphology. As JSPB07 has a very similar volume fraction it is also anticipated to have the same structure. JSPB08 was deliberately synthesised to have a lower volume fraction of PMMA (f_{PMMA} 0.12) primarily to investigate if this had any effect on phase morphology.

The phase images in figure 3.19 show patterns of both dark and light objects. The light areas correspond to the higher modulus PMMA component, and the darker areas are typical of softer material, in this example PDEA. AFM analysis of JSPB05, JSPB06, JSPB07 and JSPB08 all show some evidence of microphase separation. The phase image of JSPB03 shows the greatest degree of microphase separation, with perhaps a small indication of liquid like spherical domains. A two dimensional Fourier transform of this phase image reveals a long order domain spacing of 15.0 nm. This observation is consistent with SAXS data obtained on the same polymer. As all the polymers in this study show a pronounced structure peak in their SAXS profile it is

somewhat surprising that there is not a more defined phase separation in the AFM phase image, especially in JSPB06. However, it is important to note that the preparation method used for AFM sampling differs significantly from bulk gels used for SAXS analysis. In the case of AFM, samples were spin coated from a dilute solution, as opposed to high weight percent (40%) in the bulk gels. This will have an influence on the assembly of the gel during solvent annealing. Additionally, preferential surface interactions between the different components of the gel and the silicon substrate (SiO_X layers) will directly influence the final structure of the gel [35]. All of these variables could be used to explain the lack of well defined order in the majority of the AFM images.

Table 3.6: A summary of copolymer compositions, molecular weight and polydispersities of the PMMA-*block*-PDEA-*block*-PMMA block copolymers investigated by AFM

Copolymer I.D.	DEA volume fraction	Experimental M_n[b]	M_w/M_n
JSPB03	0.17	58941	1.38
JSPB05	0.17	79582	1.22
JSPB06	0.17	156392	1.22
JSPB07	0.16	66796	1.30
JSPB08	0.12	58400	1.22

3.8 STABILITY TESTING IN SOLUTION

3.8.1 Stability testing of PMMA-*block*-PMAA-*block*-PMMA triblock copolymers

The polyacid block copolymers synthesised in section 3.2 were subjected to testing to evaluate their suitability as chemical actuators.

JSTB02 and JSTB04 both contain a poly(methacrylic acid) midblock which expands when it is placed in a solution at a pH above its apparent pK_a. The pK_a is molecular weight dependant but can be estimated at 5.5 [21]. To test robustness 110 micron thick films of PMMA-*block*-PMAA-*block*-PMMA, which had been solvent annealed for 1 month (phase separation checked by SAXS) were placed into a solution at pH 8 (distilled water which had been adjusted to pH 8 by addition of a small amount of 1M NaOH).

At this pH the triblock is anticipated to expand. However, in actual fact both polymers placed in this solution broke into many small pieces after only a few minutes. This was of course a great disappointment and suggested a lack of structural integrity.

This lack of structural integrity is most likely a result of the high diblock content in these polymers. JSTB02 and JSTB04 contain 35% and 58% diblock respectively. The structural stability of the triblock copolymer results from bridging of PMAA domains between PMMA hydrophobic blocks. The high diblock contaminant present in these samples provides no structural integrity to the system. Its presence simply reduces the number of bridging domains in the polymer network. Any diblock will simply sit between the PMMA domains and not participate in network formation.

3.8.2 Stability testing of PMMA-*block*-PDEA-*block*-PMMA triblock copolymers

The robustness of polybase triblocks was tested in a similar manner to the polyacid. In this case, 110 micron thick films which had been solvent annealed for one week were immersed in simple HCl mineral acid solution at pH 3.6. This pH is below the pK_a of the polymer, and as this is a polybase as opposed to a polyacid the polymer is anticipated to expand. The results of the robustness testing are shown in figure 3.20. The expansion ratio in the graph was calculated according to equation 3.12,

$$ER = \frac{M_s - M_d}{M_d} \tag{3.12}$$

where M_s and M_d are the mass of the swollen and dry gel respectively.

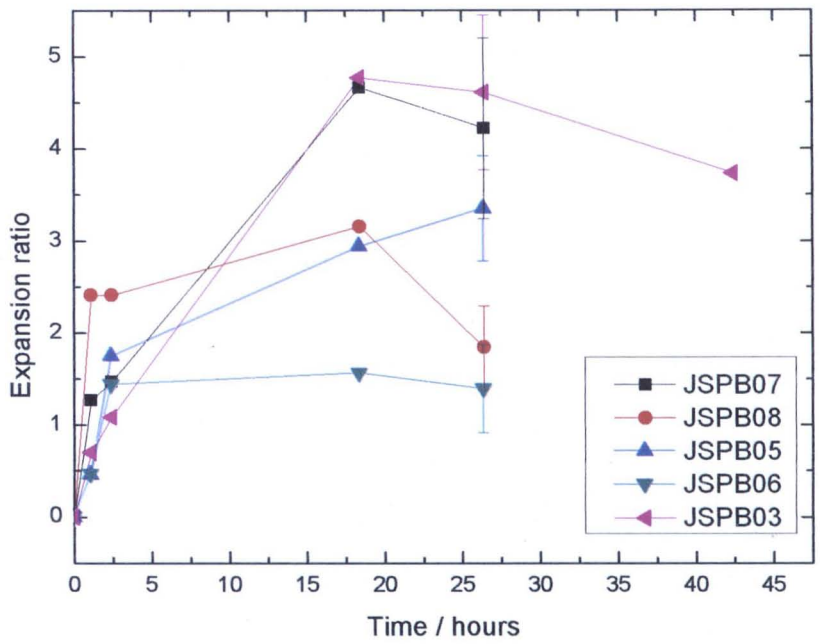

Figure 3.20: Change in the gravimetric expansion ratio as a function of time for a series of 110 micron thick films of annealed PMMA-*block*-PDEA-*block*-PMMA triblock copolymers measured in pH 3.5 HCl mineral acid.

The mass of the polymer was measured at specific time intervals. The final measurement was taken after the polymer had been immersed in solution for 45 hours. It is evident from figure 3.20 that JSPB03 had the largest expansion ratio, but more significantly it was the only polymer to remain mostly intact over a period of 45 hours. The data points for the other polymers at 45 hours are not included, and this is simply because they had broken up into many pieces and could no longer be measured. Comparison of the expansion ratio after 26 hrs indicates that JSPB03 and JSPB07 have similar levels of expansion at around 4.6. This is followed by JSPB05 at 3.3, and JSPB06 at 1.4. Assuming the polymers have reached equilibrium after 26 hrs, one may hypothesise that the higher molecular weight polymer should have the highest expansion ratio. To test this hypothesis the molecular weight of JSPB03, JSPB05, JSPB07 and JSPB06 has been plotted against their expansion ratio determined after 26 hours, as shown in figure 3.21. JSPB08 has not been included as this polymer had begun to break up.

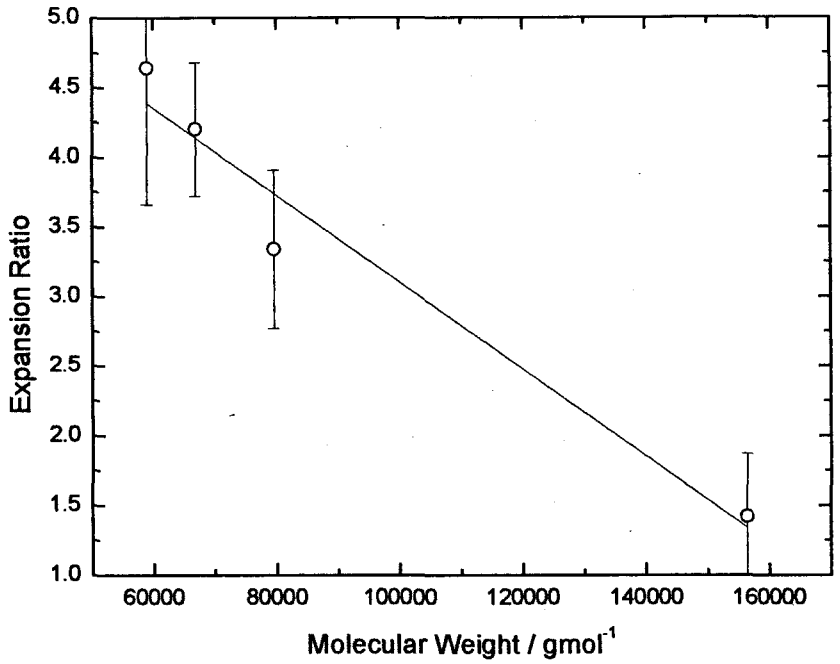

Figure 3.21: Change in the gravimetric expansion ratio as function of molecular weight for a series of PMMA-*block*-PDEA-*block*-PMMA block copolymers measured at pH 3.6 after 26hrs.

Somewhat surprisingly it would appear that the expansion ratio of the polymer decreases as the molecular weight is increased. There are a number of possible explanations for this. The expansion ratio measured after 26hrs is not a true equilibrium. Another possible explanation is the higher molecular weight polymer is more entangled and the osmotic pressure of the solution is not able to overcome the network elastic restoring force as easily, thus reducing the calculated expansion ratio. As this is a gravimetric measurement it is most likely that the expansion ratio at 26hrs is largely influenced by loss of materials and is not really a true measure. This highlights one of the issues associated with gravimetric analysis in that you are not measuring a molecular response. Further experiments will be performed in chapter four to investigate the influence of molecular weight on swelling equilibrium using SAXS.

3.9 CONCLUSION

Anionic polymerisation has been used to synthesise PMMA-*block*-PMAA-*block*-PMMA triblock copolymers. The polymers were synthesized with high control of molecular weight and narrow PDI's. In all cases, however, the polymers had bimodal distributions.

The specially designed polymers were annealed in a number of solvents, and phase separation was confirmed using SAXS. Initial stability testing of these polymers indicated that they were mechanically weak. Phase separated annealed thin films simply fell to pieces when placed in a solution above their pK_a. The mechanism of mechanical failure is most likely caused by the high content diblock content. Due to the failure of these gels synthetic efforts were direct towards the synthesis of PMMA-*block*-PDEA-*block*-PMMA triblock copolymers.

Synthesis of PMMA-*block*-PDEA-*block*-PMMA triblock copolymers was achieved using group transfer polymerisation. A range of monodisperse polymers were synthesised with relatively narrow PDI's. Annealing studies were conducted on the raw polymers using SAXS. Monitoring changes in the structure peak using SAXS gave an insight into the thermodynamics of phase separation. Initial stability tests on annealed thin films indicated the polymers to be mechanically robust, significantly more so than PMMA-*block*-PMAA-*block*-PMMA triblock copolymers.

The most robust PMMA-*block*-PDEA-*block*-PMMA triblock copolymer was JSPB03. This incidentally also had the largest swelling transition. SAXS profiles of JSPB03 had a defined structure peak, and AFM confirmed the polymer had a long order domain spacing of 15nm.

Further studies on the "static" pH response of JSPB03 are described in chapter 4.

REFERENCES

1. Li, M.-H., P. Keller, J. Yang, and A. Albouy, Advanced Materials, 2004. **16**(21): p. 1922 - 1925.
2. Nykänen, A., M. Nuopponen, A. Laukkanen, S.-P. Hirvonen, M. Rytelä, O. Turunen, H. Tenhu, R. Mezzenga, O. Ikkala, and J. Ruokolainen, Macromolecules, 2007. **40**(16): p. 5827–5834.
3. Guice, K.B., S.R. Marrou, S.R. Gondi, B.S. Sumerlin, and Y.-L. Loo, Macromolecules, 2008. **41**(12): p. 4390–4397.
4. Topham, P.D., J.R. Howse, O.O. Mykhaylyk, S.P. Armes, R.A.L. Jones, and A.J. Ryan, Macromolecules, 2006. **39**(16): p. 5573–5576.
5. Borsali, R. and R. Pecora, *Soft-Matter Characterization*. 1 ed. 2008: Springer. 160.
6. Topham, P.D., *Study of pH-Responsive Polymer Systems for use in Molecular Machines*, in *Chemistry*. 2005, Sheffield: Sheffield.
7. Ryan, A.J., C.J. Crook, J.R. Howse, P. Topham, R.A.L. Jones, M. Geoghegan, A.J.P.R.-P. rez, S.J. Martin, A. Cadby, A. Menelle, J.R.P. Webster, A.J. Gleesone, and W. Bras, Faraday Discuss, 2005. **128**: p. 55-74.
8. Bates, F.S. and G.H. Fredrickson, Annual Review of Physical Chemistry, 1990. **41**: p. 525-57.
9. Hamley, I.W., *Developments in Block Copolymer Science and Technology*, ed. I.W. Hamley. 2004, UK: John Wiley and Sons Ltd. 1.
10. Hamley, I.W., *Introduction to soft matter*. 1st ed. 2000, New York: John Wiley and Sons. 118-121.
11. Bucknall, D.G. and H.L. Anderson, Science, 2003. **302**(5652): p. 1904 - 1905.
12. Hamley, I.W., *Block Copolymers in Solution: Fundamentals and Applications*. 2005, New York: Wiley.
13. Wilkinson, N. and A.J. Ryan, *Polymer Processing and Structure Development*. 1 ed, ed. N. Wilkinson and A.J. Ryan. 1998, The Netherlands: Kluwer Academic Publishers. 301.
14. Haward, R.N. and R.J. Young, *The Physics of Glassy Polymers*. 2 ed, ed. R.N. Haward and R.J. Young. 1997, London: Chapman and Hall. 453.
15. Drolet, F. and G.H. Fredrickson, Physical review letters, 1999. **83**(21).
16. Bhowmick, A.K., *Current Topics in Elastomers Research*, ed. A.K. Bhowmick. 2008, Florida: CRC Press. 132.
17. Hanley, K.J., T.P. Lodge, and C.-I. Huang, Macromolecules, 2000. **33**(16): p. 5918-5931.
18. Abetz, V., *Block copolymers, Volume*, ed. V. Abetz. 2005, New York: Springer.
19. Matsen, M.W. and R.B. Thompson, The Journal of Chemical Physics, 1999. **111**(15): p. 7139–7146.
20. Esquenet, C., P. Terech, F. Boue, and E. Buhler, Langmuir, 2004. **20**(9): p. 3583-3592.
21. Howse, J.R., P. Topham, C.J. Crook, A.J. Gleeson, W. Bras, R.A.L. Jones, and A.J. Ryan, Nano Letters, 2006. **6**(1): p. 73-77.
22. Yao, J., P. Ravi, K.C. Tam, and L.H. Gan, Polymer, 2004. **45**(8): p. 2781-2791.
23. Tong, J.D., G. Moineau, P. Leclère, J.L. Brédas, R. Lazzaroni, and R. Jérôme, Macromolecules, 2000. **33**(2): p. 470–479.

24. Odian, G., *Principles of Polymerization* Third Edition ed. 1991, New York: John Wiley and Sons, Inc. 389.
25. Allen, R.D., T.E. Long, and J.E. McGrath, Polymer Bulletin (Berlin, Germany), 1986. **15**(2): p. 127-34.
26. C. M. Fernyhough, R.N.Y., and R. D. Tack, Macromolecules 1999. **32**(18): p. 5760-5764.
27. Brandrup, J., E.H. Immergut, and E.A. Grulke, *Polymer Handbook*. Fourth edition ed. 1999, New York: John Wiley and Sons.
28. Libera, G.K.a.M., Macromolecules, 1998. **31**(8): p. 2569–2577.
29. Shibayama, M., Takeji Hashimoto, and H. Kawai, Macromolecules, 1982. **16**: p. 1434-1443.
30. Hashimoto, T., M. Shibayama, and H. Kawai, Macromolecules, 1983. **16**: p. 1093-1101.
31. Bates, F.S. and G.H. Fredrickson, Annu. Rev. Phys. Chem, 1990. **41**.
32. Cheremisinoff, N.P., *Handbook of Polymer Science and Technology*. 1989: Taylor & Francis Ltd. 9.
33. Hashimoto, T., M. Shibayama, and H. Kawai, Macromolecules, 1980. **13**: p. 1237.
34. Takeshita, H., Y.-J. Gao, T. Natsui, E. Rodriguez, M. Miya, K. Takenak, and T. Shiomi, Polymer 2007. **48**: p. 7660.
35. Limary, R. and P.F. Green, Mat. Res. Soc. Symp, 2000. **629**: p. 2.8.1.

Chapter 4
Quantifying "static" hydrogel pH response using SAXS

4.1 INTRODUCTION

Factors affecting hydrogel behaviour in solution have been extensively studied using randomly cross-linked polymer networks [1, 2]. However, the macroscopic response measured (i.e. gravimetric, volumetric) of these systems is often far removed from the behaviour of the individual polymer chains causing the measured effect. This is due to the random distribution of chemical crosslinks that hold the gel together, which can lead to localised stresses and anisotropic expansion. This can manifest itself in mechanical failure of the gel, but more importantly it is known to have a direct effect on the measured swelling characteristics. For example, the in-homogeneous distribution of cross links in cured epoxy resins resulted in an increase in their solvent uptake by a factor of
]2 [3]. Therefore, when making comparative studies on the response of hydrogels control is needed on the cross-link distribution.

In an attempt to reduce network heterogeneities, and develop a better understanding of hydrogel behaviour at the molecular level a microphase separated A-B-A type polybase triblock copolymer (JSPB03, chapter 3) comprising of glassy self-assembled domains of poly(methyl methacrylate) (PMMA); with each domain separated by (and covalently bound to) a series of single chains of poly(2-(diethylamino)ethyl methacrylate) (PDEA) is investigated in this chapter. The chemical response of the hydrogel is governed by the PDEA chains. Structural integrity of the network during expansion is provided by the glassy PMMA physical crosslinks as discussed in chapter 3. The crosslinks are evenly distributed due to thermodynamic equilibrium achieved during self-assembly. The PMMA crosslinks also act as "markers", commonly referred to as hydrophobic stickers [4], providing the gel with an

electron density contrast, allowing structural analysis to be performed at the molecular level using X-ray scattering techniques.

Using simple buffers and mineral acids in conjunction with SAXS we will correlate the molecular response of this polymer to the single species in solution, while also evaluating the effectiveness of SAXS as a viable technique in itself for this purpose.

4.1.1 Effects of pH, salt identity and ionic strength on swelling equilibrium

The effects of pH, salt identity and ionic strength on the swelling equilibrium of ionisable polyelectrolyte hydrogels have been studied ([5, 6]). Historically, however, the experiments have almost exclusively been conducted on chemically cross-linked gels. Typically the expansion ratios are reported as a weight average expansion ratio which is determined from the ratio between dry (M_d) and swollen mass (M_s) of the gel, as shown in equation 4.1.

$$ER = \frac{M_s - M_d}{M_d} \tag{4.1}$$

Measuring the expansion ratio by mass infers a number of fundamental limitations, which are in addition to the fact that you are measuring a macroscopic response that does not necessarily reflect the response of the individual chains of the polymer.

When measuring swelling by gravimetry it is often necessary to use large gel samples. This is necessary in order to overcome the inherent propagation errors associated with measuring the weight increase in small samples. However this causes a number of problems. It is important to ensure there is always an excess of ions in the solution surrounding the gel compared to the number of free ionisable group on the polymer in itself. But when large polymer samples are used an equally large volume of solution is needed to maintain an excess. This makes multiple sampling time demanding and consumes large volumes of solution. It is also well understood that the rate of solvent diffusion in hydrogels is related to the square of the size of smallest

dimension of the gel, [7]), therefore large polymer samples must be immersed in solution for long periods of time to ensure they have reached their final equilibrium structure. Manipulation of samples also introduces errors, in the first instance one must ensure that the sample is sufficiently free from surface solution, and often during expansion samples have a tendency to fracture which results in an incorrectly measured expansion ratio.

4.1.2 Advantages of using SAXS analysis

The use of SAXS to measure the equilibrium expansion ratio offers a number of advantages. Unlike gravimetric methods there is no lower limit on the dimensions of the hydrogel. The dimension is only limited by the diameter of the x-ray beam which can be easily manipulated to the micron scale. This means that very small samples may be used which reduces both the time the sample needs to reach equilibrium and the volume of solution needed to maintain an excess of ions. In addition, as SAXS is sampling the molecular structure any loss of material due to fracture will have no effect on the expansion ratio (assuming microphase structure is retained), which would otherwise be detrimental for gravimetric analysis. Additionally any fracture in the gel can be analysed by SAXS which will help indicate the molecular mechanism of rupture [8].

As previously discussed, water uptake in hydrogels is usually reported as a mass ratio which relates the swollen mass to the dry mass of the polymer, through equation 4.1. In this work the expansion ratio is reported as a molecular unit cell, measured as the "small angle x-ray scattering (SAXS) expansion ratio."

The domain spacing measured by SAXS reflects the average distance of hard PMMA domains in the hydrogel. If one assumes that the polymer has a cubic morphology (chapter 3, section 3.7), then this domain spacing can be converted to a volume by simply cubing the value. The molecular volume can be used in equation 4.2 to produce a SAXS expansion ratio.

$$R_{SAXS} = \frac{d_e^{\,3} - d_0^{\,3}}{d_0^{\,3}} \tag{4.2}$$

where d_e = equilibrium domain spacing and d_0 = dry domain spacing

4.1.3 Experimental SAXS setup for measuring "static" response

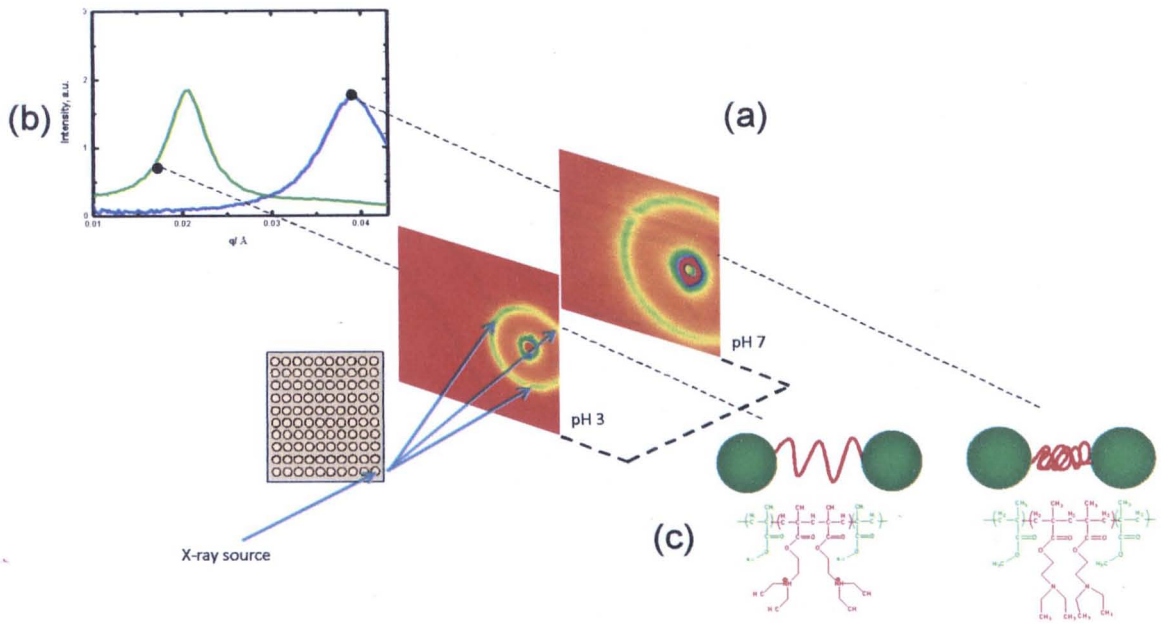

Figure 4.1: Experimental setup used to measure the molecular response of PMMA-*block*-PDEA-*block*-PMMA hydrogels. Pre-equilibrated polymer samples were loaded into an in-house built sample plate (100 samples per plate). Each sample was scanned automatically. A (a) 2D SAXS image, (b) 360 degrees integration, and (c) illustration of the molecular structure are shown for the equilibrated polymer at pH 3 and pH 7.

The molecular response of the PMMA-*block*-PDEA-*block*-PMMA hydrogels was collected using the experimental setup illustrated in figure 4.1. To facilitate an increase in the rate of sampling an in-house sample plate was constructed. This consisted of 100 holes and when used in conjunction with a computer controlled x-y-z translation stage coupled to a SAXS instrument it allowed for rapid acquisition of data. The figure also shows a typical example of the SAXS image, a 360 degrees integration of this image and the molecular structure of the polymer measured at the pH extremes, pH 3 and 7. Between the two pH values there is evidently an observable change in the polymer domain spacing; this is illustrated in the molecular cartoon as a change in the distance between the glassy PMMA domains.

4.1.4 SAXS profiles of $PMMA_{88}$-*b*-$PDEA_{223}$-*b*-$PMMA_{88}$ annealed bulk films

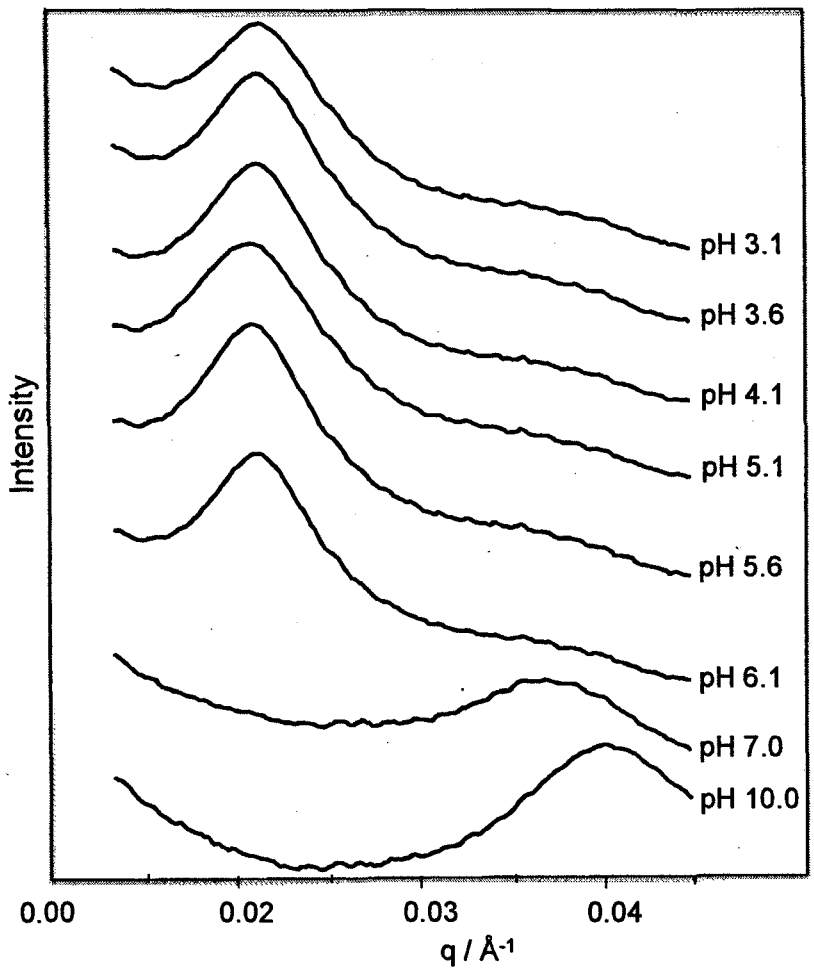

Figure 4.2: Small-angle x-ray scattering profiles of $PMMA_{88}$-*b*-$PDEA_{223}$-*b*-$PMMA_{88}$ annealed bulk films at different pH values as indicated in the figure. Measured in 0.01M citric acid (pH 3.1 –7.4) and 0.01M ethanol amine buffer (pH >8.5), ionic strength set at 0.5M using NaCl.

An example of the SAXS profile obtained for annealed films of $PMMA_{88}$-*b*-$PDEA_{223}$-*b*-$PMMA_{88}$ hydrogel immersed in two different buffer solutions (0.01M citric acid and 0.01M ethanol amine) at varying pH is shown above in figure 4.2. Each SAXS profile was created from a 360 degrees integration of the 2D SAXS image. The SAXS profile of the polymer in the solid state as indicated in chapter 3, figure 3.13 has a narrow and intense primary structure peak at q = 0.042 $Å^{-1}$. The SAXS profiles collected in citric acid buffer solutions at pH values between 3.1 to 6.1 as shown in

figure 4.2 all show a single structure peak at 0.022 $Å^{-1}$. This shift in the primary peak position at low pH values relative to the solid state polymer indicates that the molecular domains of the polymer have expanded, as $d = 2\pi/q$. As no further scattering orders are present in the SAXS profile, it is not possible to comment on the morphology of the polymer during expansion.

The SAXS profiles collected at pH values greater than 7.0 all show a single more diffuse structure peak at much greater q values. At pH 10 the polymer has a primary structure peak at 0.042 $Å^{-1}$. This is the same domain spacing as observed in the solid state polymer which implies that the polymer remains in its collapsed conformation at this pH. It is clear that the polymer conformation is controlled by manipulation of the pH.

There is an obvious dramatic shift in primary peak position between pH 6.1 and 7.0 which indicates that the polymers apparent pK_a lies within these two values. When pK_a is discussed in the context of the gel it is in effect an "apparent" pK_a emanating simplistically from the balance between the pH response (swelling pressure) of the 2-(diethylamino)ethyl methacrylate units and their hydrophobic nature at neutral pH (hydrophobic/ hydrophilic balance), coupled with the elastic retractile force of the network. A transition will occur when a particular balance of osmotic and hydrophobic forces is achieved. This effect will be investigated and discussed in greater detail later in the section.

There is also a marked difference in the peak width in the two pH extremes. At lower pH values the peak width is significantly reduced. At this pH the polymer chains are stretched due to entropic and osmotic expansion of the polymer network (see introduction, chapter 1). In this equilibrated structure all the individual polymers chains have the same length leading to a more defined structure peak. Additionally the uptake of water in the PDEA chains at low pH leads to better electron density contrast in the sample.

It should also be noted that the thin polymer films used for this study were mechanically weak. The polymer samples were immersed into buffer solutions for 24 hrs prior to SAXS analysis to ensure equilibrium was obtained. Samples immersed in solutions at pH 6.1 and below all exhibited isotropic expansion. During expansion, however, small cracks propagated in a number of the samples. Manipulation of these

samples often led to mechanical failure, characterised by tearing of the sample. As the narrow primary structure peak is still present in these samples it suggests that the mechanical failure could be a result of grain boundary imperfections. Such imperfections could be introduced into the sample during solvent casting and annealing of the sample.

Each individual SAXS profile illustrated in figure 4.2 was processed using a Gaussian fitting program (X-fit[9]) to determine the polymer domain spacing. This value was converted by equation 4.2 into a SAXS expansion ratio. All molecular expansion ratios were determined using this procedure, an example of which is given in figure 4.3.

4.1.5 The effect of pH and salt identity on the expansion ratio and apparent pK_a of $PMMA_{88}$-*b*-$PDEA_{223}$-*b*-*PMMA*$_{88}$ hydrogel measured by small angle x-ray scattering

The expansion ratio of solvent annealed thin films (2mm x 2mm) of $PMMA_{88}$-*b*-$PDEA_{223}$-*b*-$PMMA_{88}$ was measured in 0.01M citric acid and 0.01M ethanol amine buffer solution to show the effect of solution pH. Citric acid was used to buffer the pH range 3.1 to 7.4 and ethanol amine at pH values greater than 8.5. The ionic strength at each pH was fixed at a known value using a series of monovalent sodium salts. All solutions were prepared taking into account both thermodynamic temperature and ionic strength correction factors, as discussed in the appendix, section 9.6.

It is perhaps worth emphasising that there is no totally satisfactory way to measure the influence of pH on a process. For example, changing the pH of a buffer causes a shift in the balance of conjugate acid [acid] and base [base]. This is illustrated in equation 4.3.

$$[\mathrm{pH}] = pK_a + \log_{10}\frac{[\mathrm{base}]}{[\mathrm{acid}]} \tag{4.3}$$

Ultimately this directly changes the ionic strength of the solution making it difficult to differentiate the effect of ionic strength and pH. Two methods can be used to counter this, one can increase the concentration of the buffer species to maintain a

constant ionic strength at different pH values, however this will change the total buffer concentration and buffer capacity. The alternative approach which is used in this work is to maintain the imbalance of species by addition of neutral sodium salts to create a solution at constant ionic strength at different pH values. The salts used to fix the ionic

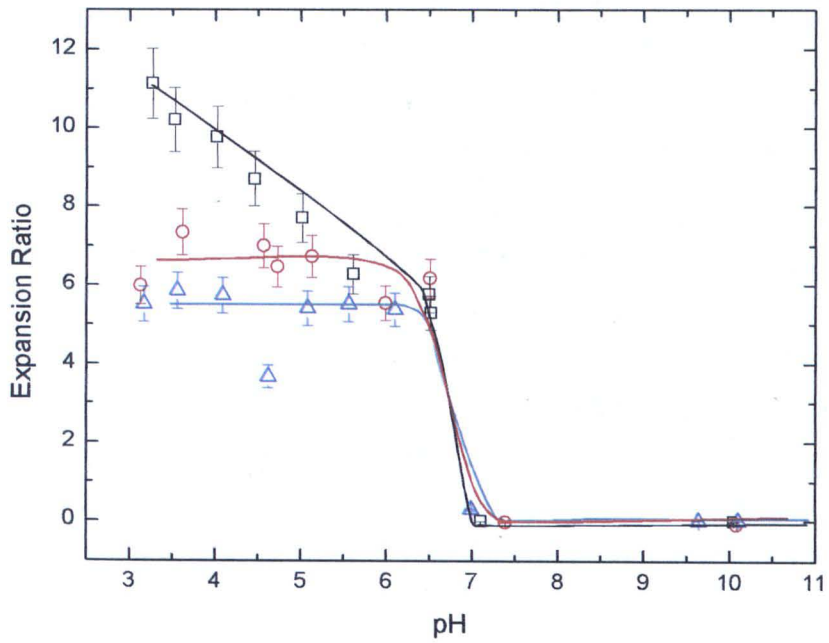

Figure 4.3: Variation of the SAXS expansion ratio of $PMMA_{88}$-*b*-$PDEA_{223}$-*b*-$PMMA_{88}$ annealed bulk films as a function of pH measured in 0.01M citric acid (pH 3.1 –7.4) and 0.01M ethanol amine buffer (pH >8.5), ionic strength set at □ 0.1M, ○ 0.3M and △ 0.5M using NaCl. Lines shown to guide the eye.

strength of the buffer were based on the Hofmeister series [10] and included sodium acetate (NaAce), sodium chloride (NaCl), sodium bromide (NaBr), sodium nitrate ($NaNO_3$), sodium iodide (NaI) and sodium thiocyanate (NaSCN).

The choice of buffer, in this case citric acid, was selected as it is able to buffer a wide pH range. This is possible because citric acid is a multivalent species with three pK_a's ranging from 3.15 to 6.40. The advantage of using a single buffer, as opposed to a series of monovalent buffers to span the same pH range, is that any effects to be attributed to specific buffer species acting alone.

Figure 4.3 shows an example where NaCl has been used to control the ionic strength. At pH values 7.0 and above the hydrogel is unexpanded and remains hydrophobic regardless of the ionic strength. As the pH is reduced below this value

a point exists when the expansion ratio increases dramatically leading to a highly swollen gel. This region/ transition can be attributed to the pK_a of the PDEA groups within the polymer, and in this example it occurs at a pH of approximately 6.8. It is also noteworthy that as the pH is further lowered below the apparent pK_a polymers swollen in 0.3M and 0.5M NaCl do not significantly change their swelling ratio. However, when 0.1M NaCl is used to fix the ionic strength there appears to be a discontinuous increase in the swelling ratio as the pH is decreased below the apparent pK_a. For example, at pH 6 the polymer has a swelling ratio of 6, which increases by almost a factor of 2 when the pH is lowered to 3.6.

The effect of pH on the expansion ratio was also measured using several other sodium salts to control the ionic strength. This investigation was undertaken to see if the identity of the salt had any effect on the apparent pK_a. In figure 4.4, the ionic strength was held constant at 0.3M using several different sodium salts which included NaCl, $NaNO_3$, NaI and NaSCN. The identity of the salt does not appear to have a significant effect on the apparent pK_a. The results are very similar to those observed in figure 4.3, where a drastic change in the swelling ratio is observed around the same pH of approximately 6.8.

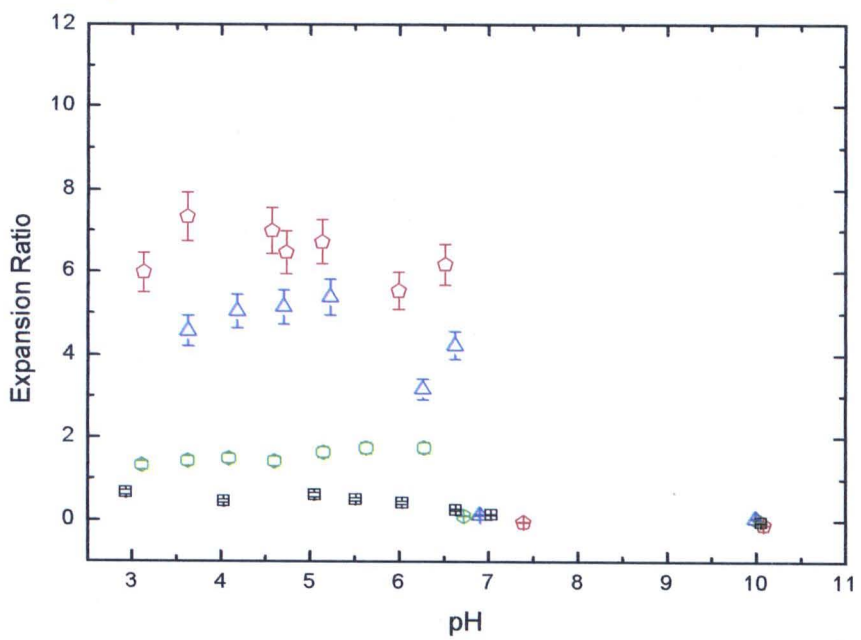

Figure 4.4: Variation of the SAXS expansion ratio of $PMMA_{88}$-*b*-$PDEA_{223}$-*b*-$PMMA_{88}$ annealed bulk films as a function of pH and salt identity, measured in 0.01M citric acid (pH 3.1 –7.4) and 0.01M ethanol amine buffer (pH >8.5), ionic strength set at 0.3M using ⬠ NaCl, △ $NaNO_3$, ⬡ NaI and □ NaSCN.

It is also worth emphasising that at a fixed ionic strength of 0.3M, there is not such a drastic discontinuous change in the expansion ratio as the pH is further lowered below the apparent pK_a. This trend was clearly evident in solutions fixed at an ionic strength of 0.1M as shown in figure 4.3. It is also apparent that at pH values below 6.8 the identity of the salt has a substantial effect on the expansion ratio. This specific effect will be discussed in section 4.1.7.

To determine if the discontinuous trend in the swelling ratio observed figure 4.3 (at 0.1M ionic strength) was salt specific, a comparison was made using NaBr and NaAce. The results are presented together in figure 4.5, which indicate that the trend is not salt specific. Solutions containing NaAce and NaBr show a similar marked discontinuous reduction in their swelling ratio as the pH is lowered from 6.8 to 3. This phenomenon was also evident in the swelling isotherms reported by Siegel and Firestone [2]. They investigated, using gravimetric analysis, the pH phase transition of a chemically crosslinked polybasic DMA/MMA 30/70 (mol%) gel swollen under identical conditions. Below the phase transition they also observed a gradual increase in the expansion ratio when the pH was lowered by upto a maximum of 30 percent.

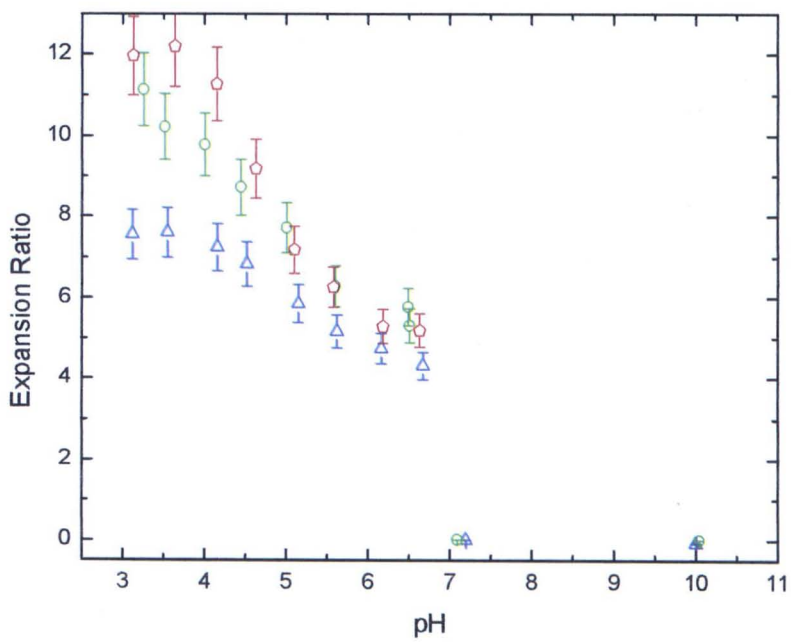

Figure 4.5: Variation of the SAXS expansion ratio of $PMMA_{88}$-*b*-$PDEA_{223}$-*b*-$PMMA_{88}$ annealed bulk films as a function of pH and salt identity, measured in 0.01M citric acid (pH 3.1 –7.4) and 0.01M ethanol amine buffer (pH >8.5), ionic strength set at 0.1M using △ NaBr, ○ NaCl, ⬠ NaAce.

However they did not discuss the underlying cause. One possible explanation for this effect would be to consider the fractional composition of species in the citric acid buffer between the pH values 3 and 7.

In the swelling isotherms in figure 4.4 and 4.5 at the pH values indicated 0.01M citric acid buffer was used to control the pH. This buffer is trivalent (having three pK_a's) and the fractional composition of individual species in the solution depends critically on the pH, as discussed in chapter 5, where a full derivation is given on how to determine the fractional composition of each species at a given pH.

Between the pH values 3.6 to 6.9 in figure 4.5, where the discontinuous swelling region is observed, the composition of ionic species changes from predominantly monovalent at pH 3.6, to divalent at pH 5 and trivalent at pH 6.5.

The change in the distribution of buffer species would appear to be the underlying cause of the discontinuous swelling region. When the buffer species are primarily monobasic the gel is highly swollen, and when trivalent species dominate the expansion is less pronounced.

It is the concentration of counter ions in the hydrogel which are fundamental for expansion, a consequence of the swelling pressure they exert. It can be postulated that less trivalent anions (having three sites to act as counterions) are needed at pH 6.5, than monovalent anions at pH 3.6 to neutralize an equal amount of charge in the gel. For this to hold true one would expect the swelling ratio to be higher at lower pH's as the concentration of monovalent species dominates. This is clearly observed in figure 4.3 and 4.5 when the ionic strength is fixed at 0.1M.

However, in figure 4.3 and 4.4, when the ionic strength is fixed at 0.3M and above, the expansion ratio below pH 6.8 does not deviate significantly with further decreases in the pH. This effect must emanate from the additional increase in the concentration of NaCl used to maintain the ionic strength.

As the ionic strength of the solution is increased, one would expect isoelectric exchange between the chloride ions in the buffer solution and citrate ions in the gel interior. This should occur following equation 4.3,

$$Cit^{z-}_{\text{gel interior}} \rightleftharpoons zCl^{-}_{\text{solution}} \qquad (4.4)$$

It follows from equation 4.4 that above a critical ionic strength all of the citrate species in the gel interior eventually become monovalent. At this stage the citrate buffer valency is no longer of importance, hence the lack of pH dependency on expansion ratio below 6.8 at 0.3M ionic strength. In other words all of the anions in the gel interior are monovalent Cl^- anions. The results suggest that the critical concentration of NaCl for complete exchange of chloride ions in the gel interior lies between 0.1M and 0.3M.

4.1.6 The effect of buffer on the swelling isotherms of $PMMA_{88}$-*b*-$PDEA_{223}$-*b*-$PMMA_{88}$ hydrogel

The expansion ratio and apparent pK_a of $PMMA_{88}$-*b*-$PDEA_{223}$-*b*-$PMMA_{88}$ was additionally investigated in a different buffer, namely 0.01M sodium phosphate. The pH was chosen between the range 6.0 to 8.5 to capture the swelling transition of the polymer. In citric acid buffer the apparent pK_a is observed around pH 6.8 as previously shown in figure 4.3. In contrast the apparent pK_a shifts to approximately 7.3 when the same polymer is studied in sodium phosphate buffer, as shown in figure 4.6.

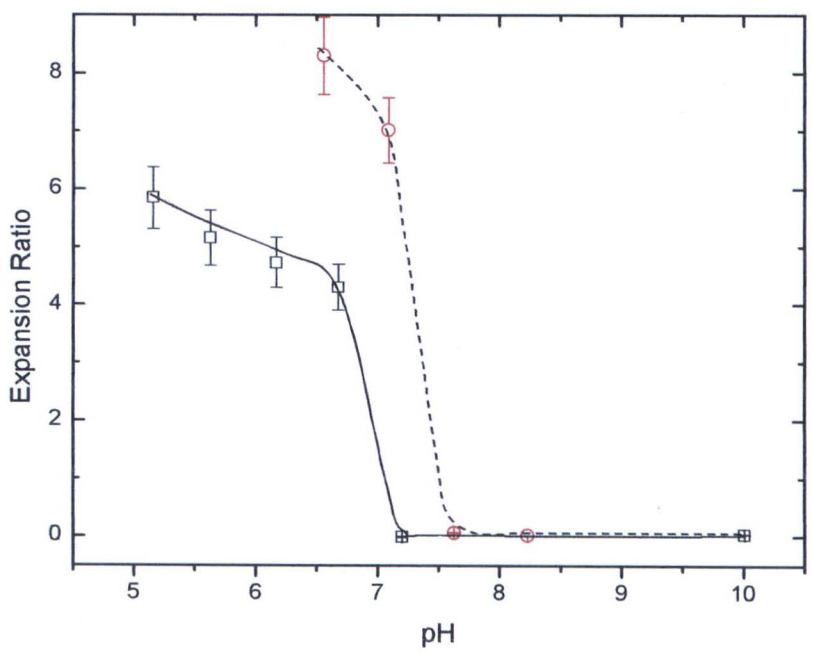

Figure 4.6: Variation of the SAXS expansion ratio with solution pH for $PMMA_{88}$-*block*-$PDEA_{223}$-*block*-$PMMA_{88}$ copolymer in □ 0.01M citric acid and ○ 0.01M sodium phosphate buffer at an ionic strength of 0.1M (NaBr). Value at pH 10 obtained using 0.01M ethanol amine. Line shown to guide the eye.

Not only does the pK_a shift to higher values it is clear that the expansion ratio just below the pK_a is higher by three units. The difference in expansion ratio at pH values below the apparent pK_a can be explained if one examines the pK_a value of the two buffers. Citric acid and sodium phosphate are both trivalent buffers, with pK_a values of 3.13, 4.77, 6.40 [11] and 2.15, 7.20, 12.33 [12] respectively. At pH 6.5 citric acid will exist primarily as a trivalent species (82% trivalent (A^{3-}), 18% divalent (A^{2-})) and sodium phosphate will be primarily divalent (70% divalent (A^{2-}), 30% trivalent (A^{3-})), see figure 4.7. The individual buffer species in the solution perform two key functions. They are responsible for protonating the polymer, but they also act as counter ions to maintain charge neutrality. The effectiveness of a buffer to act as a counter ion should depend on its valency, as previously discussed. A trivalent species has three sites available to act as counter ions, whereas a divalent has only two. At pH 6.5, citric acid which is primarily trivalent should therefore require less species to act as counter ions when compared to sodium phosphate which is mostly divalent.

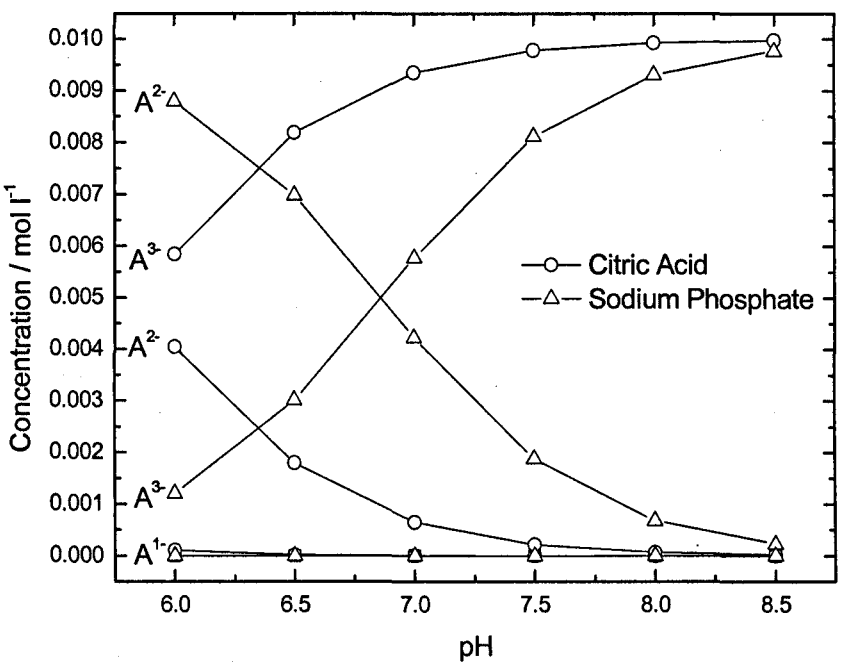

Figure 4.7: Concentration of individual buffer species (not including added salt) in 0.01M citric acid and 0.01M sodium phosphate buffer as a function of pH.

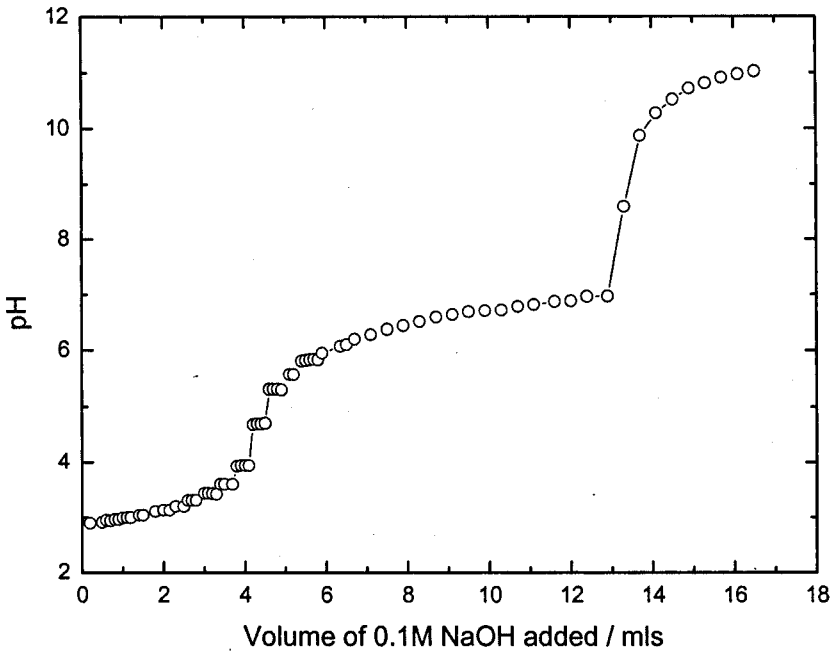

Figure 4.8: Potentiometric titration curve of $PMMA_{88}$-*b*-$PDEA_{223}$-*b*-$PMMA_{88}$. 0.1 w/w solution at pH 3 was titrated using a *0.1M* standard NaOH solution.

At pH and 6.5 polymers swollen in citric acid should therefore show a reduction in swelling pressure compared to sodium phosphate. This is observed in figure 4.6. The marked change in apparent pK_a between the two buffers is more difficult to explain. Perhaps this is associated with buffer specific effects on the pH probe perturbing the reading [13].

The apparent pK_a of the polymer was also determined by potentiometric titration for comparison. A 0.1 w/w polymer solution was pre-acidified to pH 3. At this pH the tertiary amine groups are protonated which assists dissolution of the polymer. 0.1M standardised NaOH solution was slowly titrated against the solution. Initially the pH increased, corresponding to removal of excess acid. With further addition of base a plateau region was evident, corresponding to deprotonation of the ionized amine groups. In this region further increases in pH caused the solution appearance to change from one which was initially transparent to milky, a result of decreasing hydrophilicity of the DEA. Above a critical pH, in this example, 10, the polymer

precipitated out of solution, a result of the DEA block becoming hydrophobic. The measured pK_a of 6.6 for $PMMA_{88}$-*b*-$PDEA_{223}$-*b*-$PMMA_{88}$ is comparable to the pK_a

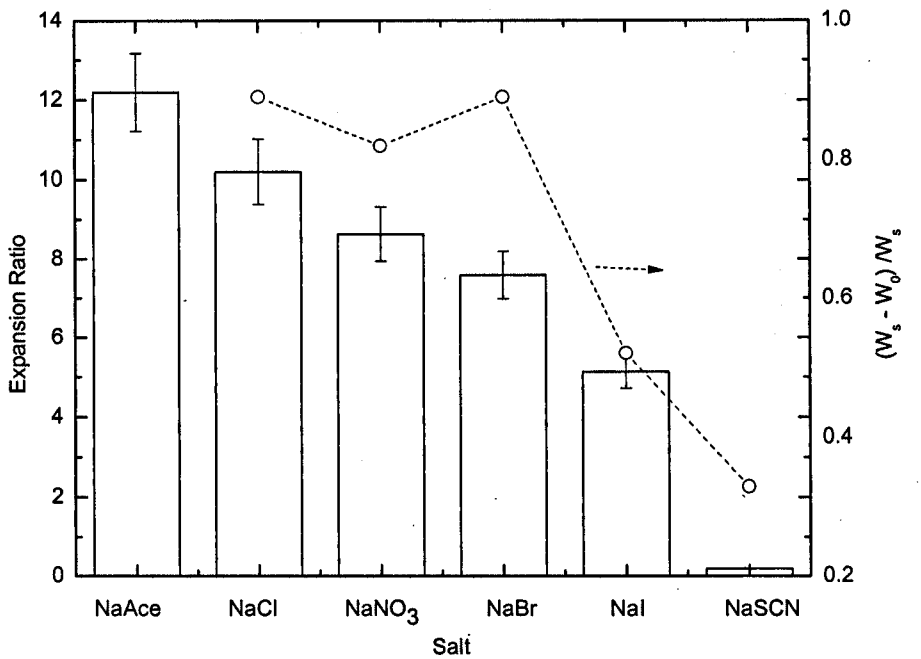

Figure 4.9: The effect of counter-ion (anion of the sodium salt) on the SAXS equilibrium swelling ratio of $PMMA_{88}$-*b*-$PDEA_{223}$-*b*-$PMMA_{88}$ annealed bulk film measured at pH 3.6 in 0.01M citric acid at an ionic strength of 0.1M. In comparison the gravimetric equilibrium swelling ratio of MMD/DMA 70/30 mol% crosslinked gels at pH 4 in 0.01M citric acid at an ionic strength of 0.1M is given on the right axis (○) [6].

measured by SAXS analysis. Interestingly, the pK_a of free PDEA chains was measured by potentiometric titration in dilute solution and found to be 6.9 [14]. The shift in apparent pK_a most likely a result in the increase in hydrophobicity of the polymer caused by the addition of PMMA [15].

4.1.7 Specific ion effects

Figure 4.9 shows the SAXS equilibrium expansion ratio obtained when an annealed thin film of $PMMA_{88}$-*block*-$PDEA_{223}$-*block*-$PMMA_{88}$ was placed in a 0.01M citric acid buffer solution at pH 3.6, using a series of monovalent sodium salts to fix the ionic strength at 0.1M. The "gravimetric" swelling results obtained by Siegel *et al* [6] on a

70/30 mol% methyl methacrylate / dimethylaminoethyl methacrylate hydrogel obtained under similar conditions are shown on the same plot.

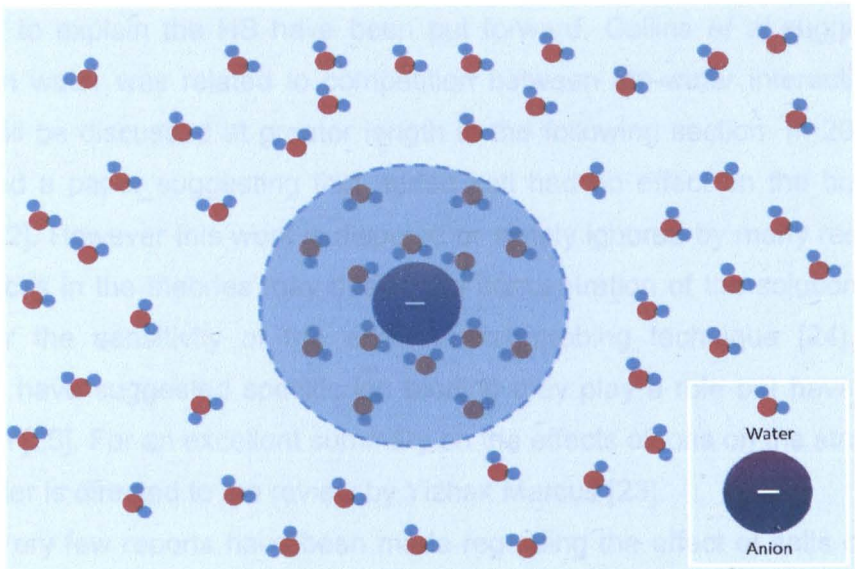

Figure 4.10: Localised ordering of water in the first hydration layer surrounding the anion. The scale is approximately correct for water and SO_4^{2-} anion.

The monovalent salts were based on the Hofmeister series (HS) ([10]). This is a series of salts which was initially indentified in 1888 where it was noted that a range of ions had varying affinities towards the precipitation of egg-white proteins, following the specific order $SO_4^{2-} > F^- > BrO_3^- > Cl^- > ClO_3^- > Br^- > NO_3^- > ClO_4^- > I^- > SCN^-$ for anions and $Li^+ > Na^+ > K^+ > Mg^{2+} > Ca^{2+} > Ba^{2+}$ for cations. It should be noted that the effect of cations is less pronounced compared with anions [16].

Since this time the Hofmeister series has been linked to many hydrogel related phenomenon, such as protein solubility, critical micelle concentration, chromatographic selectivity and surface tension [17, 18]. Generally the system under study follows the specific order of the Hofmeister series but subtle differences are known to occur [19].

To date the Hofmeister series and its principle mechanism is a strongly contested subject. Many theories have been suggested to explain the effect, the majority of which describe it in terms of the ability of the salts (anionic or cationic) to "break" or "make" bulk water structure [20]. The salts are characterised as being either chaotropic or kosmotropic in nature, where kosmotropic species (to the left of the HS series) are referred to as water structure makers. They are known to increase the local order of water, as shown in figure 4.10. In the opposite case, "structure breakers

(disorder makers)" are weakly hydrated anions; they are also referred to as salting-in ions or chaotropic ions and are known to decrease the order of water. Several other theories to explain the HS have been put forward. Collins *et al* suggested the ions effect on water was related to competition between ion-water interactions [21]. This effect will be discussed at greater length in the following section. In 2003 Omta *et al* published a paper suggesting that added salt had no effect on the bulk structure of water [22]. However this work is disputed or simply ignored by many researchers [23]. Differences in the theories may due to the concentration of the solution used in each study or the sensitivity of the experimental probing technique [24]. More recent theories have suggested specific ion binding may play a role but have received little attention [25]. For an excellent summary on the effects of ions on the structure of water the reader is directed to the review by Yizhak Marcus [23].

Very few reports have been made regarding the effect of salts on the swelling of pH responsive hydrogels. The swelling results presented in figure 4.10 indicate that the identity of the counter-ion (anion of the sodium salt) has a strong influence on the swelling of $PMMA_{88}$-*b*-$PDEA_{223}$-*b*-$PMMA_{88}$ hydrogels. In order of decreasing expansion ratio the salts follow the order given below.

$$Ace^- > Cl^- > NO_3^- > Br^- > I > SCN^- \qquad (4.5)$$

The swelling ratio results in figure 4.10 for $PMMA_{88}$-*b*-$PDEA_{223}$-*b*-$PMMA_{88}$ hydrogels clearly show the expansion ratio decreases in correlation with the position of the salt in the general Hofmeister series, with the exception of NO_3 and Br which appear in reverse order. However previous studies on specific ion effects have shown a reversal in the position of NO_3 and Br in the Hofmeister series [19].

The relationship between salt identity and expansion ratio has previously been investigated by Siegel *et al* [1]. They investigated the effect of sodium salt anions on the gravimetric equilibrium swelling ratio of a chemically crosslinked 70/30 methyl methacrylate/ N,N-dimethylaminoethyl methacrylate hydrogel, expressed as $(W_s - W_0) / W_s$, where W_s and W_0 are sample weights of swollen and the dry gel respectively. Their findings are plotted in figure 4.10. However, their results do not correlate with the findings of this work. In the work reported by Siegel there is only a small difference in the gravimetric expansion ratio between Cl^- (0.90), Br^- (0.90), and NO_3^- (0.82), with I^-

(0.52) and SCN^- (0.33) showing the greatest reduction in expansion ratio. It should also be noted that the order of the salts reported by Siegel did not follow the results presented here. They found NO_3^- had a greater effect on the expansion ratio than Br^-. Perhaps their results are not as sensitive owing to the gravimetric technique they used.

The results presented by Siegel et al were interpreted making reference to the work of Washabaugh *et al.* They investigated the mechanism of elution for several halide anions which had been passed through a non-Polar Sephadex G-10 chromatography column [21], see figure 4.11.

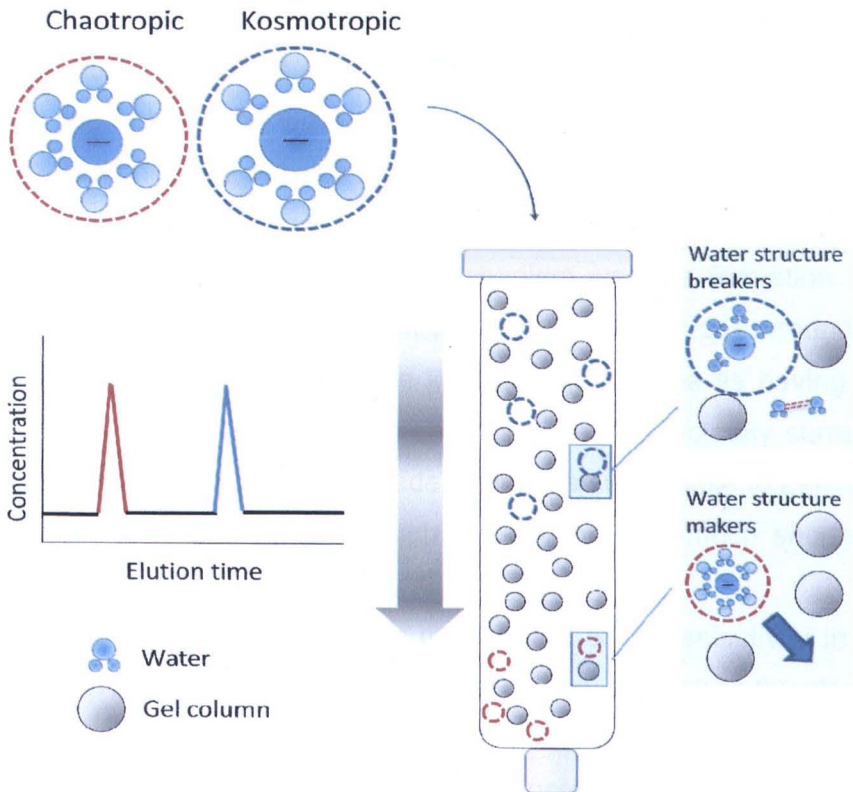

Figure 4.11: Absorption mechanism for chaotropic and kosmotropic species on a Sephadex G-10 column. Chaotropic ions remain hydrated and flow through the column unimpeded with a low retention time. Kosmotropic species are partially dehydrated in the column due to a weak bond between the anion and first hydration cage of water leading to higher retention times as compared to chaotropes.

The surface of this gel column is known to have a number of mechanisms for separation, either (1) gel sieving or (2) gel absorption. They postulated that the mechanism of separation for a specific ion depended on how weakly or strongly hydrated the solute was. They found that the mechanism of separation (interaction with the column surface) depended strongly on the identity of the specific salt eluting through the column. The salts were identified as being either chaotropic or kosmotropic in nature, as discussed earlier.

Washabaugh *et al* suggested that in chaotropic species the bond between the ion and the hydration cage of water immediately surrounding the ion was weaker than the water-water bond in the bulk solution. Therefore, when a chaotropic species was eluted through the column the weakly held hydration shell surrounding the ion was easily dehydrated. When the salt was eluted through the column the weak bond made the salt susceptible to sticking to the column, therefore increasing its retention time. They suggested the driving force for this mechanism was the formation of a strong water-water bond in the bulk solution from the weakly held water surrounding the ion [26]. Washabaugh *et al* characterised the kosmotropic species as having a stronger bond between the ion and the hydration cage of water immediately surrounding the salt. They eluded that the strong bond made them less susceptible to dehydration and as such they were found to travel through the column with much shorter retention times.

An alternative explanation for the mechanism of ion selectivity in Sephadex columns was given by Collins in a later paper [27]. They suggested the strength of the bond between the salt and surrounding hydration cage of water was interpreted by considering the ion as a point charge. As the ions increase in size (larger ionic radius) the surrounding cage of water molecules becomes progressively further away. As a result the interaction between the point charge and the hydration cage becomes weak (more diffuse electric charge). This causes the ion to become "sticky" and adhere to the surface of the gel. At a certain radius the character of the ion was found to change from one which was kosmotropic at small ionic radii to one which was chaotropic at infinite size. They identified the transition from weak to strong hydration in anionic solutes to be 1.78 angstroms.

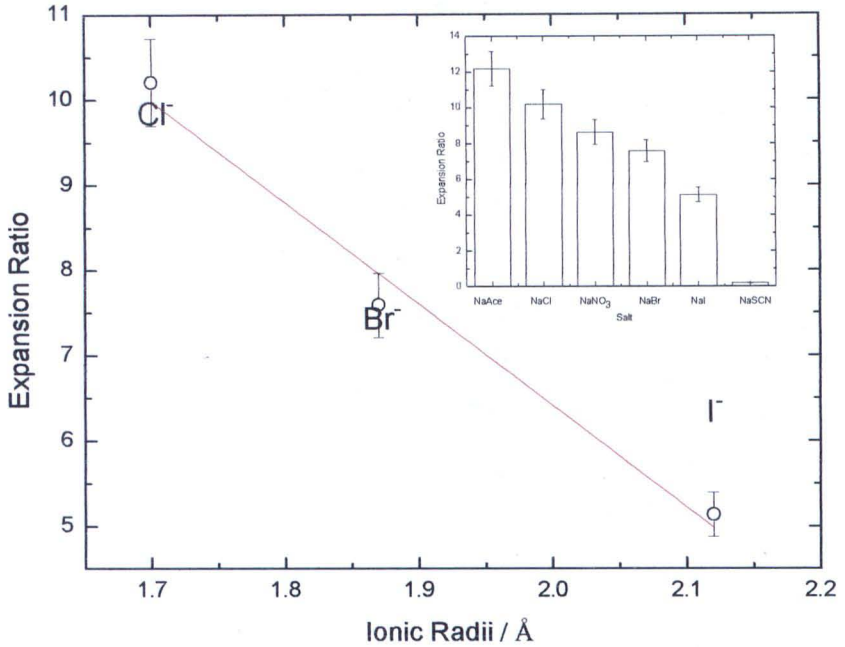

Figure 4.12: The effect of halide ion crystal ionic radius on the SAXS equilibrium swelling ratio of $PMMA_{88}$-*b*-$PDEA_{223}$-*b*- $PMMA_{88}$ annealed bulk films measured at pH 3.6 in 0.01M citric acid at an ionic strength of 0.1M, anion radius taken from ref [28]. Inset: SAXS expansion ratio as a function of salt identity at pH 3.6 and ionic strength of 0.1M.

A plot of the expansion ratio obtained using SAXS as a function of halide ion ionic radius for Cl^-, Br^- and I^- is shown in figure 4.12. It clearly shows that the expansion ratio of the polymer decreases almost linearly (R^2=0.96) with an increase in the size of the ion.

This effect was further investigated by re-plotting the graph replacing the ionic radii with the surface charge density of each ion. This was found to have an excellent correlation with an r-squared value greater than 0.99. Swelling results obtained at an ionic strength of 0.3M are also included on the graph. An r-squared value of 0.96 is obtained, showing the excellent reproducibility of this effect. A similar trend was observed by Lui *et al* [29]. They investigated the thermal gelation behavior of hydroxypropylmethylcellulose gel (HPMC), by monitoring the change in the temperature at maximum heat capacity (T_m), in a range of Hofmeister salts. They also found a linear correlation (R^2=0.99) when the surface charge density (charge on electron/ $4\pi r^2$) of the halide anions was plotted again T_m. Given that the majority of

studies, past and present, including those of Lui *et al* support the idea that the salt effect is due to their water structuring capability, this line of reasoning will be used to explain the Hofmeister effect in this study [29, 30].

The argument suggested by Collins seems to be in excellent agreement with the results obtained for the halide ion series in figure 4.13. The surface charge density of the halide ions clearly has an effect on the structuring of water. The theory also implies that NaSCN and NaI, which have the largest ionic radii should be the most weakly hydrated and therefore act as chaotropic species.

As these ions have smaller surface charge densities they are more non-polar in behaviour. As a direct result of this they should be more strongly bound to the non-polar surface of the hydrogel, leading to a greater reduction in osmotic activity and ultimately swelling compared to the kosmotropes. This is what is observed in figure 4.9.

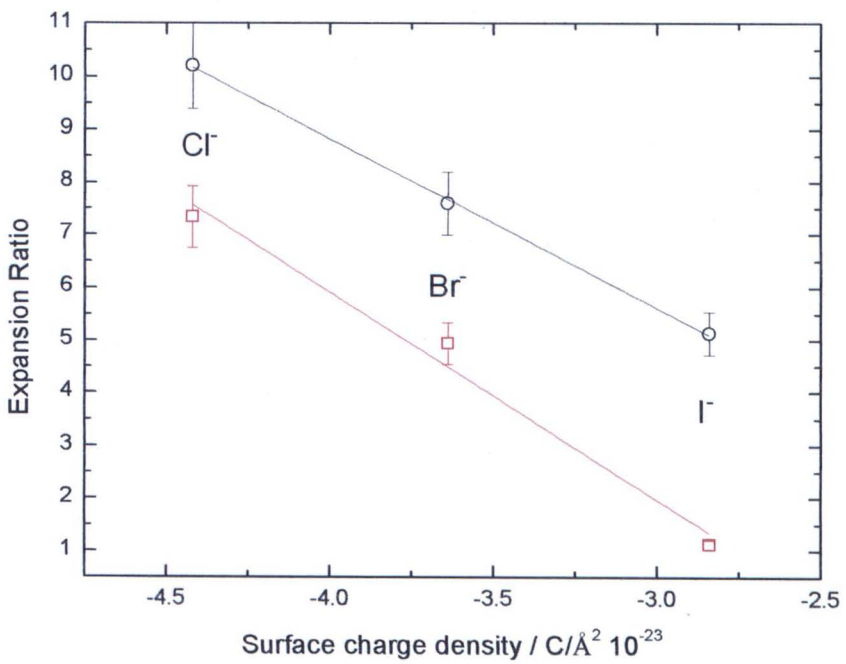

Figure 4.13: The effect of halide ion surface charge density on the SAXS equilibrium swelling ratio of $PMMA_{88}$-*b*-$PDEA_{223}$-*b*- $PMMA_{88}$ annealed bulk films measured at pH 3.6 in 0.01M citric acid at an ionic strength ○ 0.1M and □ 0.3M. Surface charge density taken from ref [28].

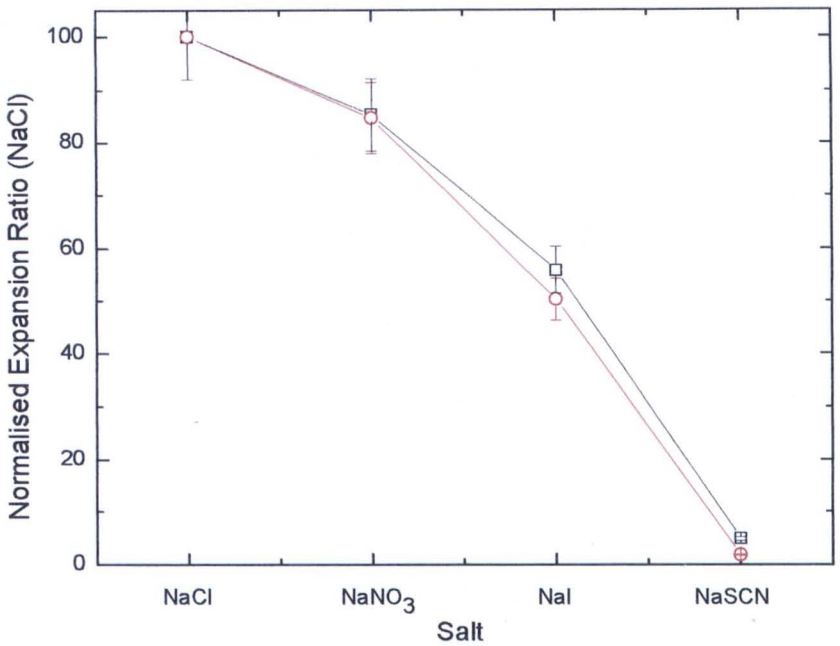

Figure 4.14: The effect of counter-ion (anion of the sodium salt) on the normalised SAXS expansion ratio of □ $PMMA_{188}$-*b*-$PDEA_{453}$-*b*-$PMMA_{188}$ and □ $PMMA_{88}$-*b*-$PDEA_{223}$-*b*- $PMMA_{88}$ bulk annealed gels measured at pH 2.7 in hydrochloric acid at an ionic strength of 0.1M.

The effect of the counter-ion identity on the expansion ratio was further investigated using a different polymer. The polymer investigated was also a PMMA-*block*-PDEA-*block*-PMMA triblock, having the same volume fraction as the material investigated in figure 4.9, but differing only by its overall molecular weight, being approximately twice as high (see table 4.1). The expansion ratio with respect to NaCl has been normalised for both polymers and is plotted in figure 4.14. Both polymers have an identical trend where a general reduction in expansion ratio is observed as one moves across the general Hofmeister series.

The salt specific change in expansion ratio between the two polymers is very similar. For example, the percentage difference in expansion ratio between NaCl and $NaNO_3$ in both polymers is in excellent agreement, a difference of exactly 15%. The change between NaCl and NaI is 55% and 50% for $PMMA_{88}$-*b*-$PDEA_{223}$-*b*-$PMMA_{88}$ and $PMMA_{188}$-*b*-$PDEA_{453}$-*b*-$PMMA_{188}$ respectively. Clearly this is a reproducible and specific effect.

4.1.8 Effect of ionic strength on swelling equilibrium

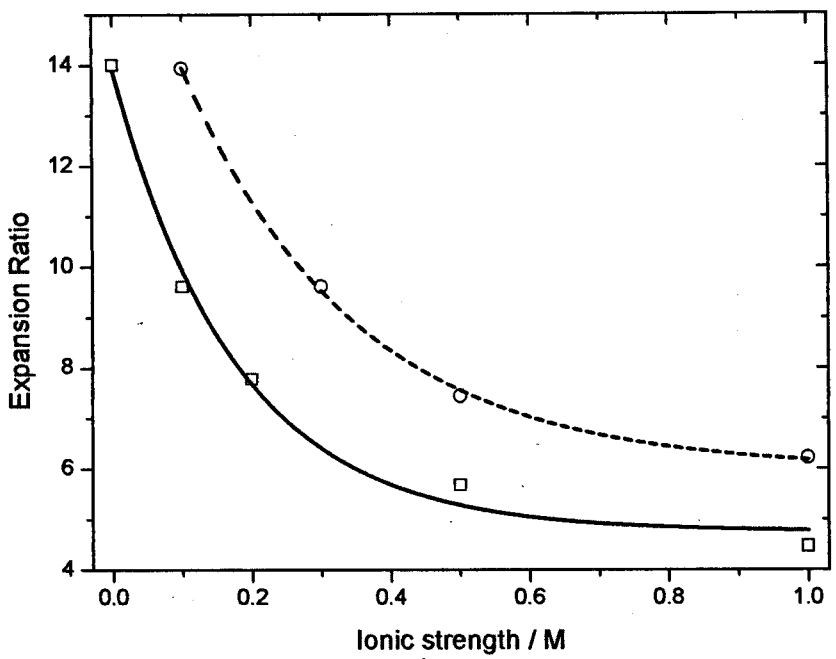

Figure 4.15. (a) Variation of the SAXS expansion ratio with ionic strength for ○ $PMMA_{180}$-*b*-$PDEA_{453}$-*b*-$PMMA_{180}$ □ $PMMA_{88}$-*block*-$PDEA_{223}$-*block*-$PMMA_{88}$ bulk annealed films in hydrochloric acid at pH 3.6. Ionic strength varied using NaCl. Lines are shown to guide the eye.

The expansion ratio of $PMMA_{88}$-*block*-$PDEA_{223}$-*block*-$PMMA_{88}$ was monitored as a function of ionic strength at a fixed pH, as shown in figure 4.15. The results indicate that the polymer is sensitive to ionic strength. The expansion ratio decreases as the ionic strength is increased. The expansion ratio of $PMMA_{180}$-*block*-$PDEA_{453}$-*block*-$PMMA_{180}$ is also included which shows a similar trend. The decrease in expansion ratio with changes in ionic strength is investigated in greater detail in chapter 5. The overall increase in expansion ratio of the higher molecular weight polymer is due to its higher charge density. When it is protonated this generates a higher osmotic pressure.

4.1.9 Effect of molecular weight on swelling equilibrium

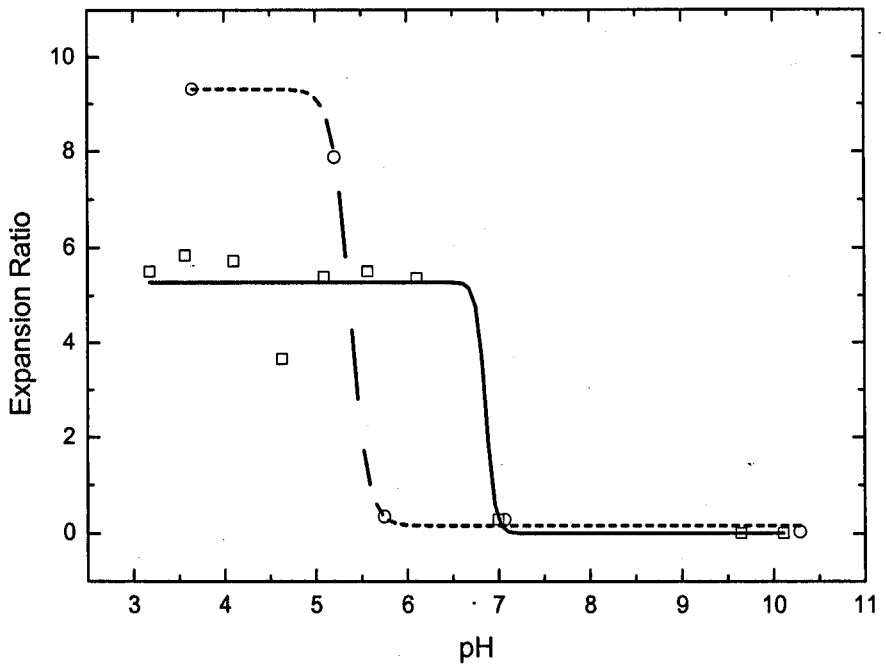

Figure 4.16: Variation of the SAXS expansion ratio with solution pH for (a) ○ $PMMA_{180}$-*b*-$PDEA_{453}$-*b*-$PMMA_{180}$ (b) □ $PMMA_{88}$-*b*-$PDEA_{223}$-*b*-$PMMA_{88}$ bulk annealed films in 0.01M citric acid at an ionic strength of 0.5M (NaCl). Line shown to guide the eye.

The effect on molecular weight on the expansion ratio was investigated compared between two $PMMA_x$-$PDEA_y$-$PMMA_x$ copolymers referred to in table 4.1. Both have the same overall volume fraction of PMMA end blocks of 0.17, the only difference between them is the overall molecular weight, one have approximately twice the degree of polymerisation. Figure 4.16 shows the expansion ratio of the two polymers as a function of pH. It is clear that the overall molecular weight has a dramatic effect on the apparent pK_a. An increase in the molecular weight by a factor of two causes a shift in the apparent pK_a by over one full unit, reducing from 6.8 in $PMMA_{88}$-*block*-$PDEA_{223}$-*block*-$PMMA_{88}$ to 5.2 in $PMMA_{180}$-*block*-$PDEA_{453}$-*block*-$PMMA_{180}$. It is also worth emphasising that in the expanded region the higher molecular weight polymer has a larger expansion ratio. This is experimentally expected as $PMMA_{180}$-*block*-$PDEA_{453}$-*block*-$PMMA_{180}$ has a higher charge density

when protonated. The water driven into the PDEA phase thus generates a higher osmotic pressure compared to $PMMA_{88}$-*block*-$PDEA_{223}$-*block*-$PMMA_{88}$.

In weak polyacid brushes it is known from pH titration curves that an increase in polymer brush graft density causes a shift to higher pK_a values. Curie et al [31] reported that an increase in grafted poly(acrylic acid) brush layer density from 18 to 8nm^2 per chain caused an apparent pK_a increase of approximately 1.5 pH units. The increase in pK_a was theoretically explained using annealed brushed theory [32, 33]. This observation is consistent with theoretical models which according to equation 4.6 [33],

$$\alpha = \left[\frac{\alpha_B}{1-\alpha_B}\sigma^{-1}(\rho_H + \rho_S)\right]^{\frac{2}{3}} \tag{4.6}$$

α = degree of ionisation in the brush, α_B = degree of ionisation in the bulk, σ = grating density of polymer chains, ρ_H = concentration of H^+, ρ_S = concentration of salt.

predict that the overall degree of dissociation in the brush under conditions of constant pH and ionic strength will decrease as the grafting density is increased. This effect has also been observed on poly(2-(diethylamino)ethyl methacrylate) brushes, where a shift in the pK_a to a lower value is observed as the brush density is increased [34].

The polymer brush theory described above was applied to the data in figure 4.16 in an attempt to explain the apparent pK_a shift observed with changes in overall molecular weight.

An illustration of the micro-domain structure of $PMMA_{88}$-*block*-$PDEA_{223}$-*block*-$PMMA_{88}$ triblock copolymer is given in figure 4.17. This material is held together by physical aggregation of the PMMA domains. One way to explain the apparent pK_a shift observed in figure 4.16 is to treat the triblock as a polymer brush. In this case one would expect that when the aggregation number of the PMMA domain is high, the polymer will behave more like a dense polymer brush, and in the opposite case of low aggregation it behaves like a loosely packed brush. Under these conditions it would be anticipated that increasing aggregation of the PMMA should lower the apparent pK_a of the material. To test this hypothesis the aggregation number of the two $PMMA_x$-*block*-

$PDEA_y$-*block*-$PMMA_x$ copolymers was calculated. The aggregation number for each polymer was calculated in the following way. Using Avogadro's number the mass of a single polymer chain of PMMA-*block*-PDEA-*block*-PMMA was calculated. As the mass fraction of the polymer is known the mass of a single PMMA chain end can be calculated. Using the density of PMMA homopolymer the mass of a PMMA chain end was converted into a volume. To calculate an approximate aggregation number the volume of a single PMMA sphere was divided by the volume of a single PMMA chain end. The volume of a single PMMA sphere was determined using the radius of each sphere which had previously been estimated using the spacing from small angle X-ray scattering and the composition (volume fraction) from NMR.

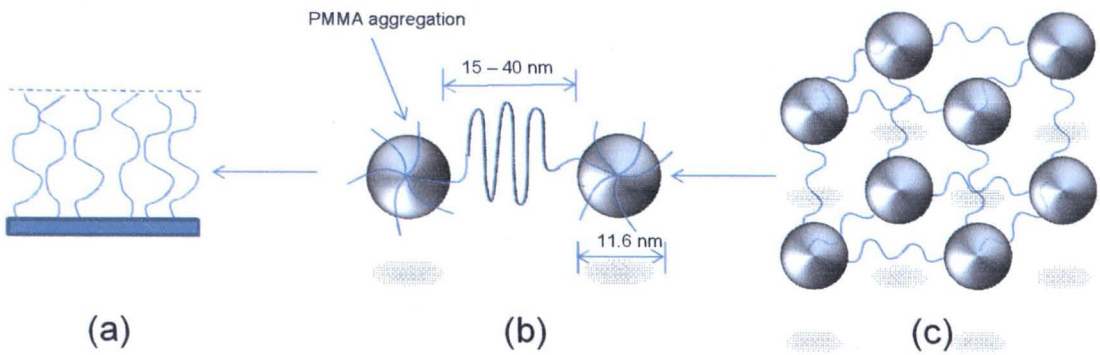

Figure 4.17: (c) micro-domain structure of $PMMA_{88}$-*b*-$PDEA_{223}$-*b*-$PMMA_{88}$, (b), illustration of the physical aggregation at each PMMA domain (a) simple polymer brush.

The aggregation number of $PMMA_{88}$-*block*-$PDEA_{223}$-*block*-$PMMA_{88}$ and $PMMA_{180}$-*b*-$PDEA_{453}$-*b*-$PMMA_{180}$ was found to be 76 and 261 respectively. This corresponds to $PMMA_{88}$-*block*-$PDEA_{223}$-*block*-$PMMA_{88}$ and $PMMA_{180}$-*block*-$PDEA_{453}$-*block*-$PMMA_{180}$ having 5.55 nm^2 and 4.79 nm^2 per PMMA polymer chain (surface area / aggregation number). Given that the lower molecular weight material has a smaller aggregation number and smaller brush density it was expected that this polymer should have the highest apparent pK_a of the two. This is in fact observed but the change in graft density is only marginal.

Table 4.1: A summary of block copolymer compositions and calculated pK_a values.

Polymer composition	M_n ($gmol^{-1}$)[a]	M_w ($gmol^{-1}$)[a]	M_w/ M_n	Volume fraction, PMMA[b]	pK_a [c]
$PMMA_{88}$-$PDEA_{223}$-$PMMA_{88}$	58941	81442	1.38	17	6.8
$PMMA_{180}$-$PDEA_{453}$-$PMMA_{180}$*	119871	152558	1.27	17	5.2

a: As determined by GPC (calibrated with poly(methyl methacrylate) standards)

b: As determined by ^1H NMR spectroscopy

c: As determined by small angle x-ray scattering

*Donated by Dr Paul Topham

4.2 CONCLUSION

This chapter has concentrated primarily on evaluating the pH response of a phase separated $PMMA_{88}$-*block*-$PDEA_{223}$-*block*-$PMMA_{88}$ hydrogel through the use of SAXS. A systematic study was undertaken to determine the effect of individual species in solution on the molecular response of the gel. There are very few reports in the literature where SAXS has been used to this effect, and one of the aims of this chapter was to evaluate the usefulness of the technique for this purpose.

The use of SAXS for measuring the static response of phase separated hydrogels has proven itself to be both a reliable and sensitive technique. The technique offers several advantages over conventional gravimetric analysis; perhaps the most important is the fact that that it measures the molecular response. The results have demonstrated that the pH response of the polymer is complex, and a thorough understanding of the swelling media is required to fully explain the results.

Although complex, the solution chemistry can be tailored to control the response of the polymer. This is particularly useful when designing chemically

actuated hydrogels. Adding salt for example, can be used to limit the extent of expansion in a controlled way.

Provisional studies were also made on another polybasic triblock having the same volume fraction of PMMA but approximately twice the overall molecular weight. Through the use of SAXS it was demonstrated that the polymer had a lower apparent pK_a, and higher expansion ratio when the pH was below the apparent pK_a. This result demonstrates one of the advantages of the *bottom-up* approach, where polymer properties can be tuned in a controlled way, making them attractive for use in a multitude of applications.

REFERENCES

1. Firestone, B.A. and R.A. Siegel, Journal of Biomaterials Science, Polymer Edition, 1994. **5**(5): p. 433-50.
2. Siegel, R.A. and B.A. Firestone, Macromolecules, 1988. **21**(11): p. 3254-3259.
3. Kishi, H., T. Naitou, S. Matsuda, A. Murakami, Y. Muraji, and Y. Nakagawa, J. Polym. Sci., Part B, 2007. **45**: p. 1425-1434.
4. Topham, P.D., J.R. Howse, O.O. Mykhaylyk, S.P. Armes, R.A.L. Jones, and A.J. Ryan, Macromolecules 2006. **39**(16): p. 5573-5576.
5. Firestone, B.A. and R.A. Siegel, Journal of Applied Polymer Science, 1991. **43**(5): p. 901-14.
6. Siegel, R.A., I. Johannes, C.A. Hunt, and B.A. Firestone, Pharmaceutical research, 1992. **9**(1): p. 76-81.
7. Tanaka, T., E. Sato, Y. Hirokawa, S. Hirotsu, and J. Peetermans, Physical Review Letters, 1985. **55**(22): p. 2455-8.
8. Guice, K.B., S.R. Marrou, S.R. Gondi, B.S. Sumerlinand, and Y.-L. Loo, Macromolecules, 2008. **41**(12): p. 4390-4397.
9. Squire, J., H. AL-Khaya, S. Arnott, J. Crawshaw, R. Denny, G. Diakun, D. Dover, T. Forsyth, A. He, C. Knupp, G. Mant, G. Rajkumar, M. Rodman, M. Shotton, and A. Windle, Fibre Diffraction Review, 2003. **11**: p. 7-19.
10. Hofmeister, F., Naunyn-Schmiedebergs Arch. Pathol, 1888. **24**: p. 247-260.
11. Christian, G.D., *Analytical Chemistry*. 2004, New Jersey: John Wiley &Sons. 298, 804.
12. Perrin, D.D. and B. Dempsey, *Buffers for pH and Metal Ion Control*. 1974, London: Chapman & Hall. 156–162.
13. Salis, A., M.C. Pinna, D. Bilaniová, M. Monduzzi, P.L. Nostro, and B.W. Ninham, J. Phys. Chem. B, 2006. **110**(6): p. 2949-2956.
14. Lee, A.S., A.P. Gast, V. Bütün, and S.P. Armes, Macromolecules, 1999. **32**(13): p. 4302–4310.
15. Triftaridou, A.I., S.C. Hadjiyannakou, M. Vamvakaki, and C.S. Patrickios, Macromolecules, 2002. **35**(7): p. 2506-2513.
16. Alexandridis, P. and J.F. Holzwarth, Langmuir, 1997(13): p. 6074.
17. Wang, J. and M. Satoh, Polymer, 2009. **50**(15): p. 3680-3685.
18. Zhang, Y. and P.S. Cremer, Current Opinion in Chemical Biology, 2006. **10**: p. 658–663.
19. Vlachya, N., M. Drechslerb, D. Tourauda, and W. Kunz, Comptes Rendus Chimie, 2009. **12**(1-2): p. 30-37.
20. Hribar, B., N.T. Southall, V. Vlachy, and K.A. Dill, J. Am. Chem. Soc, 2002. **124**(41): p. 12302–12311.
21. Washabaugh, M.W. Collins, and K. D., J. Biol. Chem, 1986. **261**(27): p. 12477-85.
22. Omta, A.W., M. F. Kropman, S. Woutersen, and H. J.Bakker, Science, 2003. **347**: p. 301.
23. Marcus, Y., Chem. Rev, 2009. **109**: p. 1346–1370.
24. M.Chaplin. *Hofmeister Series*. 2009 [cited.
25. Zhang, Y., S. Furyk, D.E. Bergbreiter, and P.S. Cremer, Journal of the American Chemical Society, 2005. **127**(41): p. 14505–14510.

26. Collins, K.D., Methods, 2004. **34**: p. 300-311.
27. Collins, K., Biophysics, 1995. **92**: p. 5553.
28. Collins, K.D. and M.W. Washabaugh, Quart. Rev. Biophys, 1985. **18**: p. 323-422.
29. Liu, S.Q., S.C. Joshi, and Y.C. Lam, Journal of Applied Polymer Science, 2008. **109**: p. 363–372.
30. Maeda, Y., T. Nakamura, and I. Ikeda, Macromolecules, 2001. **34**(5): p. 1391-1399.
31. Currie, E.P.K., A.B. Sieval, G.J. Fleer, and M.A.C. Stuart, Langmuir, 2000. **16**: p. 8324-8333.
32. Israels, R., F.A.M. Leermakers, and G.J. Fleer, Macromolecules, 1994. **27**: p. 3087.
33. Zhulina, E.B., T.M. Birshtein, and O.V. Borisov, Macromolecules, 1995. **28**: p. 1491.
34. Geoghegan, M., L. Ruiz-Pe´rez, C.C. Dang, A.J. Parnell, S.J. Martin, J.R. Howse, R.A.L. Jones, R. Golestanian, P.D. Topham, C.J. Crook, A.J. Ryan, D.S. Sivia, J.R.P. Websterc, and A. Menelle, Soft Matter, 2006. **2**: p. 1076–1080.

Chapter 5
Predicting "Static" SAXS pH response using Donnan theory

5.1 INTRODUCTION

Ideal Donnan theory has been used by researchers to predict the behaviour of ionic hydrogels, and in particular how their swelling equilibrium change with solution conditions [1-4]. Particularly relevant to the results contained in this thesis is the work by Firestone *et al* [2]. They were one of the first groups to evaluate if ideal Donnan theory could be applied to explain the behaviour of hydrogels swollen specifically in buffered solutions. They tested this by gravimetrically measuring the equilibrium expansion ratios of 70/30 mol% chemically cross-linked methyl methacrylate/ N,N-dimethylaminoethyl methacrylate hydrogels in a series of buffers, and compared the results with theoretically derived values. The aim of this chapter is to test if the theory of Firestone *et al* can be applied to predict the swelling behaviour of the phase separated PMMA-*block*-PDEA-*block*-PMMA triblock copolymers prepared in this thesis.

5.1.1 Test of the ideal Donnan Theory

Firestone *et al* [2] postulated that at equilibrium a hydrogel had a hydration level denoted by the value *H*. This value was defined as the mass fraction of gel which contained water. The precise level of hydration was controlled by the balance of three pressures [5]. The first of which was the network swelling pressure, Π_{net}. This is a thermodynamic parameter controlled mainly by enthalpic interactions between the solvent molecules and polymer (largely controlled by the Flory-Huggins interaction parameter, χ [6]). As this is purely an enthalpic interaction it can be considered independent of the ionisation state of the polymer and therefore the ionic environment. The next pressure to consider is commonly referred to as the "ion swelling pressure",

Π_{ion}. This value is dependent on both the hydration level of the gel, H and the concentration of mobile ions $\{C\}$ inside and outside of the gel. The final pressure acting on the gel is external. This external pressure can be varied to increase or decrease the level of hydration in the gel. When the gel is in a state of equilibrium the externally applied pressure can be considered equal to the internal swelling pressure of the gel as indicated below in equation 5.1.

$$\Pi_{net} + \Pi_{ion} = P_{ext} \tag{5.1}$$

Their results were obtained under conditions of free swelling, as such $P_{ext} = 0$. Equation 5.1 can therefore be re-written as

$$\Pi_{net}(H) = -\Pi_{ion}\ (H, \{C\}) \tag{5.2}$$

To test the ideal Donnan theory they postulated that ionic compositions [C] which had the same level of hydration [H] must have the same predicted values for Π_{ion}. Thus a plot of Π_{ion} vs H, where experimental values of H had been used to calculate Π_{ion} should be linear.

The ion swelling pressure in equations 5.1 and 5.2 can be theoretically derived using Donnan equilibrium theory. Donnan equilibrium refers to the unequal distribution of ions in an internal and external solution separated by a semi-permeable membrane or boundary condition. In simple terms the theory relates the concentration of ions in the external (bath) and internal solution (polymer) by

$$C_i^g = \lambda^{z_i} C_i^b \tag{5.1}$$

where λ is the Donnan ratio or Donnan partitioning co-efficient, C_i^g and C_i^b is the concentration of ions in the polymer and bath solution respectively, and z_i is the valence of the ion in question. Assuming charge neutrality in the hydrogel the Donnan ratio is calculated as the only real positive root of equation 5.4 [2, 3].

$$(1-v_p)\sum z_i C_i^b \lambda^{Zi} + \frac{\sigma_0 V_p}{1+\lambda^{-1}10^{pH-pKa}} = 0 \tag{5.4}$$

In this equation v_p is the volume fraction of polymer in the hydrogel. In a gravimetric experiment the value is calculated according to equation 5.5, where *H* is the mass fraction of polymer in the hydrogel and ρ is the density of the polymer in question.

$$v_p = \frac{(1-H)}{1+(\rho-1)H} \tag{5.5}$$

The σ_0 value introduced in equation 5.4 is the concentration of pH responsive ionisable groups in the polymer, expressed in mol l^{-1}, calculated according to equation, 5.6.

$$\sigma_0 = \frac{1000 f \rho_g}{M_w(x)} \tag{5.6}$$

where *f* is the mass fraction of pH responsive component in the polymer, ρ_g is the density of the raw polymer. In multi-component polymers this can be calculated from the weighted average of the component homopolymers using Vegard's law, $\rho = (f\rho_a + (1-f)\rho_B)$ and $M_{w(x)}$ is the molecular weight of responsive component under study, for DEA this would be 185.26gmol^{-1}. pK_a is defined as the logarithmic form of K_a, the dissociation constant for loss of a proton, defined as $-\log_{10}K_a$.

Once the Donnan ratio has been determined using equation 5.4, it is then introduced into equation 5.7 using Van't Hoff's law [7] to calculate Π_{ion}/RT, the swelling pressure.

$$\frac{\Pi_{ion}}{RT} = \Sigma C^i(\lambda^{Zi} - 1) \tag{5.7}$$

Their initial test of the ideal Donnan theory failed. A plot of *H* against the theoretically derived ion swelling pressure (Π_{ion}) proved to be non-monotonic.

5.1.2 Modified Donnan theory

However, after recognising the failure of the ideal Donnan theory they suggested an alternative Heuristic model based on Donnan theory.

Using equations 5.4 and 5.7 Firestone *et al* assumed a fictional situation where the hydration level, H, was fixed at a known arbitrary value, H^*, in their case 0.7. Then in any particular set of simulations they held the hydration level constant, and with all other variables changing according to the solution conditions they calculated the corresponding ionic swelling pressure, Π_{ion}.

Clearly, as $\Pi_{net} + \Pi_{ion} = P_{ext}$, the swelling pressure determined in the fictional case must be equivalent to the additional pressure over ambient which is required to maintain the condition (minus pressure which is applied in the absence of ionic effects) $H = H^*$.

Using this hypothesis they postulated that any condition which lead to an increase in the calculated Π_{ion} at H^*=0.7 would in-fact lead to an increased H under conditions of free swelling. This theory although not perfect quite successfully predicted how changes in solution chemistry in buffer solutions altered the expansion ratio of their polymer system.

5.2 SWELLING SIMULATION USING DONNAN THEORY

5.2.1 Effect of ionic strength and solution species on the expansion ratio

In figure 5.1 the SAXS expansion ratio of $PMMA_{88}$-*block*-$PDEA_{223}$-*block*-$PMMA_{88}$ block copolymer was measured in both simple hydrochloric mineral acid and 0.01M citric acid buffer solution at pH 3.6. The ionic strength was varied up to a maximum of 1M using NaCl. Therefore any difference in expansion ratio between the two solutions can be directly attributed to the specific species in the solution.

Figure 5.1 indicates an ionic strength dependence on the expansion ratio in the two solutions. The extent of gel swelling for both solutions in the ionic strength range 0.1 – 0.5 M decreases as the ionic strength is increased. It is also evident that the expansion ratio of the two solutions between 0.1M and 0.5M ionic strength is similar.

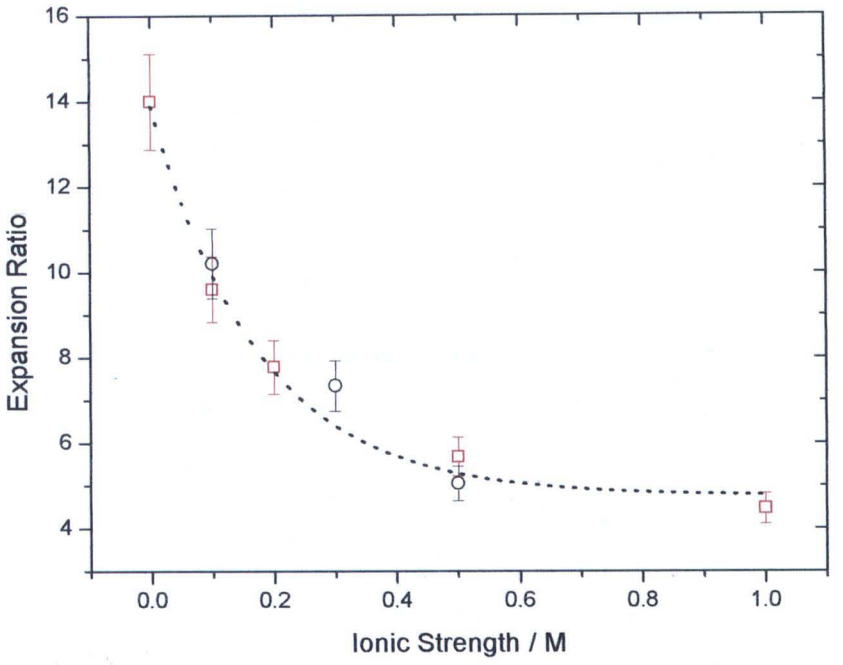

Figure 5.1: Variation of the SAXS expansion ratio with ionic strength for $PMMA_{88}$-*block*-$PDEA_{223}$-*block*-$PMMA_{88}$ annealed bulk films in ○ 0.01M citric acid and □ simple HCl mineral acid at pH 3.6, ionic strength varied using NaCl. Line shown to guide the eye.

5.2.2 Application of the modified Donnan theory

The modified Donnan equilibrium theory derived by Firestone *et al* has been used to calculate the theoretical osmotic swelling pressures inside the gel for the two solutions in figure 5.1.

The first step required to determine the theoretical swelling pressure inside a particular gel under a given set of conditions is to solve C_i^b, the concentration of ions in the external solution, as shown in equation 5.3. In buffered media containing polyprotic species such as citric acid or sodium phosphate this is not a trivial task. As citric acid was used in the majority of the swelling experiments in chapter 4 it will be used as an example here.

Citric acid shown in figure 5.2 is a trivalent acid, being capable of donating upto a maximum of three protons, with each new donating species being referred to a bronsted acid. The different species are $C_6H_8O_7$ (H_3A), $C_6H_7O_7^-$ (H_2A^-), $C_6H_6O_7^{2-}$ (HA^{2-}) and $C_6H_5O_7^{3-}$ (A^{3-})

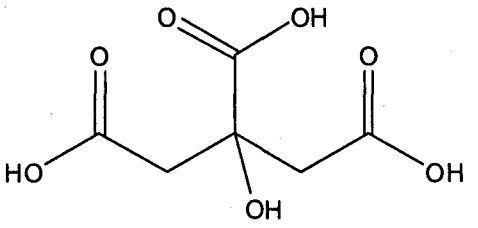

$pK_{a1} = 3.13$

$pK_{a2} = 4.76$

$pK_{a3} = 6.40$

Figure 5.2: Citric acid molecule, pK_a taken from reference [8].

In any polyprotic acid the relative fraction of each bronsted acid species in solution at a given pH is determined from its pK_a values. Citric acid has three pK_a values, 3.13, 4.76 and 6.40 [9].

To calculate the relative proportions of each species in solution an expression is needed which relates together the three acidity constants, the total concentration of citric acid and the hydronium ion concentration. To setup the expression, $C_6H_8O_7$ (H_3A) is treated as the parent acid, and the total concentration of hydronium ion is given by D. The three acidity constants required are given below [10],

$$H_3A\ (aq) + H_2O\ (l) \rightleftharpoons H_3O^+\ (l) + H_2A^-\ (aq) \tag{5.8}$$

$$K_{a1} = \frac{[H_3O^+][H_2A^-]}{[H_3A]} = \frac{D[H_2A^-]}{[H_3A]} \tag{5.9}$$

$$H_2A^-\ (aq) + H_2O\ (l) \rightleftharpoons H_3O^+\ (l) + HA^{2-}\ (aq) \tag{5.10}$$

$$K_{a2} = \frac{[H_3O^+][HA^{2-}]}{[H_2A^-]} = \frac{D[HA^{2-}]}{[H_2A^-]} \tag{5.11}$$

$$HA^{2-}\ (aq) + H_2O\ (l) \rightleftharpoons H_3O^+\ (l) + A^{3-}\ (aq) \tag{5.12}$$

$$K_{a3} = \frac{[H_3O^+][A^{3-}]}{[HA^{2-}]} = \frac{D[A^{3-}]}{[HA^{2-}]} \tag{5.13}$$

The total concentration of citric acid in solution is expressed as:

$$[H_3A]+[H_2A^-]+[HA^{2-}]+[A^{3-}]=C \tag{5.14}$$

The total concentration of citric acid in solution is now expressed by four unknown concentrations, as shown in equation 5.14. To solve this equation the acidity constants (5.9, 5.11, 5.13) need to be inputted into the expression. From right to left in equation 5.14, K_{a3} can be used to express $[A^{3-}]$ in terms of HA^{2-}, then K_{a2} can be used to express HA^{2-} in terms of H_2A^- and so forth, as shown in equation 5.15.

$$[A_3^-]=\frac{K_{a3}[HA^{2-}]}{D}=\frac{K_{a3}K_{a2}[H_2A^-]}{D^2}=\frac{K_{a3}K_{a2}K_{a1}[H_3A]}{D^3} \tag{5.15}$$

$$K=D^3+D^2K_{a1}+DK_{a1}K_{a2}+K_{a1}K_{a2}K_{a3} \tag{5.16}$$

$$f(H_3A)=\frac{[H_3A]}{C}=\frac{D^3}{K} \tag{5.17}$$

$$f(H_2A^-)=\frac{[H_2A^-]}{C}=\frac{D^2K_{a1}}{K} \tag{5.18}$$

$$f(HA^{2-})=\frac{[HA^{2-}]}{C}=\frac{DK_{a1}K_{a2}}{K} \tag{5.19}$$

$$f(A^{3-})=\frac{[A^{3-}]}{C}=\frac{K_{a1}K_{a2}K_{a3}}{K} \tag{5.20}$$

Using the general equations 5.17 – 5.20 the fractional composition of each bronsted acid species in the solution can be calculated. Only the hydronium ion concentration of the solution and pK_a value(s) of the buffer species is required. Figure 5.3 has been constructed using these equations and demonstrates how the fractional composition of species changes in a 0.01M citric acid species with changes in solution pH.

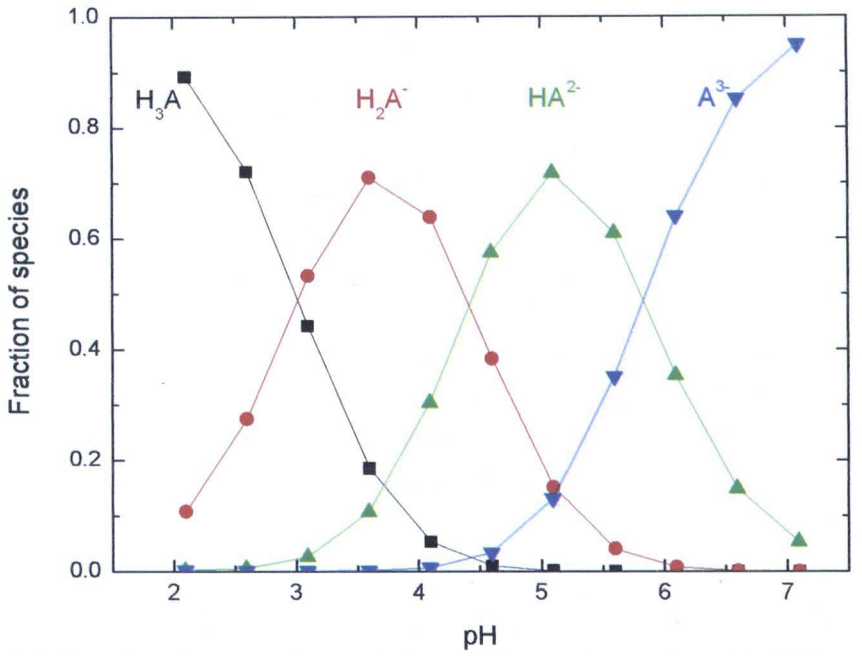

Figure 5.3: Fractional composition of citric acid species, H_3A, H_2A^-, HA^{2-} and A^{3-}, in a 0.01M citric acid buffer as a function of pH.

Complications arise in this theory when one considers that the ionic strength of the buffer changes the pK_a of the buffer species. This influence is often overlooked when preparing buffer solutions. This affect can be subtley noticed if you add salt to a prepared buffer, as both the pH and ionic strength will change. Fortunately the influence of salt on the pK_a can be predicted from the following Debye-Huckel relationship, as shown in equation 5.21 [11].

$$pK_a{}^{i} = pK_a + (2z_a - 1)\cdot\left[\frac{A\sqrt{I}}{1+\sqrt{I}} - 0.1.I\right] \qquad (5.21)$$

where $pK_a{}^{i}$ is the modified pK_a, z_a is the charge on the conjugate acid, I is the ionic strength of the solution and A is a constant which has a value of approximately 0.5 (this is a temperature dependant variable, see table 5.1 [11]). These subtle changes in pK_a have a significant effect on the concentration of species due to the logarithmic scale.

Table 5.1: Values of the temperature dependant constant A for use in equation 5.21 [11]

Temperature / °C	A
0	0.4918
10	0.4989
20	0.5070
25	0.5114
30	0.5161
37	0.5321
40	0.5262
50	0.5373
60	0.5494

Table 5.2 and 5.3 list the concentration of individual species in HCl mineral acid and 0.01 M citric acid buffer solutions respectively, as used in figure 5.1. Each solution has a pH of 3.6 with an ionic strength that varies between 0.01M to 1M (adjusted using NaCl). The concentration of each individual species was calculated using equations 5.8 to 5.21, which includes use of the ionic strength correction factor. It is immediately obvious that a change in ionic strength for the buffer solution has a significant effect on the calculated concentration of individual species in solution. In each case the concentration of salt added to adjust the ionic strength is simply the total ionic strength required minus the ionic strength due to the buffer species acting alone.

With information now known about the total concentration of all ionic species in the external solution surrounding the gel, it is possible to calculate the Donnan partitioning co-efficient. The first step required to achieve this is to input the individual concentrations of each species into equation 5.4, along with several experimental variables for the polymer under study, these include σ_0, v_p and pK_a. For $PMMA_{88}$-*b*-$PDEA_{223}$-*b*-$PMMA_{88}$ 6.8 was used for the pK_a as determined in chapter 4. σ_0 was calculated following equation 5.22 (using the density values in chapter 3 for DEA and MMA).

$$\sigma_0 = \frac{1000 f \rho_g}{M_w(x)} = \sigma_0 = \frac{1000 \times 0.7 \times 1.08}{185.26} = 4.08 \qquad (5.22)$$

The Donnan ratio is calculated as the only real positive root of equation 5.4. Due to the complexity of this calculation the root was solved using Maple 13 software. Once the Donnan partitioning co-efficient is known for each species this number is then inputted into equation 5.7 to give a theoretical swelling pressure.

The calculated theoretical swelling pressures listed in table 5.2 and 5.4 have been plotted in figure 5.4. Two different v_0 values have been used to simulate the data, namely 0.3 and 0.25. These values were chosen as they fit the data quite well. It should be noted that the value of v_0 has an influence on the swelling pressures, with a lower value causing a shift in the data to lower values of *I*, and an overall reduction in the swelling pressure.

Table 5.2: Concentration of ionic species at different ionic strengths in a hydrochloric acid solution at pH 3.6. The calculated theoretical osmotic swelling pressure inside the $PMMA_{88}$-*block*-$PDEA_{223}$-*block*-$PMMA_{88}$ hydrogel is determined for each ionic strength solution. σ_0 = 4.09, v_p = 0.3/0.25, pK_a = 6.8, M_w (DEA) =185.26gmol^{-1}. Ionic strength adjusted using sodium chloride.

Ionic strength / M	Salt concentration added to maintain ionic strength / 10^{-3} M		Acid concentration to adjust pH / 10^{-4} M		Donnan Ratio v=0.3 10^{-2}	Donnan Ratio v=0.25 10^{-2}	Osmotic pressure v=0.3/ M	Osmotic pressure v=0.25/ M
	$[Na]^+$	$[Cl]^-$	$[H]^+$	$[Cl]^-$				
0.01	0.97	0.97	2.51	2.51	0.62	0.78	1.60	1.26
0.05	4.97	4.97	2.51	2.51	2.90	3.72	1.62	1.25
0.1	9.97	9.97	2.51	2.51	5.74	7.35	1.55	1.17
0.2	19.97	19.97	2.51	2.51	11.32	14.43	1.39	1.02
0.3	29.97	29.97	2.51	2.51	16.70	21.10	1.25	0.89
0.5	49.97	49.97	2.51	2.51	26.58	32.81	1.01	0.69
0.8	79.97	79.97	2.51	2.51	38.84	46.23	0.77	0.50
0.9	89.97	89.97	2.51	2.51	42.26	49.76	0.71	0.46
1.0	99.97	99.97	2.51	2.51	45.39	52.91	0.66	0.42

Table 5.3: Concentration of individual ionic species at different ionic strengths in a 0.01M citric acid buffer prepared at pH 3.6. σ_0 = 4.09, v_p = 0.3/0.25 pK_a = 6.8, M_w (DEA) =185.26gmol^{-1}. Ionic strength adjusted using sodium chloride.

Ionic strength / M	Concentration of Citric acid species / 10^{-6} M			Salt concentration added to maintain ionic strength / 10^{-2} M		Acid concentration to adjust pH / 10^{-4} M		Donnan Ratio v=0.3 10^{-2}	Donnan Ratio v=0.25 10^{-2}
	$[A^{3-}]$	$[HA^{2-}]$	$[H_2A^{-}]$	$[Na]^+$	$[Cl]^-$	$[H]^+$	$[Cl]^-$		
0.01	0.18	67.47	71.42	4.02	4.02	2.51	2.51	3.21	3.66
0.05	0.39	90.26	71.21	4.02	4.02	2.51	2.51	5.06	5.98
0.1	0.61	106.03	70.79	8.97	8.97	2.51	2.51	7.85	9.01
0.2	0.93	124.6	70.09	18.9	18.9	2.51	2.51	12.4	15.4
0.3	1.20	135.23	69.63	28.9	28.9	2.51	2.51	17.4	21.8
0.5	1.45	144.55	69.18	48.9	48.9	2.51	2.51	27.0	33.2
0.8	1. 43	144.00	69.21	78.9	78.9	2.51	2.51	38.9	46.4
0.9	1.37	141.69	69.32	88.9	88.9	2.51	2.51	42.5	50.0
1.0	1.29	138.76	69.47	98.9	98.9	2.51	2.51	45.6	53.1

Table 5.4: Theoretical osmotic swelling pressure inside a $PMMA_{88}$-*b*-$PDEA_{223}$-*b*-$PMMA_{88}$ hydrogel determined in 0.01M citric acid at varying ionic strength adjusted using NaCl.

Ionic strength / M	Osmotic pressure v=0.3/ M	Osmotic pressure v=0.25/ M
0.01	0.95	0.75
0.05	1.24	0.98
0.1	1.34	1.04
0.2	1.31	0.97
0.3	1.21	0.87
0.5	1.00	0.68
0.8	0.77	0.50
0.9	0.71	0.46
1.0	0.66	0.42

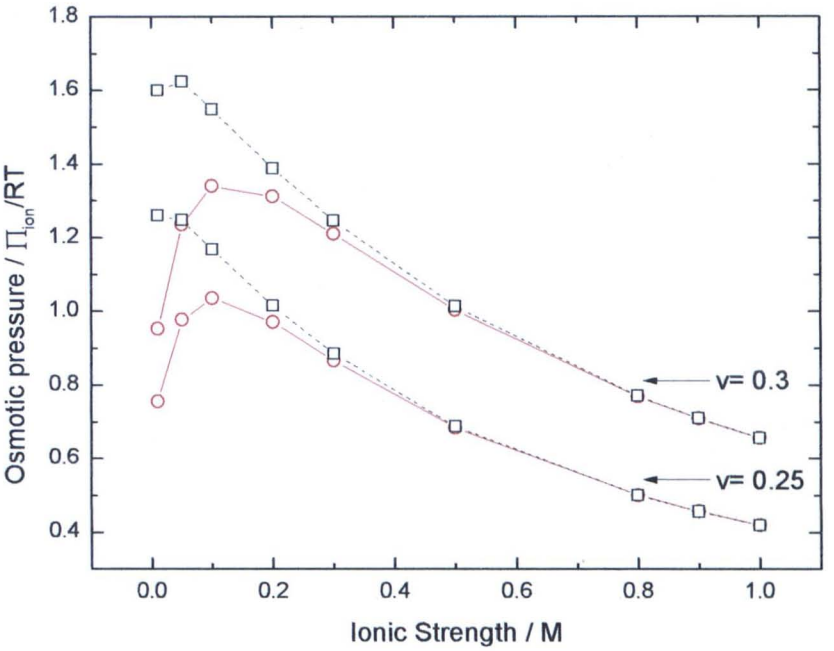

Figure 5.4: Theoretical osmotic swelling pressure for $PMMA_{88}$-*block*-$PDEA_{223}$-*block*-$PMMA_{88}$ measured in both ○ 0.01M citric acid buffer, and □ simple mineral acid at pH 3.6 using NaCl to change the ionic strength between 0M and 1.0M. Data points taken from table 5.2 and 5.4.

Donnan theory simulations indicate that in the ionic strength range 0.1M -1.0M both the buffered and un-buffered solutions have a similar osmotic swelling pressure. Appreciable differences are evident when the ionic strength is lowered below 0.1M. Clearly there is a maximum in the swelling pressure for buffered media at around 0.1M which begins to reduce as the ionic strength is further lowered; this is not observed in the un-buffered case which continues to rise. This marked difference at low ionic strength is due to the presence of trivalent species in the buffer, as less trivalent species are required to maintain electroneutrality thus exerting a smaller swelling pressure. This was discussed in chapter 4 along with an isoelectric exchange argument which explains why you see a maximum in the swelling pressure. In the current study the concentration of salt in the buffered media was not measured below 0.1M so it is not possible to confirm the theoretical curve at this value.

$PMMA_{88}$-*block*-$PDEA_{223}$-*block*-$PMMA_{88}$ hydrogels swollen in simple mineral acid in figure 5.2 show a general reduction in their expansion ratio as the ionic strength is increased. This is entirely consistent with the theoretical predictions which follow a similar trend. This trend is also observed for gels swollen in buffer solution between the ionic strength values 0.1M to 0.5M. Simulations also indicate that the swelling pressure of the two solutions is similar in the ionic strength range 0.1M -0.5M which is consistent with the swelling results.

This general reduction in the osmotic pressure is due to the ideal Donnan effect, and can be explained if one inspects equation 5.23,

$$(1-v_p)\sum z_i C_i^b \lambda^{zi} + \frac{\sigma_0 V_p}{1+\lambda^{-1}10^{pH-pK_a}} = 0 \qquad (5.23)$$

It is evident that as the ionic strength is progressively increased, the total concentration of species in solution, C increases, and to satisfy the electroneutrality condition $z_i C_i = 0$, the Donnan partitioning co-efficient approaches unity.

5.3 CONCLUSION

The internal osmotic swelling pressure inside $PMMA_{88}$-*block*-$PDEA_{223}$-*block*-$PMMA_{88}$ hydrogels was qualitatively calculated using modified Donnan equilibrium theory. The results indicate that the molecular response of the hydrogel to changes in the ionic strength is driven primarily by the ionic osmotic swelling pressure.

REFERENCES

1. Chiu, H.-C., T. Hsiue, and W.-Y. Chen, 2004, Polymer. **45**(5): p. 1627-1636.
2. Firestone., B.A. and R.A. Siegel, Journal of Biomaterials Science, Polymer Edition, 1994. **5**(5): p. 433-50.
3. Rieka, J. and T. Tanaka, Macromolecules, 1984. **17**: p. 2916-2921.
4. Tanaka, T., Scientific American 1981. **124**: p. 138.
5. Flory, P.J., *Principles of Polymer Chemistry.* 1953, New York: Cornell University Press. 595.
6. Flory, P.J., Journal of Chemical Physics, 1942. **10**: p. 51-61.
7. Benedek, G.B. and F.M.H. Villars, *Physics with Illustrative Examples from Medicine and Biology, v. 2: Statistical Physics.* 2000, New York: Springer-Verlag. 525.
8. Christian, G.D., *Analytical Chemistry.* 2004, New Jersey: John Wiley &Sons. 298, 804.
9. Windholz, M., S. Budavari, R.F. Bluemettic, and E.S. Otterbein, *The Merck Index.* 10th Edition ed. 1983: Merck and co. 330-331.
10. Atkins, P. and J.d. Paula, *Elements of Physical Chemistry.* 3 ed. 2000, Oxford: Oxford University Press.
11. Beynon, R.J. and J.S. Easterby, *Buffer Solutions The Basics*, ed. R. J.Beynon, T. A.Brown, and C. Howe. 1996, Oxford: Oxford University Press. 1.

Chapter 6
Quantifying "kinetic" hydrogel pH response using SAXS

6.1 INTRODUCTION

To date most swelling kinetic studies performed on pH responsive hydrogels have been conducted by means of gravimetric analysis. Gels are often prepared as a disc and during the course of their expansion the samples are periodically weighed [1-7]. Comparison between the initial dry mass of the gel (M_0) and expanded mass (M_s) gives an expansion ratio, as shown below in equation 6.1.

$$ER = \frac{M_s - M_0}{M_0} \tag{6.1}$$

6.1.1 Limitations of gravimetric swelling kinetics

Unfortunately using gravimetric techniques to measure swelling ratios has a number of limitations. From an experimental point of view, the samples need to be weighed periodically to measure the uptake of water. To measure fast dynamic response in hydrogels, in the order of minutes, more frequent sampling is required. This may simply not be possible, and can also lead to several problems. Repeated manipulation of the sample can result in mechanical failure and ultimately cracking of the gel. Evidently this will have a detrimental effect on the calculated expansion ratio. To make this effect less pronounced the frequency of sampling has to be reduced. Clearly this makes gravimetric analysis a less attractive method, significantly reducing its usefulness for measuring fast kinetics.

6.1.2 Alternative methods to measure swelling kinetics

Methods used to overcome the problems associated with gravimetry include the use of video microscopy [6, 8, 9]. This technique measures the change in the macroscopic size of the gel during swelling. Although this technique can be useful, one must consider that gels can swell anisotropically. Samples can twist during expansion and this makes measuring the size inaccurate. Additionally, to visualise a hydrogel in water there must be a difference in the refractive index of the gel and the surrounding solution. However, as the gel swells and accommodates more solution its refractive index begins to approach that of the solution. With conventional microscopy, in which a real image of the material under study is formed by refraction or reflection, it becomes increasingly difficult to visualise such objects in water as the refractive indices are so similar. The advantage of this technique as opposed to gravimetric methods is that it is an *in-situ* technique and does not require any manipulation of the sample. This reduces the chance of errors which are associated with gravimetric analysis and allows swelling to be monitored with higher resolution.

6.1.3 Measuring kinetics in hydrogels with greater resolution

The problems which are associated with measuring kinetics gravimetrically clearly present an opportunity to design a new *in-situ* analysis method. Any new technique should enable the kinetics to be measured with both high accuracy and high resolution. Another very significant problem with gravimetry as already discussed in chapter 4 is that you are measuring the macroscopic response. Therefore all information about the response of the polymer at the level of single polymer chains is lost.

6.1.4 Evaluating the use of SAXS for measuring swelling kinetics

Small angle X-ray scattering (SAXS) is one possible technique to overcome this problem. This technique can be easily adapted for *in-situ* analysis and additionally it allows the molecular response of the material to be analysed.

To test the effectiveness of SAXS for measuring the swelling kinetics of hydrogels a pH responsive A-B-A type polybasic triblock copolymer was utilised, where A and B represent poly (methyl methacrylate) (PMMA) and poly(2-(diethylamino)ethyl methacrylate) (PDEA) respectively [10]. This polymer undergoes microphase separation to form a "liquid like" BCC structure composed of PMMA spheres in a matrix of pH responsive PDEA. SAXS can be used to measure the average distance between the hard PMMA domains, as described in chapter 4. When the polymer expands the distance between the PMMA domains increases. This is representative of both a molecular and macroscopic increase in the size of the polymer.

6.1.5 Factors effecting swelling kinetics

It is perhaps worth emphasising at this point that the rate of solvent uptake in hydrogels is limited by several factors. Some of these are related to the polymer properties, (i.e size and shape of the gel) whilst others are related to the solution properties used to swell the gel.

Tanaka et al have previously demonstrated that the rate of solvent diffusion in hydrogels is related to the square of the size of smallest dimension of the gel [11]. In the context of chemical actuation applications, fast switching requires the gel dimensions to be as small as possible. And when swelling rates are particularly high techniques such as gravimetry do not offer the resolution required to quantify the response.

The rate of swelling in hydrogels is also strongly dependant on the chemical identity of the species which are used to swell the gel. Such effects have been investigated by Siegel *et al.* They investigated the swelling kinetics on a chemically crosslinked, methyl methacrylate/ dimethylamino ethyl methacrylate gel [4], which swells in acidic conditions. They prepared gels as circular disks between 330 and 370 microns in thickness. Swelling was measured gravimetrically and the expansion ratio was determined using the formula expressed in equation 6.1. Due to the thickness of samples used in their study, swelling was typically measured in excess of 6 hours, at which point samples were demonstrated to have reached final equilibrium.

Using a series of buffers and mineral acids prepared at different concentrations they performed a systematic study to identify if there was any noticeable difference in swelling rates between the different media. They identified several key differences. Gels swollen in buffer showed a greater rate of expansion compared to the same gel swollen in mineral acid at the same pH. In buffered solution they found that the rate of expansion was related to the concentration of buffer. Buffers prepared at higher concentration had a greater rate of swelling. Additionally they observed that for efficient protonation of the polymer it was necessary that the pK_a of the buffer was lower than the pK_a of the polymer.

It was suggested that the enhanced rate of expansion in buffered systems was due to the "stealthing ability" of the proton within the buffer. At the very beginning of expansion a hydrogel is largely in its uncharged state. As the polymer begins to expand, the chains within the polymer start to protonate. As more of the polymer begins to expand a cloud of positive charge begins to accumulate on the surface of the gel. This charge acts as a barrier, also referred to as a Donnan barrier, shown in figure 6.1. This barrier makes it more difficult for free dissociated protons, such as those found in hydrochloric acid to enter the core of the gel. This phenomenon explains why the rate of expansion is often reduced in simple mineral acid solutions.

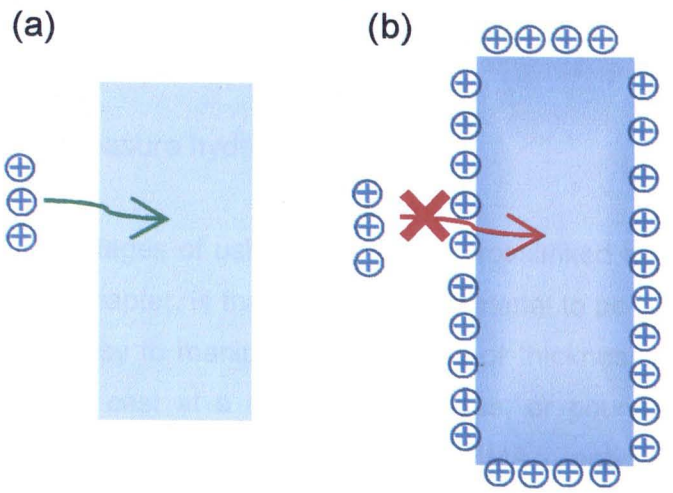

Figure 6.1: (a) Hydrogel largely in its uncharged state at the beginning of expansion (b) Donnan barrier formed at the surface of a polymer during the course of protonation. The barrier hinders the transport of free protons to the polymer core and therefore reduces the rate of expansion.

When a buffer is used to swell a gel the concentration of dissociated and un-dissociated species depends on several factors. These include the pK_a's of the buffer species, the local pH and the concentration at which the buffer was prepared. All these variables are encompassed in equation 6.2, where C_{AH} is the concentration of un-dissociated buffer in the parent acid form, C_{AT} is the total concentration of buffer, pH is the negative log of the hydrogen ion concentration and pK_a is the acid dissociation constant. Siegel et al also found that the highest rate of swelling was in buffer which had a pK_a lower than the pK_a of the gel. Additionally they discovered that the pH of the solution needed to be lower than the pK_a of the buffer.

$$C_{AH} = \frac{C_{AT}}{1+10^{pH-pK_a}} \tag{6.2}$$

They explained the enhanced rate of swelling in buffers in the following way. When the pH of the solution is below the pK_a of the buffer (greater than 1 unit), the majority of the buffer is in the un-dissociated form. In this situation the un-dissociated buffer component can enter the polymer core without feeling any electrostatic repulsion from the Donnan charge barrier (see figure 6.1). The buffer acts as a "stealth proton", masking its charge until it becomes dissociated upon protonation in the gel interior. The buffer therefore provides both the charge and counter-ion.

6.1.6 Using SAXS to measure hydrogel kinetics

One of the advantages of using a physically crosslinked hydrogel, like the one investigated within this chapter, is that it allows the material to be processed with more control. It is relatively easy to manipulate the shape or thickness of the sample. The material can be solvent cast at a specified thickness, or poured into a mould if a specific shape is required. The $PMMA_{180}$-$PDEA_{453}$-$PMMA_{180}$ polymer used for swelling experiments within this chapter was processed as a thin film. It was 80 microns in thickness and approximately 5mm x 5mm in length and width. The film thickness was kept as small as possible to facilitate an increase in the expansion rate. The lower limit

on the thickness of the sample was related to the scattering power of the material. Eighty microns was found to be the optimum thickness. The length and width of the

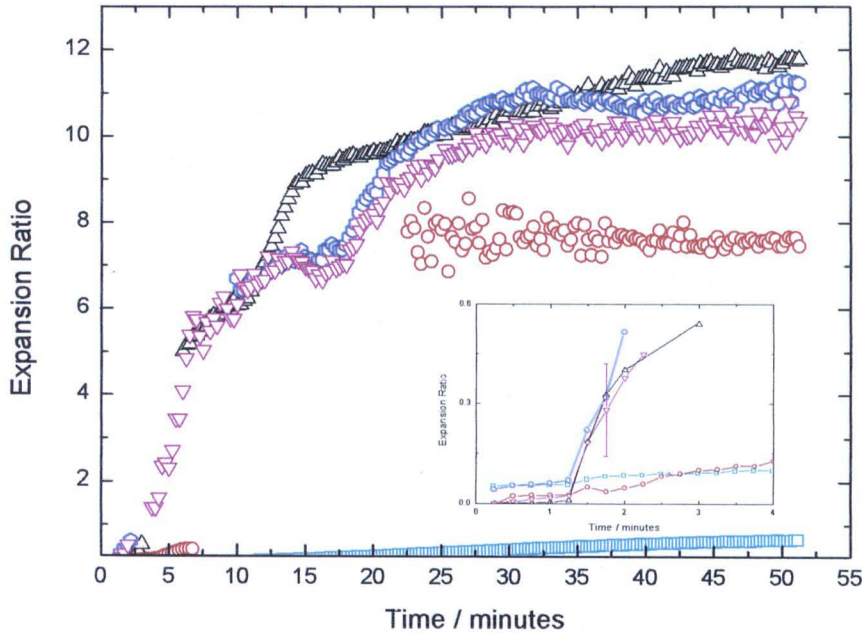

Figure 6.2: Change in the expansion ratio of an 80 micron thick film of $PMMA_{180}$-$PDEA_{453}$-$PMMA_{180}$ in □ hydrochloric acid, ▽ 0.01M citric acid, ○ 0.01M acetic acid, △ 0.03M acetic acid and ⬡ 0.05M acetic acid at pH 3.7 at an ionic strength of 0.1M (NaCl). Inset: Exploded view of the onset on swelling.

sample was limited mainly by the size of liquid cell. A detailed diagram of the liquid cell can be found in the appendix, section 9.3. In a typical swelling experiment a piece of the film was fixed inside the liquid cell. A continual flow of solution was then pumped through the liquid cell, and 2D SAXS images of the gel were taken every fifteen seconds.

Each 2D scattering pattern was integrated to determine the domain spacing of the polymer. This value was input into equation 6.3 to determine the expansion ratio, as already discussed in chapter 4.

$$R_{SAXS} = \frac{d^3 - {d_0}^3}{{d_0}^3} \tag{6.3}$$

d = equilibrium domain spacing and d_0 = dry domain spacing

Figure 6.2 shows the kinetic expansion data collected for an 80 micron thick annealed film of $PMMA_{180}$-$PDEA_{453}$-$PMMA_{180}$ copolymer swollen in a range of different solutions. These solutions included several buffers, namely acetic acid and citric acid, and a simple hydrochloric mineral acid. The concentration of each buffer was varied between 0.01M and 0.05M at a fixed ionic strength of 0.1M using NaCl, at a pH of 3.7. The pH was specifically chosen as it is far below the pK_a of the polymer.

Swelling data was collected over a period of fifty minutes with a time resolution of 15 seconds. The results indicate there is a significant difference in swelling rates between buffered solutions compared to simple mineral acid at the same pH. Over a period of 50 minutes polymer swollen in mineral acid shows very little increase in its expansion ratio, less than 0.5 a unit. The same polymer swollen in buffer show much faster rates of swelling. After approximately 30 minutes the increase in swelling in the buffered solutions starts to plateau signifying the polymer has reached its maximum equilibrium expansion ratio. The expansion ratio at equilibrium for 0.01M citric acid, 0.05M acetic acid and 0.03M acetic acid is 10.3, 11.0 and 11.7 respectively. 0.01 M acetic acid has a significantly lower value of 6.5. This will be explained later.

It is clear from figure 6.2 that the initial onset of expansion and final equilibrium can be resolved; however, there are regions in between where no data is present. These areas will be explained in greater detail later.

Expanding upon figure 6.2, the very onset of expansion was investigated. The results are shown in figure 6.3. Within a period of three minutes polymer swollen in hydrochloric acid and 0.01M acetic acid show the slowest rate and overall increase in expansion. The rate of expansion has been estimated from the gradient of the curve. The remaining three buffer solutions show a much greater increase in swelling. However there is very little difference in the rate of expansion between the three; it could be argued that 0.05M acetic acid has a slightly higher rate. Clearly the overall amount of expansion in all solutions is small, however, SAXS has demonstrated its ability at resolving the molecular expansion ratio in short time scales, which would have been difficult to achieve with another technique.

The results presented in figure 6.2 clearly demonstrate that the Donnan shielding effect discovered by Siegel is equally applicable to this polymer system. That is to say the rate of swelling in HCl is significantly reduced due to a charge build up on the surface of the hydrogel with impedes further influx of H^+.

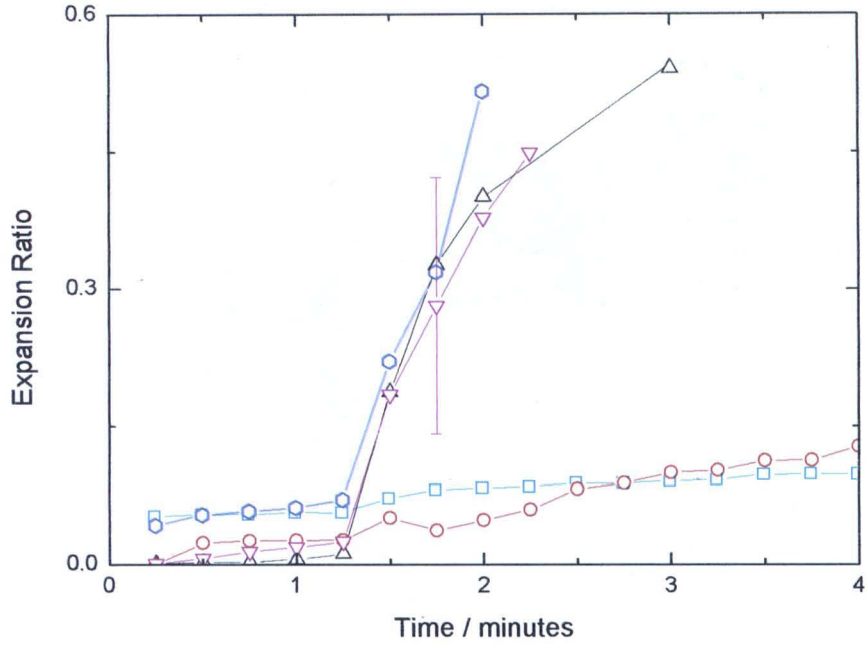

Figure 6.3: Change in the expansion ratio of an 80 micron thick film of $PMMA_{180}$-$PDEA_{453}$-$PMMA_{180}$ measured in □ hydrochloric acid, ▽ 0.01M citric acid, ○ 0.01M acetic acid, △ 0.03M acetic acid and ⬡ 0.05M acetic acid at pH 3.7 at an ionic strength of 0.1M (NaCl). A representative error bar is shown for one data point.

Further examination of figure 6.3 indicates that the rate of swelling is much faster in 0.03M and 0.05M acetic acid compared to 0.01M acetic acid. This is due to the buffers prepared at higher concentration having more H^+ available to protonate the gel and thus enhances the rate of expansion.

A diagram demonstrating how SAXS was used to measure the pH response of phase separated thin films of $PMMA_{180}$-$PDEA_{453}$-$PMMA_{180}$ polymer is shown in figure 6.4. The illustration shows both the macroscopic and molecular response of the polymer, indicated using microscopy and SAXS images respectively. The microscopy images show how the polymer in its initially dry state begins to expand, going through an intermediate stage where both an unexpanded core and an expanded periphery are present. Once the polymer has reached equilibrium a single phase is present.

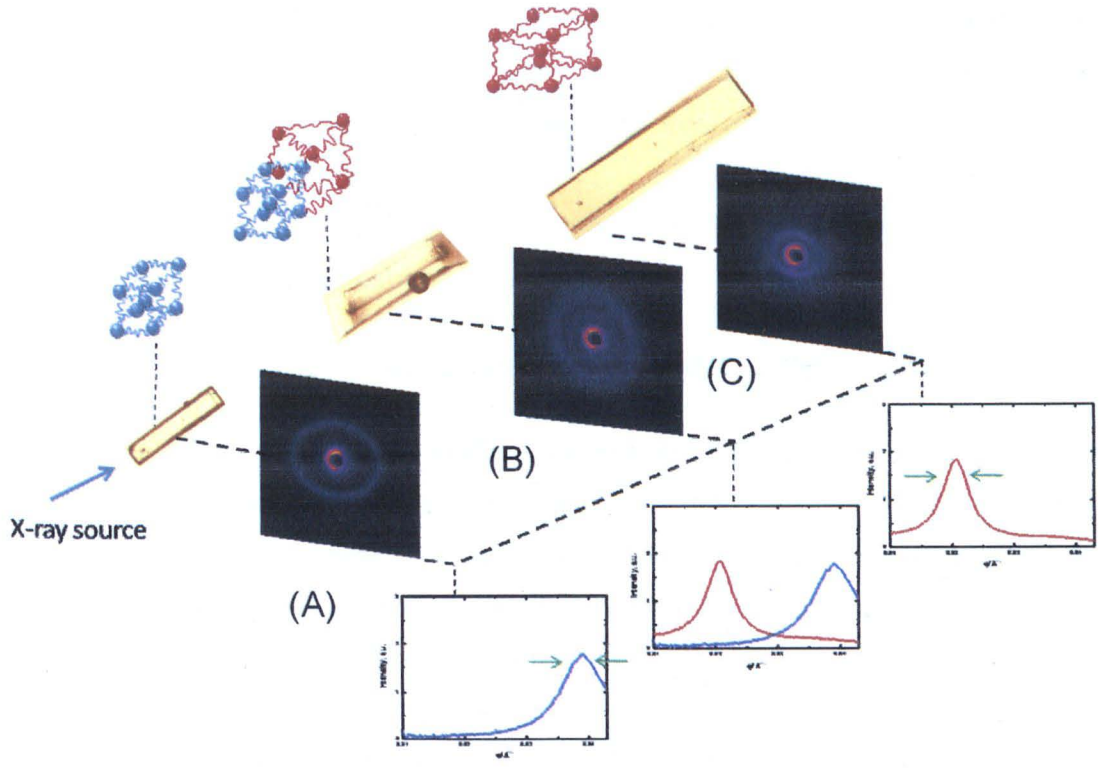

Figure 6.4: A schematic illustration showing the macroscopic and molecular changes in the pH responsive of PMMA-*block*-PDEA-*block*-PMMA during the course of expansion, three stages are shown (a) initial dry polymer (b) intermediate expansion and (c) full equilibrium expansion. Integration of the 2D SAXS data at each stage are also shown illustrating how the peak maximum and peak width changes during the course of expansion.

These three stages are captured in much greater detail using SAXS. The graphs in figure 6.4 are an integration of the 2D SAXS data. They show the primary structure peak of the polymer. The position of this peak represents the domain spacing of the polymer, simplistically this is the distance between PMMA glassy domains. This domain spacing was input into equation 6.3 to calculate the SAXS expansion ratio. The 2D SAXS image shown in figure 6.4a is what is typically observed for polymers in the dry state. They have a single circular ring.

When the polymer is immersed in solution it goes through an intermediate swelling regime, where it contains parts which are both swollen and un-swollen. In the 2D SAXS pattern in figure 6.4b you can see two circular rings. The position of each ring represents the domain spacing of the polymer. The ring closest to the beam stop

represents the expanded periphery of the polymer and the ring further away represents the unexpanded core. As the polymer continues to expand the ring gets smaller and becomes closer to the beam stop, this represents an increase in the molecular size of the polymer.

At final equilibrium as shown in 6.4c a single ring is present which represents the final domain size of the expanded polymer.

6.1.7 Change in structure peak half-height peak width during expansion

In addition to measuring the change in expansion ratio for each polymer, the change in half height peak width was also determined. The half height peak width of the structure peak represents the distribution of chain lengths between the PMMA domains. A more "polydisperse" sample which has a greater distribution of different lengths should have a larger peak width.

The change in half height peak width during the course of expansion was determined using the "x-fit" Gaussian peak fitting program. An example of a typical peak fitting result is shown in figure 6.5.

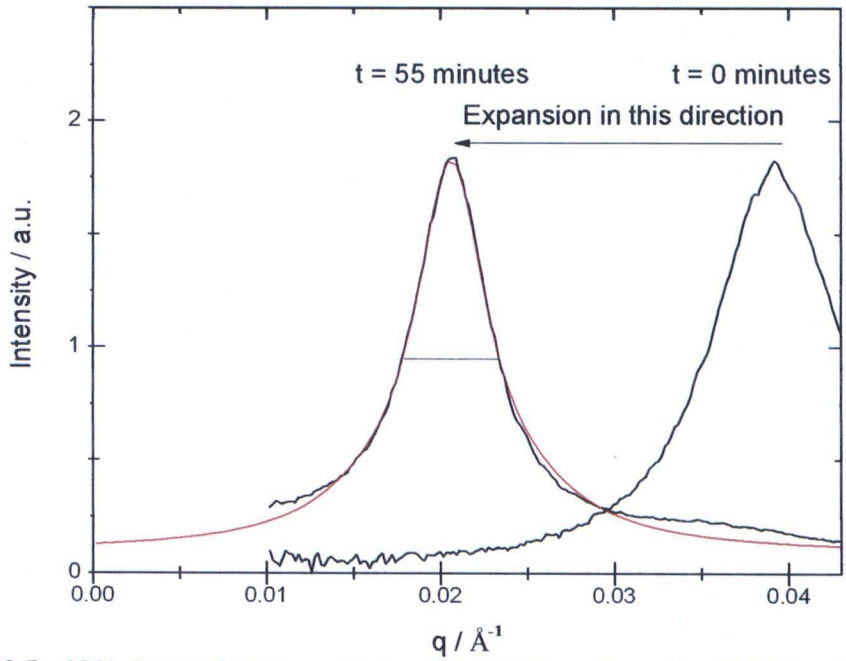

Figure 6.5: 360° integral traces of the 2D SAXS pattern for $PMMA_{180}$-$PDEA_{453}$-$PMMA_{180}$ swollen in 0.01M citric acid, at time = 0 and 55 minuses. Gaussian peak fitting used to determine the half height peak width (example shown for the expanded structure peak only).

In addition to measuring the peak width the program was also responsible for tracking the change in peak position. In the example shown in figure 6.5 the peak at time = 0 has a half height peak width of 0.00766 $Å^{-1}$. During the course of expansion the peak position moves to a lower value of q, and additionally the peak width has reduced to 0.00549 $Å^{-1}$.

The dynamic change in half height peak width during expansion is shown for several cases in figures 6.6 – 6.8. In each figure, the change in peak width is calculated using equation 6.4, where σ_0 represent the peak width of the initially unswollen gel and σ_t is peak width at a given time of swelling.

$$\Delta\sigma = \sigma_t - \sigma_0 \qquad (6.4)$$

This equation infers that a "positive change in peak width" corresponds to a situation where the polymer chains are becoming more disperse than the sample at t=0. In the opposite case, where negative changes in peak position are reported, the chains are becoming less disperse than the dry sample.

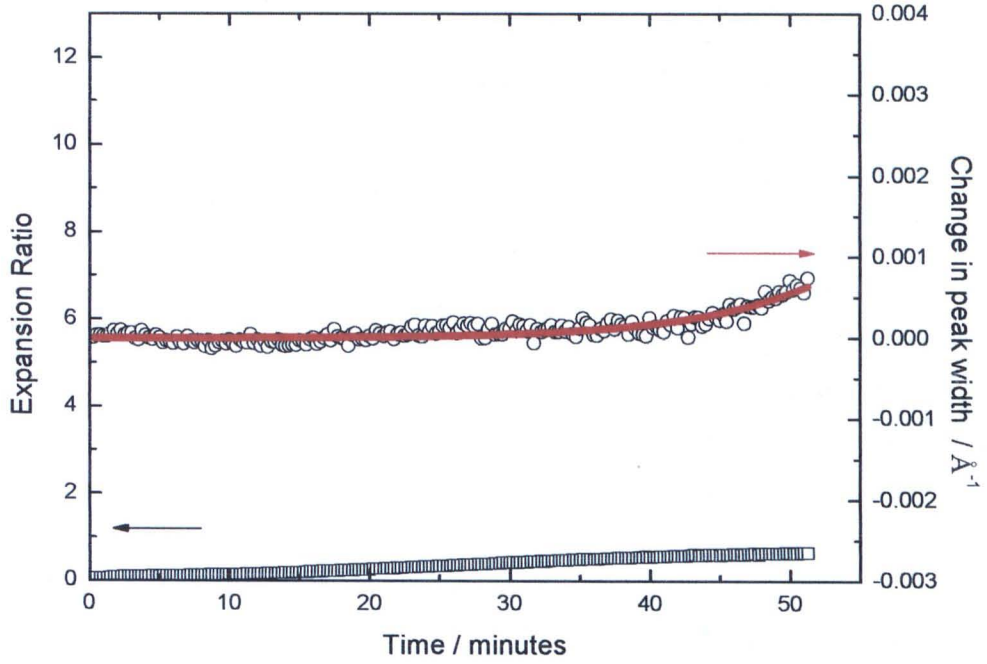

Figure 6.6: Change in the (a) □ expansion ratio (b) ○ peak width, of an 80 micron thick film of $PMMA_{180}$-$PDEA_{453}$-$PMMA_{180}$ measured in HCl at pH 3.7 at an ionic strength of 0.1M (NaCl).

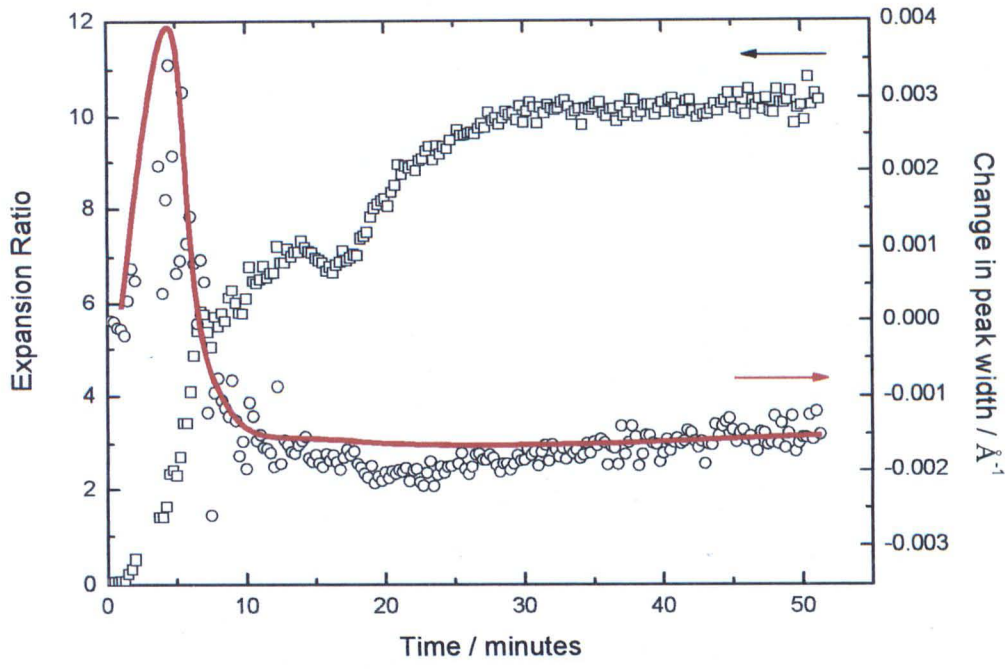

Figure 6.7: Change in the (a) □ expansion ratio (b) ○ peak width of an 80 micron thick film of $PMMA_{180}$-$PDEA_{453}$-$PMMA_{180}$ measured in 0.01M citric acid at pH 3.7 at an ionic strength of 0.1M (NaCl). Best fit line drawn "by hand" to help visualise the data.

Polymer expanded in mineral acid in figure 6.6 shows no significant change in the peak width during the first 55 minutes of expansion. This is expected as there is only a small change in the domain spacing during the same period.

Polymer swollen in 0.03M and 0.05M acetic acid show a significant change in their peak width during expansion. In the dry unswollen gel at t=0, the change in peak width is zero (i.e. peak width – reference peak width). As swelling commences there is a positive change in the peak width. The magnitude of this positive change in peak width continues to rise until it reaches a maximum. This corresponds to the polymer chains at their most poydisperse. This is followed by a sharp decrease. The change in peak width continues to fall, going through zero until it reaches a final value of approximately -0.002. Being a negative value, it means the polymer chains have become less disperse than in the original dry polymer. Once at -0.002 (after 20 minutes) the value does not deviate and remains approximately the same.

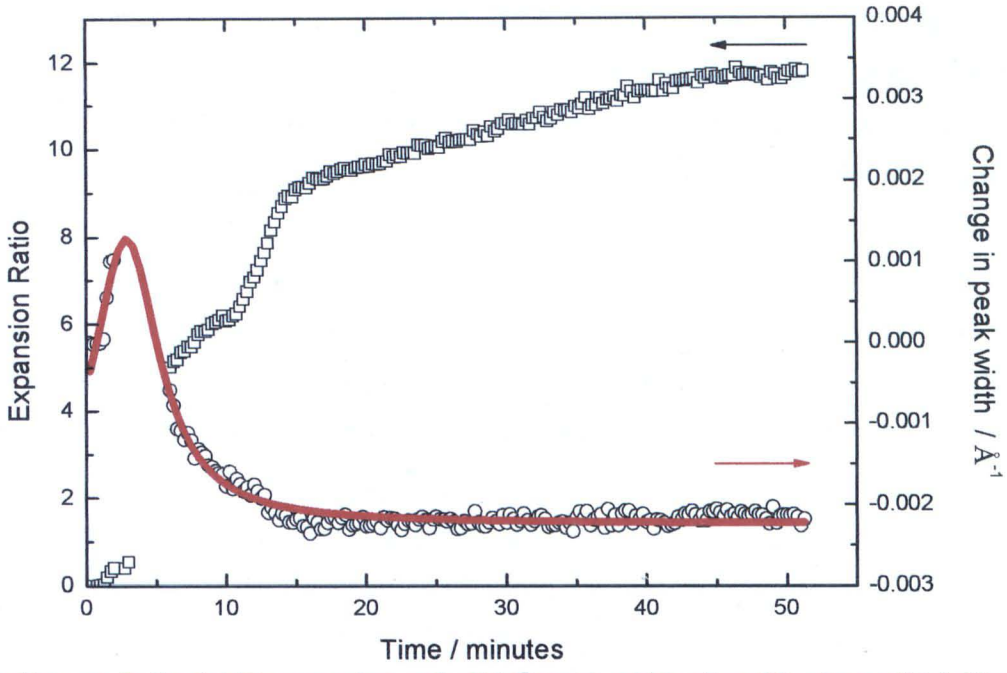

Figure 6.8: Change in the (a) □ expansion ratio (b) ○ peak width of an 80 micron thick film of $PMMA_{180}$-$PDEA_{453}$-$PMMA_{180}$ measured in 0.03M acetic at pH 3.7 at an ionic strength of 0.1M (NaCl). Best fit line drawn "by hand" to help visualise the data.

To understand the physical origin of the change in peak width one must consider the molecular structure of the polymer. In dry annealed material the polymer chains are locked into structure and are unable to move freely. This is because the glass transition temperature of PMMA is above room temperature which essentially locks in the structure of the gel. In the dry state the width of the structure peak is controlled by how well the polymer undergoes phase separation. To a large extent this will depend on the physical characteristics of the polymer, where mono-modal and low polydispersity material would be anticipated to show the narrowest structure peak (see chapter 3).

The change in peak width during expansion represents a change in the distribution of chain lengths between the PMMA domains (the micellar core separation). This is due to the chains expanding at different rates (assuming the x-ray beam goes through the entire sample), a process which is driven by diffusion kinetics. The observations in figure 6.7 and 6.8 can be explained in the following way. In the beginning of expansion you have a broadening in the peak width because not all chains are expanding at the same rate. Chains at the surface of the gel expand faster

than chains in the core as it takes time for the solution to diffuse through the polymer. When the polymer begins to reach equilibrium all of the chains have almost fully expanded and should therefore all be the same length. This results in a narrowing of the half height peak width which is what is observed. What is perhaps interesting is that the fully expanded polymer has a narrower peak width than the initially dry material. This can be explained if one considers how the molecular structure of the polymer changes in the different expansion regions. In the dry gel the length of chains between PMMA domains is similar, but as they are entangled there is a slight distribution of lengths. However, in the equilibrium expanded region all the chains are now fully stretched due to Donnan osmotic pressure overcoming the restoring force of the network. As they all have the same length there is a narrowing in the observed peak width compared to the dry polymer.

It is also evident that in 0.03M and 0.05M acetic acid the change in peak width remains approximately constant beyond twenty minutes of swelling, but the domain spacing continues to rise slightly during this period. This would suggest that swelling after twenty minutes must have reached a diffusion limit, i.e. all the polymer chains are swelling at the same rate.

6.1.8 Missing data points in the kinetic traces

In several of the kinetic swelling plots there are quite a few missing data points. The region of missing data is almost always just after the initial onset of swelling. This problem was encountered for several reasons.

2D SAXS images taken of the initially dry polymer films all had circular scattering rings. When the polymer films were immersed in solution the material would initially begin to swell in an isotropic fashion, maintaining a flat surface. During this time it was possible to collect the 2D SAXS data which was subsequently analyzed by 360 degrees integration.

As swelling continued, however, the polymer no longer expanded isotropically. It would typically fold on itself to reduce the surface area of the gel exposed to water. This caused a number of problems. In some cases the polymer folded away from the cross-section of the x-ray beam. Clearly no SAXS data could be collected in this period. This was only a small issue as the position of the cell was changed to bring the

polymer back into the beam, therefore only losing a few frames of data. However, analysis of the 2D SAXS profile in this region was problematic. An example of the 2D SAXS image collected during this period is shown in the figure 6.9a.

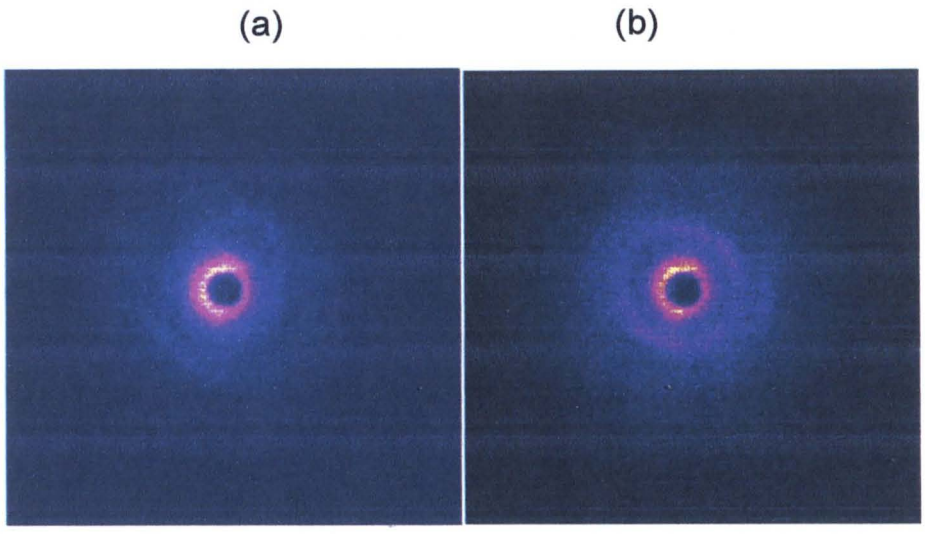

Figure 6.9: 2D SAXS image collected of thin annealed film of $PMMA_{180}$-$PDEA_{453}$-$PMMA_{180}$ after (a) five and (b) 7 minutes of swelling in 0.03M acetic acid.

After approximately five minutes of swelling the 2D SAXS image of the gel is elongated in two regions, and additionally the scattering intensity is rather weak. The presence of directionality in the scattering pattern makes it almost impossible to accurately determine the domain spacing of the polymer in a consistent manner. In order to measure the domain spacing it is important to avoid such orientational effects. The swelling results presented in figure 6.2 and 6.3 are plotted from 2D SAXS data where there is minimal influence of orientation in the scattering data.

The problem of orientation in most cases only persisted in the very beginning of expansion. Once the polymer had gone through this initial transition period the film began to unfold and flatten out. This is caused by the build up of osmotic swelling pressure within the gel. After the polymer went through this transition the orientation in the SAXS pattern was no longer present, as shown in figure 6.9b (inner ring). Not all of the gels behaved in this way. The swelling behaviour of gel swollen in 0.01M acetic acid is shown in figure 6.10. As the polymer expands the scattering ring decreases in size as illustrated in figure 6.10b. As expansion continues the intensity is weak and the

sharpness is lost as shown in figure 6.10c. Most significantly in this sample is the presence of orientation in the equilibrium structure as shown in figure 6.10d. This figure further illustrates the problem associated with integrating the 2D SAXS data to determine the domain spacing. This problem manifests itself in figure 6.2 as a significant reduction in the equilibrium expansion ratio compared to the other polymers. It is also evident from figure 6.2 that polymer swollen in 0.01M citric acid and 0.05M acetic acid both have a small depression in the expansion ratio after approximately 14 minutes. The fact that it occurs at the same time for both polymer is interesting. Again, this effect likely emanates from very subtle differences in the orientation of the scattering ring.

The inherent problem of sample twisting could be due to several reasons. It is most likely a result of pre-stress in the sample, which may emanate from the technique used to process the polymer films.

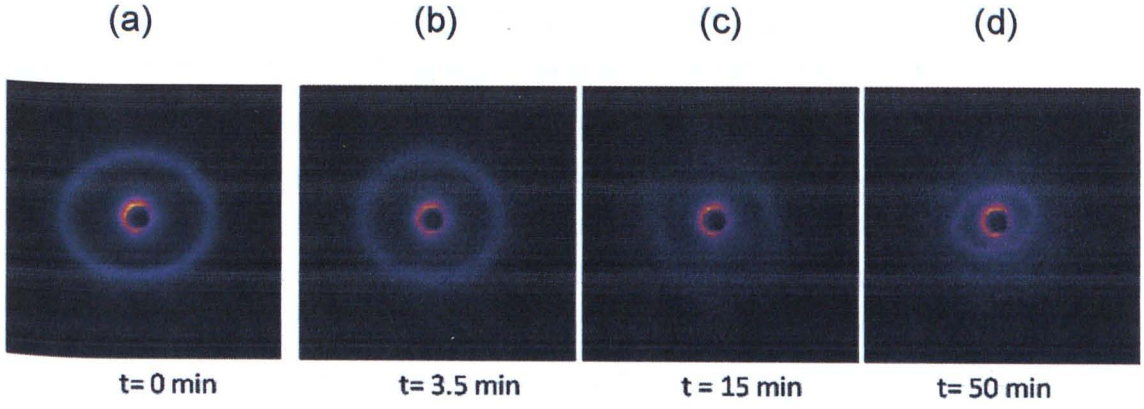

Figure 6.10: 2D SAXS image collected of thin annealed film of $PMMA_{180}$-$PDEA_{453}$-$PMMA_{180}$ after various amounts of time swollen in 0.01M acetic acid.

To produce the desired self-assembled structure the polymer was solution cast as a thin film and solvent annealed using THF. During this casting process stress may be put into the polymer film. The presence of stress in the polymer films is evident from the SAXS profile as an elliptical scattering ring. A number of the dry films did show evidence of significant orientation but these samples were discarded and not used for kinetic analysis. Stress can also be put in the film when the sample is cut. If this is not done carefully it can cause the film to stretch.

To remove any residual stress the cast polymer films used for kinetics were typically solvent annealed for one week. In this time period the polymer chains have time to reach equilibrium, and the circular ring in the SAXS profile confirms this.

However, twisting of the polymer during expansion would suggest the polymer has a "memory affect" retaining some knowledge of the casting process. Additionally the small size of the sample increases the probability that the polymer will twist.

6.2 CONCLUSION

SAXS analysis does offer an alternative technique for measuring swelling kinetics. It is particularly useful for measuring the onset of swelling in hydrogels which have fast swelling rates. Clearly this would not be possible with gravimetric techniques. The other major advantage of SAXS is that it allows the molecular nature of the polymer to be probed. This was demonstrated by measuring the change in structure peak width during expansion, which revealed the diffusive behaviour of the material. Unfortunately the method of sample preparation and size of polymer has made measuring the domain spacing problematic. Although this is clearly a sensitive technique, this in itself brings with it another set of problems in relation to orientational effects. This limits the effectiveness of the technique, however, not all polymers exhibited this problem which suggests that judicial choice of processing parameters and film dimensions could improve the situation.

REFERENCES

1. Chou, L.Y., H.W. Blanch, J.M. Prausnitz, and R.A. Siegel, Journal of Applied Polymer Science, 1991. **45**: p. 1411-1423.
2. Firestone, B.A. and R.A. Siegel, Journal of Applied Polymer Science, 1991. **43**: p. 901-914.
3. Firestone, B.A. and R.A. Siegel, Journal of Biomaterials Science, Polymer Edition 1994. **5**(5): p. 433-50.
4. Firestone, B.A. and R.A. Siegel, Journal of Applied Polymer Science, 1991. **43**: p. 901-914.
5. Siegel, R.A., I. Johannes, C.A. Hunt, and B.A. Firestone, Pharmaceutical Research, 1992. **9**(1): p. 76.
6. Parísa, R., J.M. Barrales-Riendaa, and I. Quijada-Garrido, Polymer, 2009. **50**(9).
7. Caykara, T. and I. Aycicek, Journal of Polymer Science: Part B: Polymer Physics, 2005. **43**: p. 2819-2828.
8. Topham, P.D., *Study of pH-Responsive Polymer Systems for use in Molecular Machines*, in *Chemistry*. 2005, Sheffield: Sheffield.
9. De, S.K., N.R. Aluru, B. Johnson, W.C. Crone, D.J. Beebe, and J. Moore, J. Microelectromech. Syst, 2002. **11**(5): p. 544-555.
10. Topham, P.D., J.R. Howse, O.O. Mykhaylyk, S.P. Armes, R.A.L. Jones, and A.J. Ryan, Macromolecules 2006. **39**(16): p. 5573-5576.
11. Tanaka, T., E. Sato, Y. Hirokawa, S. Hirotsu, and J. Peetermans, Physical Review Letters, 1985. **55**(22): p. 2455-8.

Chapter 7

Quantifying Hydrogel Response using Laser Light Scattering

7.1 INTRODUCTION

The ability to measure the molecular response of PMMA-*block*-PDEA-*block*-PMMA hydrogels using SAXS has been demonstrated in both chapter 4 and 6. The technique proved to be an excellent method for measuring the "static" pH, ionic strength and salt specific response of the material. However, although the principle can be applied to kinetics, complex experimental setup and sample processing issues made it both challenging and problematic.

One of the greatest advantages of SAXS over other techniques is that it measures the response of the hydrogel at the molecular level. Although SAXS analysis presents a significant step forward in understanding hydrogel behaviour it suffers several pitfalls. For example, SAXS relies on the polymer sample being comprised of some sort of molecularly ordered structure. However, perhaps the most significant issue is the use of SAXS itself. For time-resolved experiments on the time scale of minutes one cannot rely on conventional x-ray sources but instead must turn to high intensity beam lines which can only be found at synchrotron radiation sources. This is obviously not an ideal situation due to the expense and rather limited amount of beam time available to researchers.

Clearly, it would be desirable to be able to use a complimentary *in situ* method, one which has most of the advantages of SAXS, including its sensitivity and non-invasiveness, but which is more widely accessible. In a previous study by Topham *et al* [1], the affine nature of self-assembled PMMA-*block*-PDEA-*block*-PMMA triblocks has been demonstrated, which indicated that the response of the polymer in the nm

range scaled up to a macroscopic response. This presents an opportunity to design a new tool for measuring the response of PMMA-*block*-PDEA-*block*-PMMA hydrogels.

The response of a hydrogel to a changing chemical environment has often been tailored to sensor applications. For example the use of hydrogels as pH sensors [2] or slightly more complex glucose sensors [3] In this function the hydrogel acts as a transducer, where a change in the property of the hydrogel is converted into a response signal. In chapter 4, the PMMA-*block*-PDEA-*block*-PMMA hydrogel can also be considered a transducer, where the change in domain spacing is the response signal, and calibration of this signal gives information about the molecular response of the material (i.e. the expansion ratio). Other approaches have been used to create hydrogel sensors; Asher *et al* [3] fabricated a transducer based on optical changes. They polymerised a colloidal crystalline array (CCA) of spheres into a hydrogel. The hydrogel was found to shrink and swell reversibly in the presence of specific analytes, namely metal ions and glucose. The incorporated CCA diffracted light in the visible range, the wavelength depending on the lattice domain spacing. This gave rise to a strong colour emission. It was found that a volume change of 0.5 % in the hydrogel shifted the diffraction wavelength by approximately 1 nm. Other work using the concept of changes in optical properties has been reported by Lowe *et al* [4] They fabricated a holographic pattern onto the surface of a pH-sensitive hydrogel. By monitoring the change in the diffraction wavelength (colour) of the hologram as a function of pH in a variety of media they were able to characterise the shrinkage and swelling response. They reported a response of 165 nm per pH unit. However, these techniques generally rely on complicated photosensitive or photo masking [5] techniques to create the polymeric sensors.

The concept of monitoring optical changes within a hydrogel in the form of a "diffraction grating" has been applied to the $PMMA_{88}$-*b*-$PDEA_{223}$-*b*-$PMMA_{88}$ triblock copolymer discussed in the chapter 4 and 6. A polymeric grating was manufactured by solvent casting $PMMA_{88}$-*b*-$PDEA_{223}$-*b*-$PMMA_{88}$ (JSPB03) onto the surface of a quartz diffraction grating template. This is a very simple procedure in contrast to the complicated techniques used by other researchers. For example, the hologram created by Lowe required complicated photosensitization techniques. Changes in the optical properties of the grating were measured at different pHs and in a range of solutions prepared from the Hofmeister salts introduced in chapter 4. The grating was

also used to measure the kinetics of swelling and de-swelling. To test the accuracy and usefulness of this technique the results of mesoscopic scattering will be compared with those obtained from gravimetric and SAXS analysis under identical conditions.

7.1.1 Diffraction grating theory

A diffraction grating is an optical component, the primary purpose being to disperse light into a spectrum. The grating consists of many parallel and equidistant slits, typically in the order of several thousand per cm. If the slit separation of each gap is narrow relative the wavelength of light, diffraction causes each slit to act as a centre of secondary disturbance. These scattering centres create semi-circular wave fronts, which in a few specified directions may combine constructively to produce a continuous wave front or destructively in which case no wave front will be present. Figure 1a shows a typical interference pattern created by a large number of slits. Figure 7.1 demonstrates the origin of the interference pattern created by a diffraction grating. It shows a ray of path difference *p* being brought to a Point P,

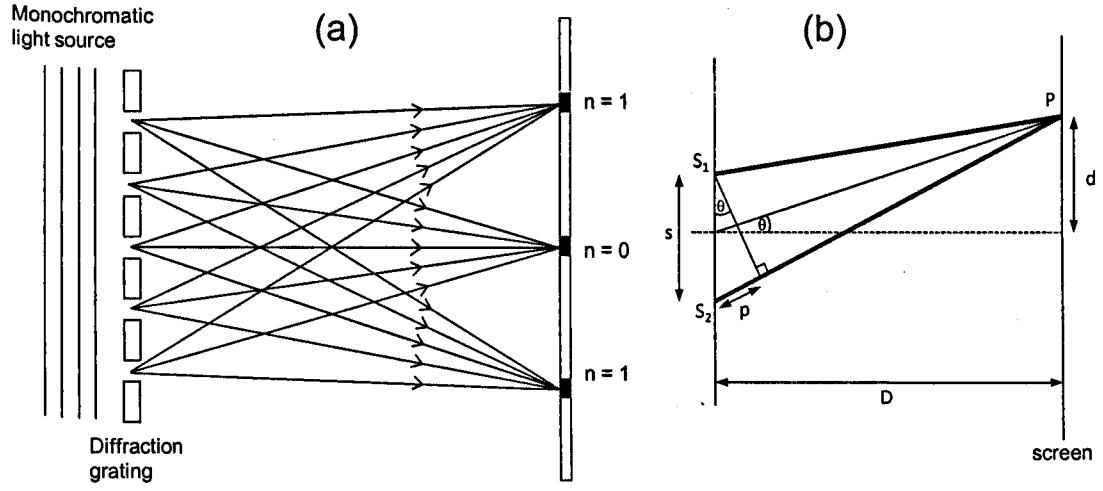

Figure 7.1: (a) Diffraction at the slits of an optical diffraction grating. (b) the geometry used to calculate the grating slit separation (s).

where $\sin\theta = p/s$ (7.1)

and p is the path difference (S_2P - S_1P) for waves that are superimposed at point P.

$$\tan\theta = d\,/\,D \tag{7.2}$$

if θ < 1/10 rad (distant screen assumption) then, i.e. $\tan\theta = \sin\theta$

$$\frac{d}{D} = \frac{p}{s} \tag{7.3}$$

it then follows that

$$p = \frac{ds}{D} \tag{7.4}$$

The superposition of waves will be constructive when n is an integer, i.e. when

$$p = \frac{ds}{D} = n\lambda \tag{7.5}$$

This can re-arranged to $d = \frac{n\lambda D}{s}$ (7.6)

where d is the displacement from the centre line, s is the slit separation (separation of the centres of neighbouring gaps), λ is the wavelength of incident light and D is the distance between the grating and the screen.

7.1.2 Processing of the polymeric diffraction gratings

An optical diffraction grating was engraved onto the surface of a quartz plate (approximately 2cms x 2 cms) using photolithography. Quartz was chosen due to its resistance to solvent and reusability. An AFM image of the quartz grating surface is presented in figure 7.2a.

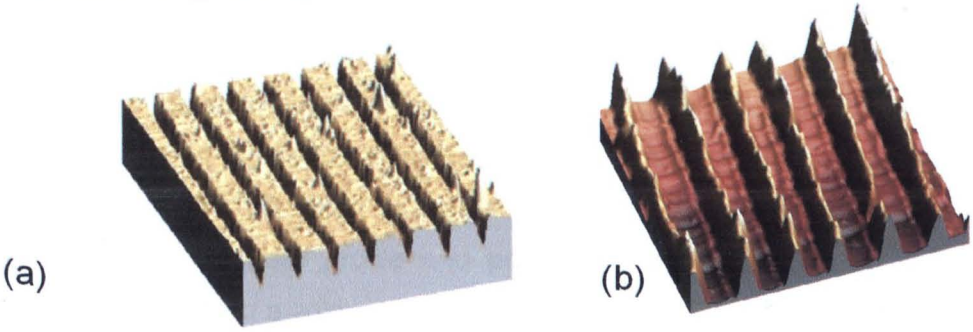

Figure 7.2: AFM images of an (a) optical diffraction grating "mould" in fused quartz (b) $PMMA_{88}$-*b*-$PDEA_{223}$-*b*-$PMMA_{88}$ polymeric diffraction grating formed by replication from it, obtained in contact mode. Both gratings have a spectral period of 2 microns.

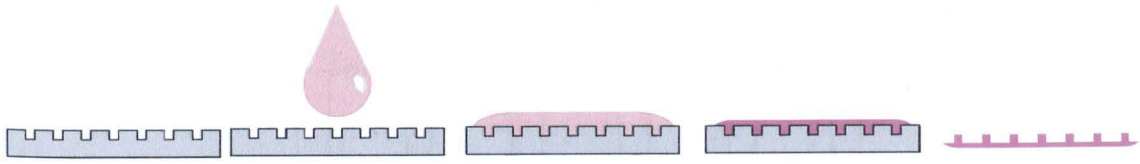

Figure 7.3: Casting method used to create the polymeric diffraction grating.

This grating was used as a master template, and all polymeric gratings were created from it. To create the polymeric diffraction grating the polymer was dissolved in THF. This is a good solvent for both DEA and MMA. The polymer solution was prepared at 30 weight percent. A high concentration was used to favour network formation, but not too high to ensure it would flow freely into the grooves of the grating. (see appendix, section 9.7). The solution was then poured on to the surface of the quartz grating template to create a thin film. The grating was then put into a solvent rich environment of THF and annealed for several days. An illustration of the technique demonstrating how the grating is created from the master template is shown in figure 7.3.

Once the cast polymer was sufficiently annealed it was removed from the surface of the quartz by plasticisation in water. Figure 7.4 shows an AFM surface depth profile of the template, and a polymeric grating created from it. The quartz grating has a regular array of slits with an average separation of 2 microns. Comparison between the template and polymeric grating indicates the casting method was successful, leaving behind a negative copy. The mesoscopic pH response of the polymeric film was monitored by measuring the change in the laser scattering pattern. The setup used to measure this is shown in figure 7.5. A 632nm helium neon laser was suspended above the polymer grating. The laser beam was projected through the sample, and the diffraction spots were projected onto a white surface directly below the film. The intensity profile and position of the diffraction spots were measured quantitatively using a colour camera.

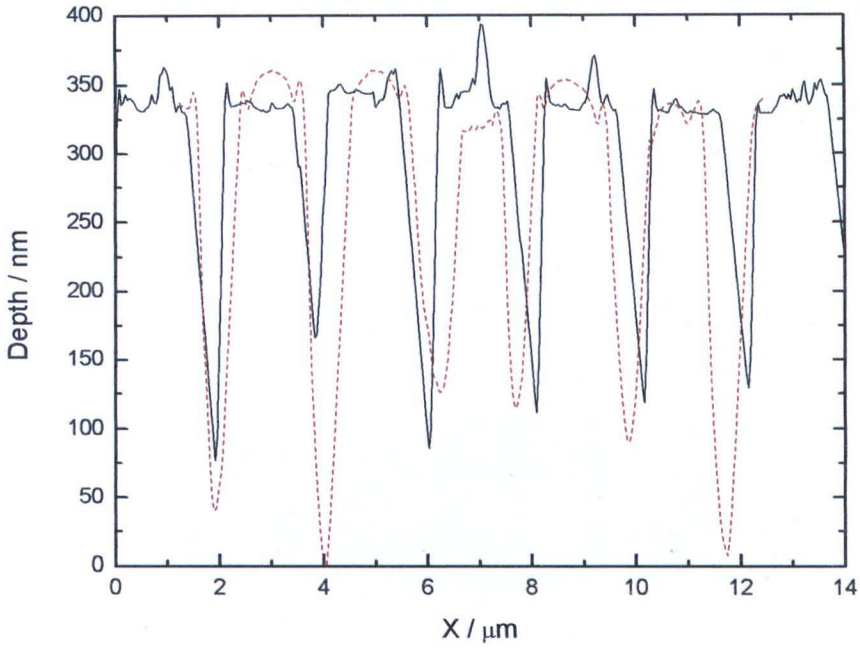

Figure 7.4: Depth profile analysis of the (black) fused quartz optical diffraction grating (red) $PMMA_{88}$-*b*-$PDEA_{223}$-*b*-$PMMA_{88}$ polymeric diffraction grating.

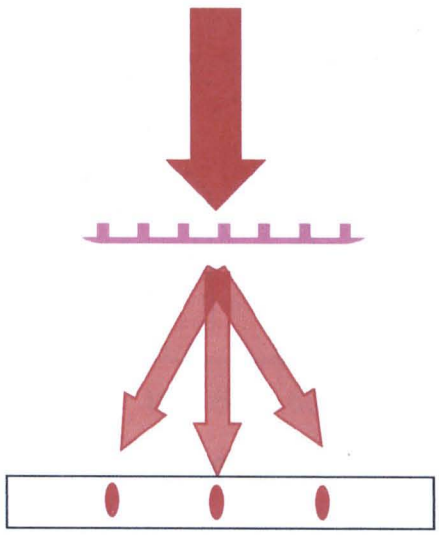

Figure 7.5: Illustration demonstating the princple used to record the diffraction spots of the polymermeric diffraction grating, a 632nm Helium-Neon laser was used for the source of light. The change in the position of the diffraction spots was recorded using video microscopy.

For static scattering experiments the polymeric grating was suspended in a Petri dish. This allowed the solutions to be rapidly changed. A new piece of polymeric grating was used for each solution measurement. For dynamic experiments a specially designed liquid cell was used. This allowed the change in the scattering pattern to be monitored continuously with changes in the solution pH. A representative laser scattering pattern generated by the imprinted polymer sample in solution is shown as an intensity image in Figure 7.6a clearly showing the diffraction orders either side of the direct beam.

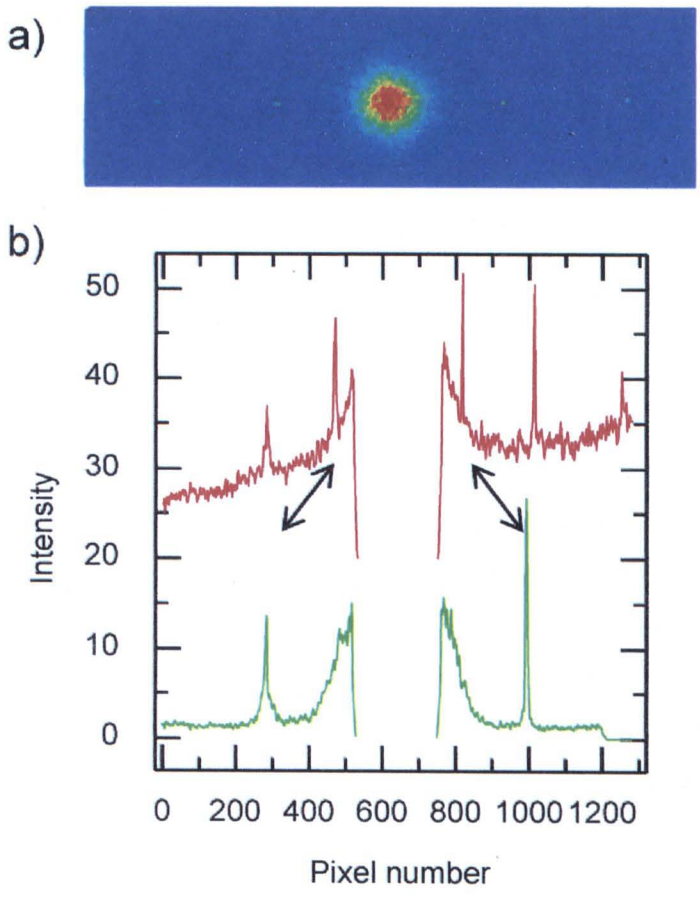

Fig 7.6: a) A typical laser diffraction pattern from the imprinted gel. b) Vertically integrated laser scattering patterns for the gel in distilled water at pH 7.0 (fully collapsed, —), in citric acid buffer at pH 3.6 (expanded, —). The direct beam has been removed and the scattering patterns shifted vertically to aid visualisation.

The intensity images were vertically integrated using Labview software and the obtained 1D scattering patterns for the gel in two different conformations (expanded and collapsed) are shown in Figure 7.6b. The 1D data also show that the polymer diffraction grating was highly ordered.

With this scattering technique, a large movement in the peak position is observed, which corresponds to the gel expanding and collapsing. The scattered angle is inversely proportional to the period of the diffraction grating and so as the material expands, the diffraction pattern moves towards the direct beam (Figure 7.6b). Additionally, the accuracy of this technique can be tuned by altering the distance between the sample and detector; the larger the distance, the higher the sensitivity to changes in the imprinted grating structure.

To determine the periodic spacing using laser light scattering equations 7.7 was used which is derived in section 7.1.1.

$$s = \frac{m\lambda D}{d} \tag{7.7}$$

where s is the repeat length of the diffraction grating, d is the scattering vector (measured as half the distance between 1st order peaks), m is the diffraction order, λ is the incident beam wavelength, and D is the distance between the sample and the detector. By measuring the position of the diffracted beam one can precisely determine the repeat length of the imprinted polymer structure.

7.1.3 Comparing Gravimetric, mesoscopic and molecular equilibrium swelling behaviour

To demonstrate the suitability and effectiveness of this simple technique a systematic study was conducted on the response of the hydrogel to two distinct parameters, namely pH and counter ions. The imprinted grating technique will display responses on the micron length scale (10^{-6} m), halfway between the length scales measured by SAXS and gravimetric analysis. The counter ions chosen for this are taken from a sequence of ions known as the Hofmeister series as discussed in chapter

4. These ions were found to have a specific effect upon the swelling of the gel. The counter ion study was carried out at pH 3.6, such that the gel was expanded and the counter ion effect would manifest itself as reduced swelling of the gel

To test this technique the results of mesoscopic scattering were compared with those obtained from gravimetric and SAXS analysis under identical conditions. To compare the results of the studies on a single scale, the response of the gel is expressed in terms of an expansion ratio. This is defined as $(\sigma_{eq} - \sigma_{ref})/ \sigma_{ref}$, where σ_{eq} is the equilibrium length in a given solution and σ_{ref} is the dry length.

Both SAXS and laser light scattering of the diffraction grating generate results in terms of a unique length scale. SAXS measures the microphase separated length (defined by the polymer molecular weight and relative volume fractions of the polymer constituents), whereas laser light scattering measures the single length scale for the period of the 1D diffraction grating. Gravimetric analysis, however, will return a result in terms of mass. Consequently, this has been converted into a volume response, assuming a constant density of 1.0 g cm^{-3} (an approximation which also takes into account the change in density with swelling) and the cube-root taken to generate a macroscopic length scale for comparison with the other two techniques.

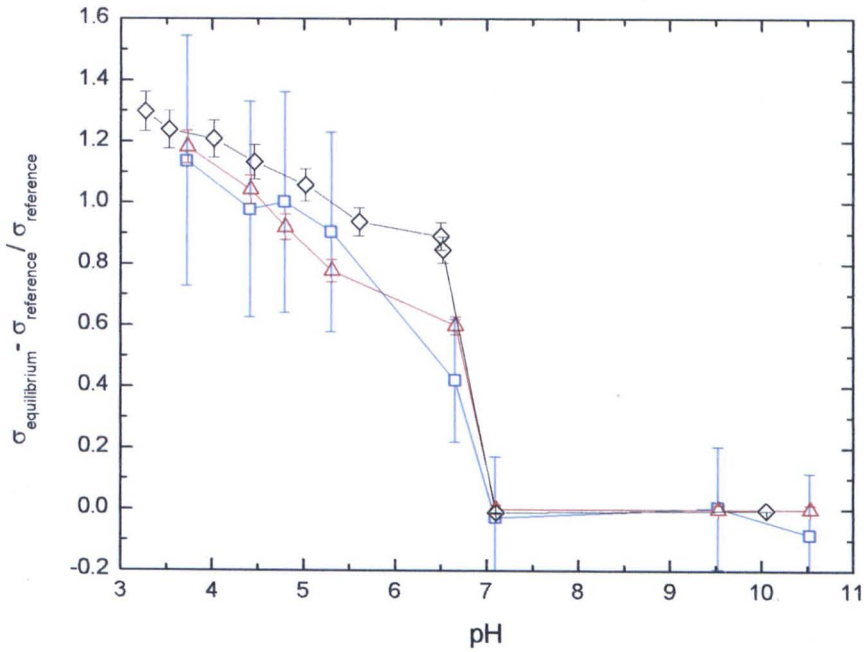

Figure 7.7: Variation of the relative change in ◇ molecular domain spacing, △ surface grating separation and □ extrapolated gravimetric length, as a function of pH in 0.01M citric acid (3.6-7.1) and ethanol amine buffer (>9).

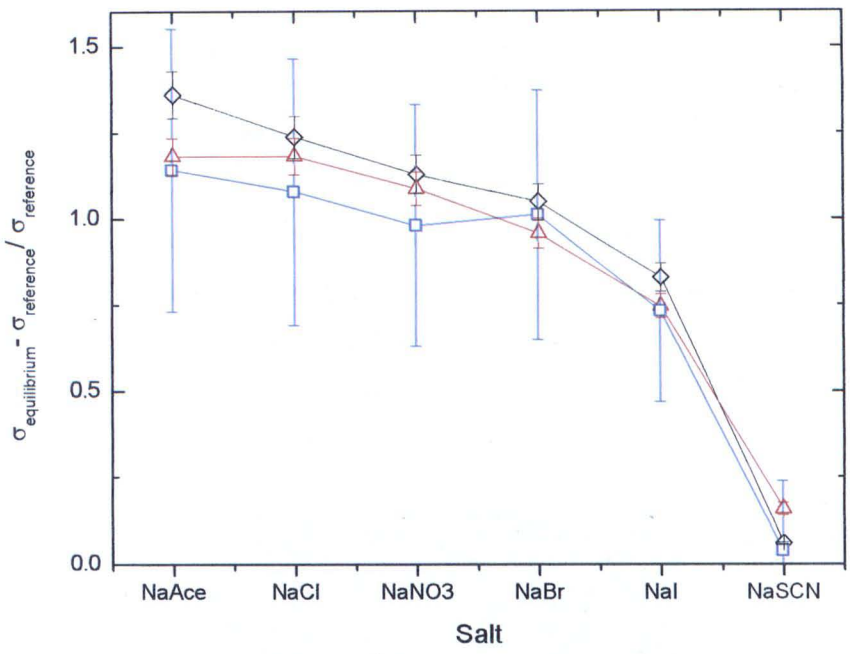

Figure 7.8: Variation of the relative change in ◇ molecular domain spacing, △ surface grating separation and □ extrapolated gravimetric length, as a function of sodium salt identity measured in 0.01M citric acid at pH 3.6 at an ionic strength of 0.1M.

Figure 7.7 and 7.8 shows that the same trend is observed using the three techniques for measuring the hydrogel response in the counter ion study and across the pH range investigated. Furthermore, the data for the grating more closely matches that for the SAXS studies than the gravimetric analysis, which is prone to more significant experimental errors. All of the analytical techniques used here show that the pK_a of the triblock copolymer lies between pH 6.5 and pH 7.0.

The three techniques are clearly complimentary, each probing a different length scale; nano, micro, and macroscopic. However, of the three techniques, it is the laser and x-ray scattering techniques which offer high resolution and high frame rate dynamic studies of the response. Of these two analytical tools, it is the laser scattering which is more accessible in most laboratories.

7.1.4 Mesoscopic diffraction response kinetics

To demonstrate the effectiveness of this technique for *in situ* studies, the polymer diffraction grating technique was used to measure the hydrogel response in a dynamic experiment. The imprinted grating was placed into a solution which was alternated between 0.05 M citric acid or 0.05 M ethanol amine at pH 3.6 and 11.5 respectively, the ionic strength was fixed at 0.1 M using NaCl.

Figure 7.9 shows the results from the vertically integrated laser diffraction pattern as a function of time along with analysis of a typical region from the dynamic data pH-experiment.

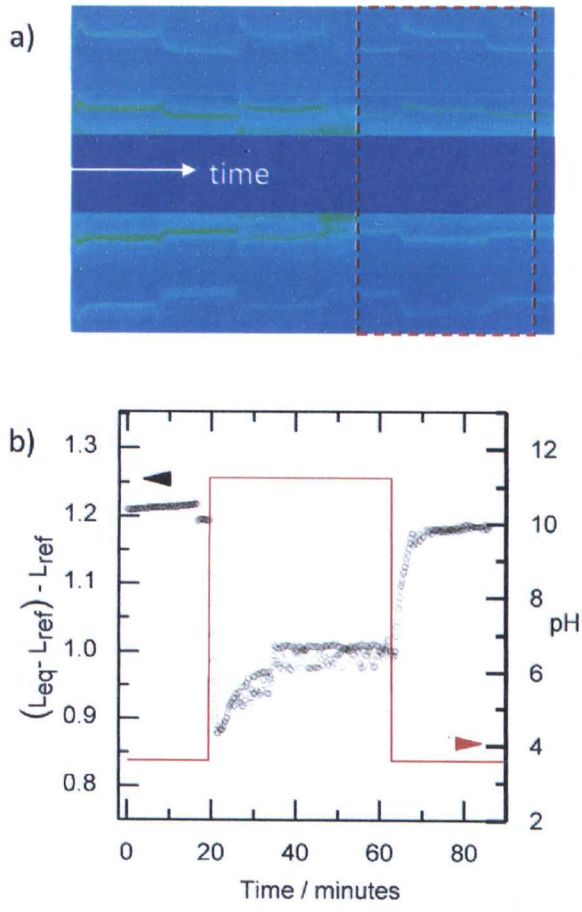

Fig 7.9: (a) Integrated 2D scattering patterns as a function of time for the gel in a manually oscillating pH environment. 0.01M citric acid (pH 3.6) and 0.01M ethanol amine (pH 11.5) at an ionic strength of 0.1M (NaCl). (b) Expansion ratio as a function of time for a single pH oscillation as highlighted in red in part a.

Figure 7.9a shows the reproducible movement of the scattering peaks as the gel expands and collapses in response to a changing pH environment. This dynamic, *in situ* method allows one to clearly determine when equilibrium is reached, demonstrating its applicability in measuring the kinetics of hydrogel response. Each transition, both expansion and collapse, is associated with a short outward movement of the scattering peaks. This can be attributed to small residual stresses in the surface causing small fluctuations/waves over the surface of the gel. This effect slightly alters the angle of incidence for the incoming beam, presenting a narrower grating to the beam.

In spite of this, the data clearly show that laser light scattering is an appropriate analytical tool for measuring dynamic hydrogel response, without the need for ordered nanostructure nor the costs associated with SAXS. Moreover, if SAXS and laser scattering are carried out simultaneously (and subsequently calibrated), one then has the basis of a technique where materials can be probed in a laboratory set-up to yield molecular level information simply through extrapolation.

7.2 CONCLUSION

The imprinting of a microscale morphology into an optically transparent medium, in combination with laser scattering has demonstrated itself to be an accessible and accurate method for measuring both the static and dynamic response of pH-responsive hydrogels. Results obtained herein indicate that the three length scales measured, macro by gravimetry, micro by optical diffraction and nano (molecular) by SAXS are comparable to each other for a pH-responsive triblock copolymer.

The *in situ* nature of this technique is particularly useful for measuring fast dynamic structure response in hydrogel systems. This is a clear advantage when compared to other laboratory scale experiments, such as gravimetric analysis, which are often limited to measuring kinetics over long time periods. Moreover the combination of SAXS and laser light scattering allow *in situ* studies and address the issues of spatial hysteresis. However, the laser light scattering technique is easily transferable to other systems which offer suitable optical transparency and will find particular use for cross-linked systems which do not possess a well-defined

microstructure.

For the first time, the simple approach of casting a curable polymer to generate a defined topography has been proven to be an inexpensive and effective analytical route to measuring hydrogel response on the microscopic scale.

REFERENCES

1. Topham, P. D., Howse, J. R., Crook, C. J., Gleeson, A. J., Bras, W., Armes, S. P., Jones, R. A. L., and Ryan, A. J., 2007, **256**, 95.
2. Richter, A., Paschew, G., Klatt, S., Lienig, J., Arndt, K.-F., Hans-Jürgen, and Adler, P., *Sensors*, 2008, **8**, 561.
3. Holtz, J. H. and Asher, S. A., *Nature*, 1997, **389**, 829.
4. Marshall, A. J., Blyth, J., Davidson, C. A. B., and Lowe, C. R., *Anal. Chem*, 2003, **75**, 4423.
5. Zhang, N. and Knoll, W., *Anal. Chem*, 2009,, **81**, 2611.

PUBLICATIONS

1. Joshua M. G. Swann, Wim Bras, Jonathan R. Howse, Paul D. Topham and Anthony J. Ryan, Quantifying Hydrogel Response using Laser Light Scattering, Soft Matter, submitted.

Chapter 8
Summary and Future Work

8.1 SUMMARY

The main aim of this project was to use SAXS as a tool to quantify the molecular response, both "kinetic" and "static" of phase separated triblock copolymers, namely PMMA-*block*-PDEA-*block*-PMMA and PMMA-*block*-PMAA-*block*-PMMA. The first objective was the synthesis of the block copolymers and this was achieved using Group Transfer and Anionic polymerisation.

Whenever PMMA-*block*-PMAA-*block*-PMMA block copolymers were synthesised a significant amount of diblock contamination was always present. Thin films of this material were solution cast and annealed. SAXS analysis revealed phase separation in the cast material. These annealed films were found to be mechanically weak. When immersed in a solution above their pK_a they simply broke up into many pieces. The most likely cause of this failure is the high level of diblock contamination. The structural integrity in the triblock copolymers is largely a result of the physically cross-linked network, and diblock contamination simply reduces the number of chains involved in bridging. Recent work Guice *et al* [1] has demonstrated the importance of bridging domains on the mechanical strength of ABA type triblock copolymers. Other parameters are known to have an effect on the mechanical properties, such as the polydispersity of the PMMA end groups. If there is an uneven distribution of PMMA chains then a number of the smaller chains will not be involved in network formation which will ultimately reduce the mechanical strength [2]. That is why anionic polymerisation was used in an attempt to produce narrow molecular weight material.

Synthesis of PMMA-*block*-PDEA-*block*-PMMA block copolymers was more successful, producing monodisperse high molecular weight materials with PDI's around 1.2. Morphological development in solvent-cast films was followed using SAXS by monitoring changes in the structure peak. This revealed the thermodynamically controlled phase separation of the system. A series of the annealed block copolymers were

immersed in a solution at pH 3.6. At this pH the block copolymer expands. By measuring the change in their mass over a period of the 45hrs the robustness of the material was evaluated. JSPB03 was found to be the most robust material. Having successfully synthesised and processed a robust phase separated material the second part of the project focused on evaluating its molecular response through the use of SAXS.

The "static" SAXS response of the material was evaluated by measuring the change in its structure peak at different pH's and ionic strengths using a range of salts. The structure peak was subsequently converted into an equilibrium expansion ratio. Changes in pH were accomplished using a controlled set of buffers, namely citric acid, sodium phosphate and ethanol amine. The ionic strength of the buffers was fixed using a series of salts from the Hofmeister series, namely NaAce, NaCl, NaBr, NaI, $NaNO_3$ and NaSCN. Measuring the equilibrium response of the hydrogel using SAXS was found to be very accurate. Buffer, salt and pH specific effects could be easily resolved with high resolution.

"Kinetic" studies performed on the hydrogel were less successful. During expansion of the material pre stress in the thin films caused them to fold which made evaluating the domain spacing problematic. This was only observed just after the onset of swelling so it was still possible to resolve the majority of the kinetic data. By monitoring changes in the half height peak width during expansion it was possible to observe diffusion within the material at the molecular level. This is something which would clearly not be possible with gravimetric techniques.

Due to the enormous cost and limited beamtime available at synchrotron sources a novel method was used to evaluate the response of the hydrogels. A quartz diffraction grating was used to create a micron-sized periodic structure on the surface of a thin film of the polymer and the resulting diffraction pattern was used to calculate the swelling ratio of the polymer film *in situ*. The technique has been proven to be an inexpensive and effective analytical tool for measuring hydrogel response on the microscopic scale. It is as cheap as gravimetry but has the accuracy of SAXS.

8.2 FUTURE WORK

The kinetic results obtained using the diffraction grating technique at this stage are only preliminary and further in depth studies are required. Initial studies would investigate the effect of decreasing the thickness of the imprinted films to see if this overcomes the problems associated with residual stress.

Clearly the robustness of PMMA-*block*-PMAA-*block*-PMMA triblock copolymers needs to be improved. A possible route to achieve this while maintaining a phase separated structure is to incorporate a reversible UV-cross-linking unit on to the PMMA end groups. After synthesis and post-annealing of the sample the microphase separated structure can be chemically locked through the UV cross-links. Such an investigation would allow a direct comparison between the robustness of a phase separated physically and chemically cross-linked gel. Reversible cross-linking of micelles has been reported in the literature using the UV cross-linker 7-(2-Methacryloyoxyethoxy)-4-methylcoumarin [3]. An alternative strategy might be the formation of nanocomposites using either PMMA particles or clay platelets.

In relation to molecular diffusion studies the phase separated material could be exploited using microfocus SAXS. Using a microdrop dispenser similar to what is found in a conventional bubble jet printer picoliter volumes of solution can be deposited at a specific point on the subms time. Coupled with microfocus SAXS this would allow spacially resolved diffusion kinetics to be collected.

REFERENCES

1. Guice, K. B., Marrou, S. R., Gondi, S. R., Sumerlin, B. S., and Loo, Y.-L., *Macromolecules* 2008, **41**, 4390.
2. Tong, J. D., Moineau, G., Leclère, P., Brédas, J. L., Lazzaroni, R., and Jérôme, R., *Macromolecules*, 2000, **33**, 470.
3. Jiang, J., Qi, B., Lepage, M., and Zhao, Y., *Macromolecules* 2007, **40**, 790.

Appendix

Theoretical background and experimental methods

9.1 BLOCK COPOLYMER SYNTHESIS - THEORY

Block copolymers with well-defined structures can be synthesised using a variety of different strategies [1]. Herein, a description of the techniques used in this thesis will be presented with the relevant fundamental theoretical background. An emphasis will be placed on the synthesis of triblock copolymers. This will commence with a description of anionic polymerisation which is one of the oldest and most versatile methods to synthesise block copolymers with complex architecture.

9.1.1 Anionic polymerisation

9.1.1.1 Introduction to anionic polymerisation

Anionic polymerisation is a 'living' chain polymerisation which is free from termination or chain transfer. This living nature was first identified by Szwarc in 1956 [2]. In anionic polymerisation the propagating active centres remain 'living' and in the absence of terminating species the addition of monomer will simply increase the degree of polymerisation.

The method is commonly used for the synthesis of block copolymers as it allows one to produce polymers with predetermined molecular weight, controlled architecture and low molecular weight distribution.

In order to produce polymers with low molecular distribution (Poisson distribution) a number of criteria need to be met.

1. The rate of initiation must be greater than or equal to the rate of propagation. This ensures that all chains grow for the same period of time.
2. No termination or chain transfer should occur at the active centre.

3. The propagation steps should be irreversible.

The molecular weight in an anionic polymerisation is controlled by the degree of conversion and stochiometry of the reaction. For a mono-functional initiator under ideal conditions with no chain transfer or termination, the molecular weight at 100% conversion of monomer can be predicted using equation 9.1.

M_n = mass of monomer (g) / moles of initiator (mol) (9.1)

9.1.1.2 Monomers which are susceptible to anionic polymerisation

Anionic polymerisation is limited to monomers which can be roughly classified into two categories. Diene, vinyl and carbonyl containing monomers which contain one or more double bonds, and cyclic monomers which contain a ring capable of being opened by an incoming nucleophile.

9.1.1.3 Mechanism

An ideal anionic 'living polymerisation' in the absence of any chain termination or transfer will involve the following elementary steps, initiation and propagation. The living polymerisation of methyl methacrylate is shown in figure 9.1. In solution the initiator, BuLi exists as a cluster, but can be viewed simply as $n\text{-}Bu^-$ associated with Li^+ counterion. In the initiation step the carbanion initiator reacts with the double bond on the backbone of the monomer unit. This leads to the formation of a carbanion site on the monomer. The newly formed carbanion centre will react with another monomer molecule regenerating further reactive intermediates. Propagation will continue to occur until all of the monomer has been consumed. Premature termination of a living system can be induced by addition of a protic impurity into the polymerisation. In this example methanol is added which reacts with the active centre and renders it inactive.

In general, monomers used in anionic polymerisation must possess an electron withdrawing substituent or double bond, capable of stabilising the carbanion intermediate formed in the transition state for monomer addition. This is further demonstrated in figure 9.1. The negative charge produced during the initiation step is resonance stabilised over the monomer carbonyl group.

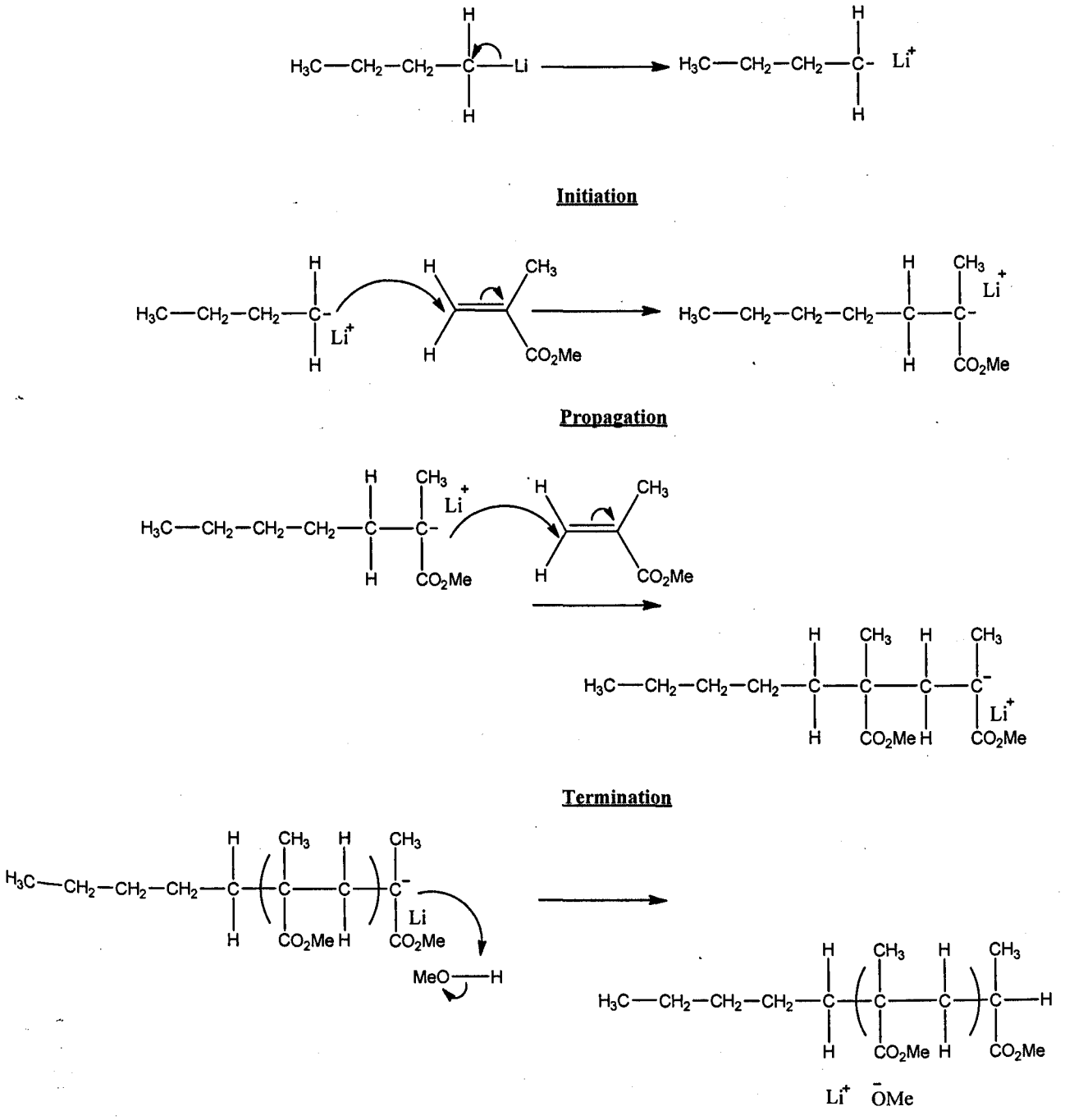

Figure 9.1: General mechanism for the living anionic polymerisation of methyl methacrylate. *sec*-butyl lithium is used as the initiator, and the terminating species is methanol.

9.1.1.4 Initiators used in anionic polymerisation

The choice of initiator strongly depends on the electrophilicity of the monomer being used. If the initiator is weak this will lead to slow initiation resulting in an increase in the molecular weight distribution. More reactive initiators may react adversely with the monomer inducing premature chain termination. This termination mechanism is observed when BuLi is used as an initiator in the polymerisation of alkyl methacrylates. BuLi attacks the expected double bond but also the carbonyl double bond. This results in fewer than 50 % of initiator molecules initiating a chain [3].

The reactivity of alkyl lithium initiators such as BuLi is strongly dependant on their degree of association in solution. When the initiators are less associated they are more reactive. The degree of association can be controlled by the choice of solvent. Aromatic solvents reduce the degree of association compared with non-aromatic solvents.

9.1.1.5 Methacrylate Polymerisation – Undesirable chain termination

When methacrylate and acrylate monomers are used in anionic polymerisation there are a number of undesirable side reactions which can lead to chain termination and other undesirable side reactions.

The initiating species can react with the carbonyl group of the monomer forming the corresponding alkoxide and ketone, as illustrated in figure 9.2 [4]. This particular side reaction can be minimised if one uses initiators which are less reactive and contain bulky sterically hindered groups.

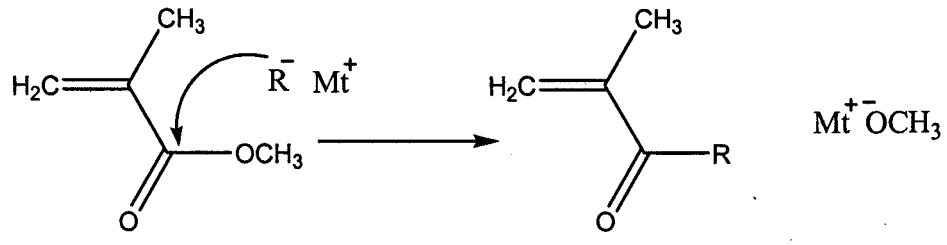

Figure 9.2: Chain termination – reaction of the monomer carbonyl group with the initiator.

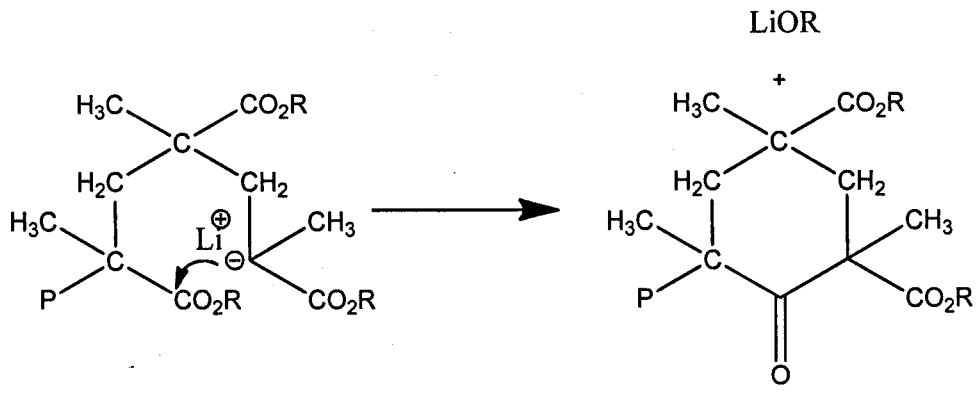

Figure 9.3: Chain termination – unimolecular backbiting.

The primary termination mechanism is thought to be a unimolecular chain backbiting reaction, as shown in figure 9.3 [4]. The carbanionic living centre is able to react with the penultimate ester group on the polymer chain. An energetically favourable six membered ring is formed with the ejection of an alkoxide group. Alkoxide is a poor nucleophile and is not able to reinitiate the polymer chain. This undesirable side reaction may be avoided by running the reaction at low temperatures (~ -78°C), as at low temperatures the rate of propagation is approximately 10^4 faster than the rate of termination.

A breakthrough in the polymerisation of acrylate/ methacrylate monomers was discovered by Teyssie and co-workers [5]. They noticed that the addition of LiCl salt to the polymerisation of t-butyl acrylate had a dramatic effect on the molecular weight distribution. When LiCl was used the molecular weight distribution reduced from 3.61 to 1.2 [6]. LiCl is now routinely used in methacrylate polymerisations. It is understood to be a sigma co-ordinating salt cable of forming a four membered complex with lithium and the growing chain end.

9.1.1.6 Synthesis of triblock copolymers by anionic polymerisation

There are several methods which can be used to create triblock copolymers using anionic polymerisation. Each particular method has negatives and positive points. Due to the living nature of anionic polymerisation it is possible to create triblocks by sequential monomer addition. In this reaction scheme the first monomer is polymerised, followed immediately by polymerisation of the second

monomer and so on. However, this method suffers two main drawbacks. Living polymerisation is highly susceptible to termination from impurities. With each monomer addition to the living polymer the change of termination is increased. This causes the formation of undesirable diblock and or homopolymer it the monomers are not pure enough. It is also important to point out that this procedure relies on the first living polymer being able to initiate the second monomer. If this condition is not fulfilled the polymer will be ill defined.

To circumvent this problem researchers have created symmetric triblocks using difunctional initiators. Difunctional initiators are organometallic compounds which have two anionic sites on the same chain, which are both capable of initiating polymerisation. To create a symmetrical triblock (A-B-A) the difunctional initiator is reacted with the first monomer to form the midblock. This is followed by addition of the second monomer to create the end blocks. One of the disadvantages of using a difunctional initiator is the fact that the monomers must be of high purity. This is necessary to avoid deactivation of both or one of the active sites with could lead to the formation of triblock with undesirable impurities.

9.1.2 Group Transfer Polymerisation (GTP)

9.1.2.1 Introduction to GTP

Group transfer polymerisation (GTP) was discovered by Webster and co-workers at DuPont in 1983 [7]. It is a method used predominantly for the polymerisation of methacrylate and acrylate monomers. GTP allows one to produce polymers with controlled architecture and low molecular weight distributions. GTP is related to classical anionic polymerisation where control is achieved through the livingness of the polymerisation, i.e all the chains grow simultaneously with little or no chain termination. Unlike anionic polymerisation of methacrylate which typically requires initiation at -80°C; GTP can be carried out at room temperature and above. In comparison with ionic and radical polymerisations GTP is much less sensitive to impurities and is also tolerant to a wide variety of monomer functionalities such as allylic groups, amines and epoxides [8].

9.1.2.2 Mechanism of GTP

GTP was so named as it was believed at the time of its discovery that a silane group transferred to the growing chain end after the addition of each monomer unit. The original mechanism is based on an associative pathway, as shown in figure 9.4.

A nucleophilic catalyst binds to the silane group activating it towards the monomer. A hypervalent intermediate is formed and the silane group transfers to the incoming monomer unit. The associative mechanism assumes that the silane group remains on the polymer chain during the polymerisation step.

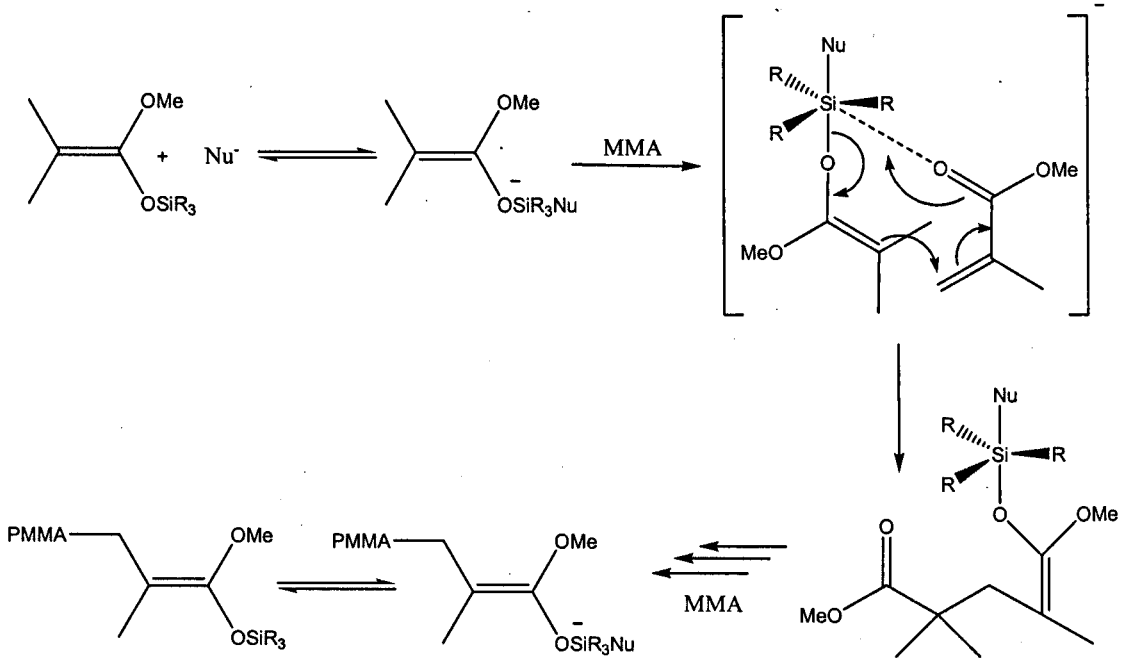

Figure 9.4: Scheme 1: Associative pathway.

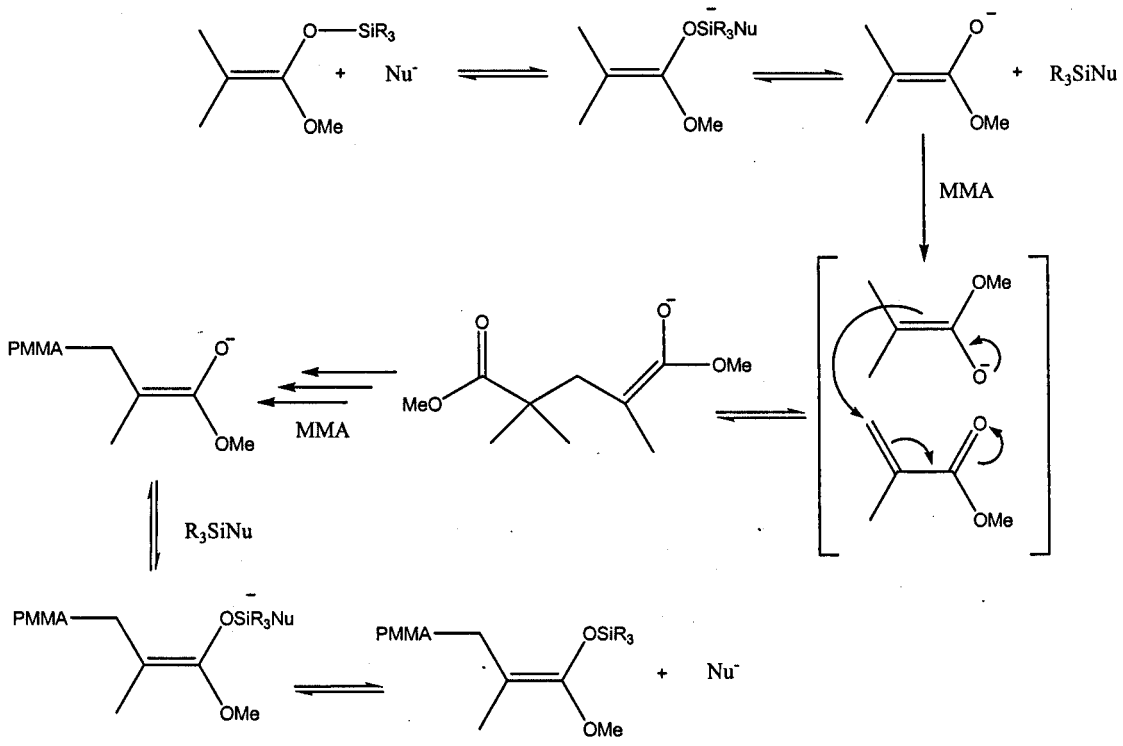

Figure 9.5: Scheme 2 Dissociative pathway.

Based on current findings it is now believed that the associative route is incorrect [9]. The currently accepted mechanism lies with a dissociative pathway as shown in figure 9.5. In this pathway the nucleophilic catalyst again binds to the silane group, but a reversible cleavage step produces a reactive enolate end which adds to the monomer.

9.1.2.3 Synthesis of triblock copolymers by GTP

Using suitable bifunctional initiators, ABA type triblock copolymers can be synthesised in a two step monomer addition procedure. The use of 1,4-Bis methoxytrimethylsiloxymethylene) cyclohexane (BMMC) discovered by Steinbrecht and Bandermann [10] has recently been reported in the Armes group [11] for the synthesis of BAB and ABA triblock where A = 2-(dimethylamino)ethyl methacrylate and B = 2-(diethyl amino)ethyl methacrylate.

9.2 BLOCK COPOLYMER SYNTHESIS

9.2.1 General analytical methods

Melting points were determined with a Sanyo Gallenkamp melting-point apparatus and are uncorrected. ^{1}H and ^{13}C NMR spectra were recorded on a Bruker AC-250 (MHz) instrument. Electrospray mass spectra were recorded on a Waters Micromass LCT ESSystem. Solid state infrared spectra were obtained with a Perkin-Elmer RX I FT-IR spectrophotometer coupled with a Durasampl IR II SensIR© diamond ATR accessory.

NMR splitting patterns have been defined as follows: s (singlet), d (doublet), dd (doublet of doublet), t (triplet), m (multiplet), and br (broadsignal). Quat. C (quaternary carbon). Coupling constants (J values) are listed in hertz (Hz). All yields reported are unoptimized.

9.2.2 Solvent purification

Tetrahydrofuran (THF) was dried over Na-benzophenone complex for three days (a deep purple colour indicated the solvent was free from moisture and oxygen). When used in anionic polymerisation the solvent was further purified over styryllithium.

9.2.3 Monomer purification

2-(Diethylamino) ethyl methacrylate (DEA) was passed through a basic alumina column to remove protic impurities. The monomer was then stirred over calcium hydride for 24 hrs to remove final traces of moisture. Immediately before use the monomer was distilled and stored at -78°C.

Methyl methacrylate (MMA) was passed through a basic alumina column to remove protic impurities. The monomer was then stirred over CaH_2 for 48 hrs. For anionic polymerisation the monomer was then distilled onto a 10% w/w $AlEt_3$ solution [12]. When a persistent yellow/green colour was observed the monomer was distilled and stored at -78°C.

Tertiary butyl methyl methacrylate (ter-BuMA) was stirred over CaH_2 for 48 hrs and then distilled onto a 10% w/w $AlEt_3$ solution [12]. When a persistent yellow/green colour was observed the monomer was distilled and stored at -78°C.

9.2.4 Bifunctional initiators synthesis for use in GTP polymerisations

9.2.4.1 1,4-Bis (methoxytrimethylsiloxymethylene) cyclohexane (BMMC)

(a)

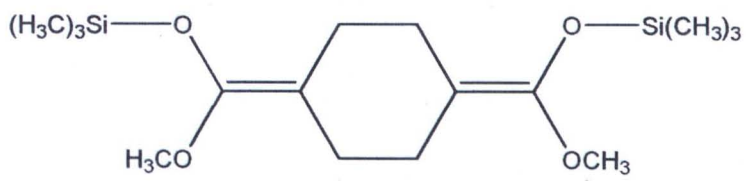

(b)

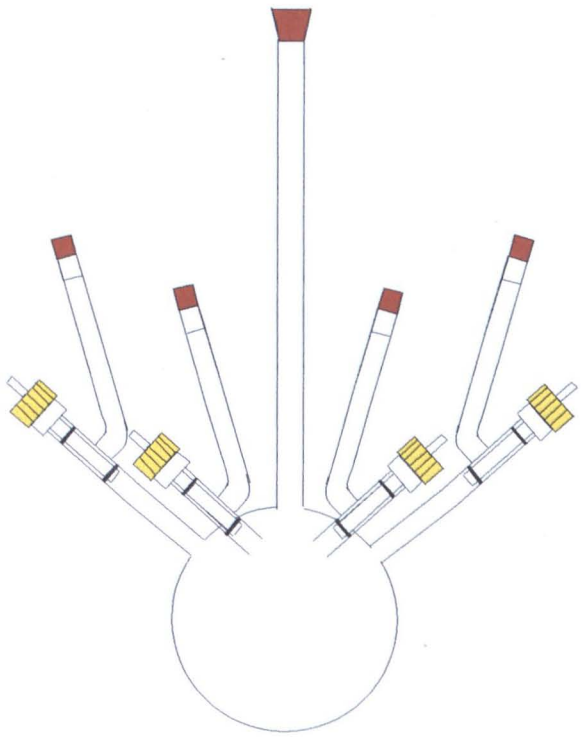

Figure 9.6: (a) 4-Bis (methoxytrimethylsiloxymethylene) cyclohexane (BMMC) (b) Specially made glass reactor used for the synthesis of BMMC.

BMMC was prepared using a literature recipe [13]. Synthesis of BMMC was carried out in a specifically designed four armed 250 ml round bottom glass reactor fitted with a magnetic stirrer and contact thermocouple, as shown in figure 9.6b. All

glassware was dried overnight prior to assembly in a 125-180°C oven, and flame dried immediately before use.

100 mls of dry THF was distilled into the reactor and at the same time (11.7 mls 88. 3 mmol) of diisopropylamine was transferred via syringe into one of the side arms. The side arm was thoroughly purged with nitrogen, and then the isopropylamine was slowly added to the THF. To a second side arm was transferred (33 mls 88.3 mmol) of n-BuLi, which was also thoroughly purged with nitrogen. The temperature of the solution in the reactor was reduced to -78°C and the n-BuLi was then added dropwise over a period of15 minutes. The reaction mixture was allowed to return to room temperature and stirred for a further two hours. To a third side arm was added (6 mls 33 mmol) of dimethyl 1,4-cyclohexane dicarboxylate, which was thoroughly purged with nitrogen. The reaction solution was once again cooled to -78°C and the diester was added dropwise over a period of 30 minutes. The solution was allowed to stir for a further two hours. To a fourth side arm was added (14.8 mls, 117 mmol) of trimethysilyl chloride. Following repeated degassing with nitrogen, the trimethysilyl chloride was added to the reaction mixture and stirred for a further two hours, before being allowed to warm slowly to room temperature.

Solvent was removed under *vacuo* and dry hexane (approx 30 mls) was then added. The solution was filtered and n-hexane removed using rotary evaporation. Evaporation of solvent yielded an oily residue that was distilled from impurities under high vacuum.

^{1}H ($CDCl_3$) = (ppm) 0.20 (s; 18H; $Si(CH_3)_3$); 2.04 (s; 4H, CH_2); 2.10 (s; 4H, CH_2); 3.50 (s, 6H, OCH_3).
MS ES$^+$, MH^+ = 345

9.2.5 Catalyst synthesis for use in GTP polymerisations

9.2.5.1 Tetrabutylammonium Hydrogen Bisbenzoate (TBABB)

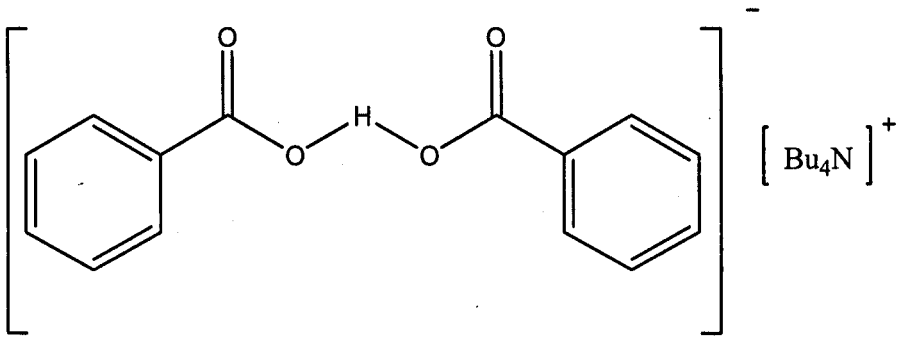

Figure 9.7: Tetrabutylammonium Hydrogen Bisbenzoate (TBABB).

TBABB as illustrated in figure 9.7 was prepared using a literature recipe [14]. **Example**. Benzoic acid (2 g, 16 mmol) was dissolved in 40% aqueous tetrabutylammonium hydroxide (15.9 mls). The solution was thoroughly mixed with gentle heating for a minimum of 15 minutes. A uniform solution resulted which was extracted five times using dichloromethane (5 x 15 mls).

Benzoic acid (2g, 16 mmol) was added to the dichloromethane extract and thoroughly mixed. $MgSO_4$ was added to the extract. The solution was filtered and the solvent was removed under *vacuo*. Dry THF (15 mls) was added to dissolve the residual solid followed by careful addition of diethyl ether (50 mls) down the sides of the flask The solution was left to stand at room temperature overnight resulting in needles of bioxyanion. The solid was dried under high vacuum (10^{-5} Pa) for 1 week.

^{1}H ($CDCl_3$) (ppm) = 1.00 (t, 12H, CH_3); 1.44 (m, 8H, $C\underline{H_2}CH_3$); 1.64 (m, 8H, $CH_2C\underline{H_2}CH_2CH_3$); 3.20 (m, 8H, NCH_2); 7.39 (m, 6H, Ar m, p); 7.97 (d, 4H, Ar o).

Elemental Analysis: C 73.93, H 10.0 N 2.95 Expected C 74.19 H 9.75 N 2.88.

9.2.6 Synthesis of PMMA-*block*-PDEA-block-PMMA triblocks

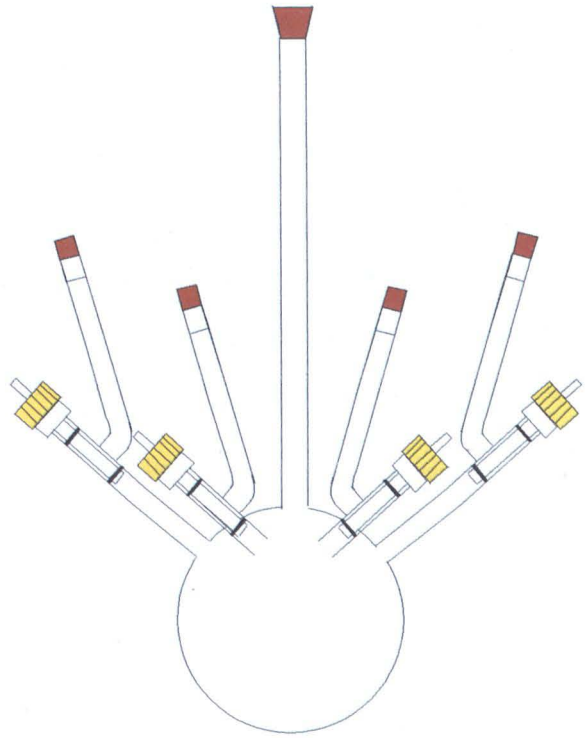

Figure 9.8: Reactor used for the synthesis of PMMA-*block*-PDEA-*block*-PMMA triblock copolymers.

PMMA-*block*-PDEA-*block*-PMMA copolymers were prepared using a modified literature recipe [15]. All GTP reactions were carried out in a specially designed four armed glass reactor fitted with a magnetic stirrer and contact thermocouple, as shown in figure 9.8. Each arm of the reactor contained a Young's tap and rubber septum. All glassware was dried overnight in a 125-180°C oven prior to assembly. The following description outlines the general procedure used in a GTP reaction. Quantities of monomer and initiator used will depend on the target molecular weight.

In a typical polymerization, 2 mol % of TBABB (relative to initiator) was added to the reactor. The reactor was then put under high vacuum and flamed. Dry THF (200 mls) was vacuum distilled into the reactor and the solvent was stirred to ensure complete dissolution of the catalyst. BMMC was transferred using a glass syringe into one of the side arms, which was then immediately purged with dry nitrogen. The initiator was then added to the reaction solution and stirred for 30 minutes. During this

time DEA and MMA monomer were transferred via cannula into their respective side arms of the reactor. Both side arms were thoroughly purged with dry nitrogen. When stirring of the initiator was complete DEA monomer was added to the solution. The reaction exotherm was recorded using the contact thermocouple. When the exotherm abated a sample aliquot was removed for analysis and MMA monomer was immediately added to the solution. The solution was stirred overnight to ensure complete polymerization of MMA. Finally methanol was added to the solution, which was subsequently stirred for 1 hour to terminate the reaction. The solution was transferred into a round bottom flask and the solvent removed under *vacuo*. A white solid precipitated which was dried under high vacuum for five days.

9.2.7 Bifunctional initiators synthesis for use in anionic polymerisations

9.2.7.1 1,2-bis-(4-benzoylphenyl)ethane

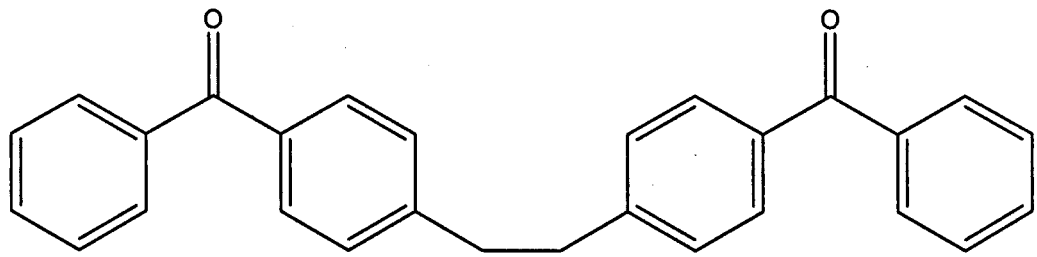

Figure 9.9: 1,2-bis-(4-benzoylphenyl)ethane.

1,2-bis-(4-benzoylphenyl)ethane as illustrated in figure 9.9 was prepared using a literature recipe [16]. To an ice-cooled suspension of $AlCl_3$ (70.40g, 0.53 mol) in 1,2-dichloroethane (120 mls) was slowly added benzyl chloride (61.76g, 0.44 mol) in 1,2 dichloroethane (40 mls) under an N_2 atmosphere.. The reaction mixture was allowed to return to room temperature and 1,2-diphenylethane (40.1g, 0.22mol) in 1,2-dichlorethane (50 mls) was added. The reaction mixture was stirred overnight resulting in the formation of a deep red solution. The solution was poured onto ice (300 mls), and then extracted into diethyl ether. A precipitate formed between the aqueous and organic layer. The aqueous layer was discarded and the precipitate collected. The organic layer was washed with distilled water resulting in the formation of more

precipitate. The precipitate was further purified by recrystallisation using a mixture of cyclohexane/ THF (1:2).

9.2.7.2 1,3-bis (1-phenylethenyl) benzene

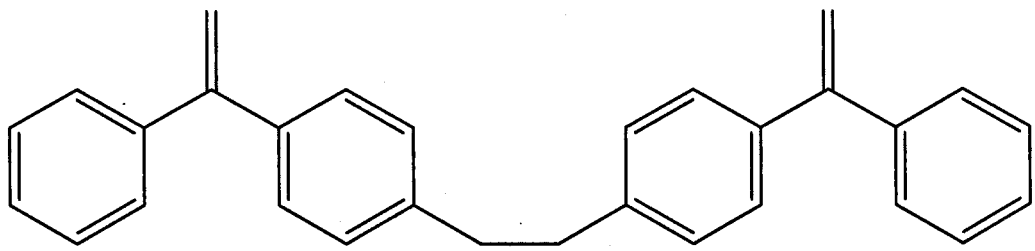

Figure 9.10: 1,3-bis (1-phenylethenyl) benzene.

To a solution of methyltriphosphoniumbromide (20.07 g, 0.056 mol) in THF (100 mls) was added dropwise n-BuLi (32 mls, 2.5M in hexanes) at 0°C under an N_2 atmosphere. Dichloromethane (4 mls) was then added to the solution followed by 1,2-bis-(4-benzoylphenyl)ethane (9.03 g, 0.023 mol), the reaction was stirred overnight. The solution was filtered leaving behind a white solid. The solid was washed with THF until the solvent ran clear. Solvent from the filtrate was removed under *vacuo* leaving behind a brown solid, which was further purified by recrystallisation in the minimum amount of acetone/ methanol (1/9).

^{1}H ($CDCl_3$) (ppm) = 2.95 (s, 4H, CH_2); 5.40 (d, 1H, CH); 5.45 (d, 1H, CH); 7.1 (d, 4H, CH Ar); 7.25 (m, 14H, CH Ar).

^{13}C ($CDCl_3$) (ppm) 37.56 ($\underline{C}H_2)_2$; 113.83 (C=$\underline{C}H_2$); 127.67, 128.15, 128.25, 128.31 (Ar $\underline{C}$H) 139.17, 141.39, 41.65 (quat C), (149.86($\underline{C}$=CH_2)

9.2.8 Synthesis of PMMA-*block*-PMAA-*block*-PMMA triblocks

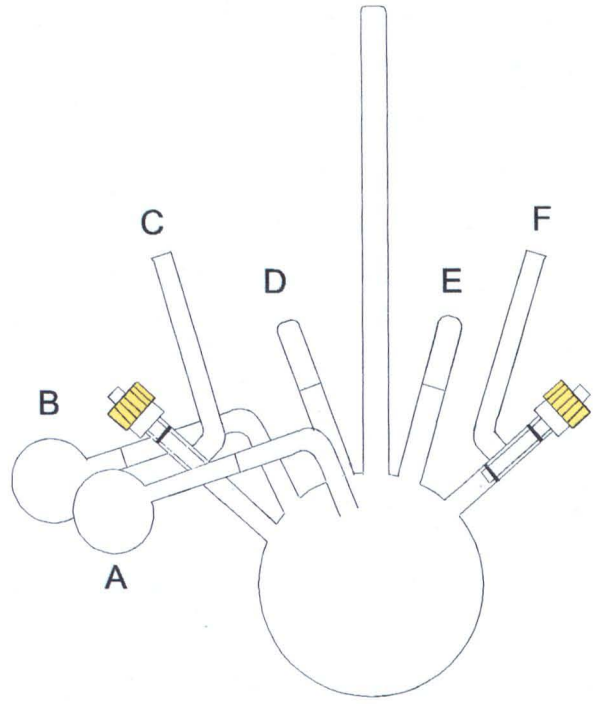

Figure 9.11: Reactor used for the synthesis of PMMA-*block*-PMAA-*block*-PMMA triblock copolymers.

PMMA-*block*-PMMA-*block*-PMMA copolymers were prepared using a modified literature recipe [17]. All anionic polymerizations were carried out using glass break seals whenever possible for the transfer of monomers and reagents. All glassware was dried prior to assembly overnight in a 125-180°C oven.

The following description outlines the general procedure used in a typical polymerization. Quantities of monomer and initiator have not been included as a range of polymers were synthesized with different molecular weights.

A specially designed reaction vessel was used as shown in figure 9.11. Four breakseal ampoules containing MMA (A), ter-BuMA (B), degassed methanol (5 mls) (D) and sec-BuLi (solution in cyclohexane) (E) were connected to the reactor. (C) LiCl (solution in THF) and (F) DDPE (solution in THF) were stored in ampoules fitted with a Youngs tap. The reactor was first flamed under high vacuum. THF (250 mls) was distilled into the reactor, the ampoule of LiCl (10 times molar excess compared to initiator) was then added to the solution while maintaining continuous stirring. After

dissolution of LiCl the ampoule of sec-BuLi was added to the solution. Using a methanol/solid CO_2 bath the contents of the reactor were then cooled to -78°C. The DDPE solution was then slowly titrated, resulting in the formation of a blood red solution. Cold ter-BuMA was added to the reaction mixture with vigorous stirring, causing the red colour to immediately disappear. The reaction was left stirring at -78°C for a further 90 minutes. Cold MMA was then added to the solution with vigorous stirring. After a further 30 minutes the reaction was terminated by addition of degassed methanol (approximately 5 mls).

The polymer was precipitated in a methanol/water mixture (90/10), filtered off and dried under high vacuum.

9.2.9 Hydrolysis of PMMA-*block*-terBuMA-*block*-PMMA

PMMA-*block*-terBuMA-*block*-PMMA copolymer (2 g) was added to a round bottom flask and dissolved in dichloromethane (DCM) (20 mls). A five times molar excess of trifluoroacetic acid was then added under nitrogen and the solution was stirred at room temperature for 24 hours. After 24 hours the DCM was removed by rotary evaporation. A white solid precipitated which was subsequently dissolved in dioxane (20 mls). The polymer was then precipitated in hexane.

9.3 GPC ANALYSIS

9.3.1 Theory of GPC analysis

Gel permeation chromatography (GPC), also referred to as size exclusion chromatography (SEC) is a method for determining the molecular weight distribution and molecular weights of polymers. The method involves the permeation of a dilute polymer solution through a special column containing microporous beads of cross-linked polymer, typically polystyrene [18] (other porous material can be used including glass beads and silica gels). The diameters of the beads are comparable in size to the molecular coils in solution.

Polymer coils permeate through the column in two ways. Some will pass through the beads, and others pass through the interstitial volume (the volume occupied between the beads).

Lower molecular weight polymers which have a smaller coil diameter (and hydrodynamic volume) are able to penetrate into the beads more easily compared to larger polymers. The passage of smaller molecules through the column is therefore slower than larger molecules, which consequently travel through the interstitial volume. Transport through the interstitial volume is thus faster than through the beads. The amount of time it takes for the polymer to permeate through the column increases as the molecular weight is lowered.

The concentration of polymer eluting through the column is continuously measured as a function of time using a suitable detector. The specific type depends on the properties of the polymer and eluting solvent, examples include UV, refractive index, viscosity, light scattering or a combination of several detectors.

To determine accurate molecular weight information it is necessary to calibrate the column. To achieve this a series of well characterised calibration standards are eluted through the column.

A plot of log M_c. $[\eta]_c$ vs retention volume (V_r) for a given solvent and temperature is used to construct a universal calibration plot, where M_c is the molecular weight and η_c is the intrinsic viscosity of the calibrant. This relationship was first identified by Benoit *et al* [19] which is possible by assuming the hydrodynamic volume

of the polymer is related to the product of intrinsic viscosity and molecular weight. If there is a valid universal calibration curve for the system then,

$$\log M_c . [\eta]_c = \log M_u . [\eta]_u \quad (9.2)$$

where the subscript c and u represents the calibrant and polymer under study respectively.

As polymer chains swollen in the eluting solvent may swell to a different extent compared to an equal molar mass sample of the calibrant polymer, there hydrodynamic volume may not necessarily be the same. These subtle differences can be taken into account using the Mark-Houwink parameters [20], $[\eta]=KM^a$, determined from solution viscometry, where K and a are empirical constants.

Application of this equation allows the molecular weight of a polymer to be determined even if it is of a different type to the calibrant.

9.3.2 GPC Setup

*9.3.2.1 GPC analysis of PMMA-block-P(ter-*BuMA*)-block-PMMA triblock samples*

Molecular weights and molecular weight distributions of PMMA-*block*-P(*ter*-BuMA)-*block*-PMMA triblock copolymers were evaluated using triple detector gel permeation chromatography (GPC). The system was equipped with a dual refractometer/ viscometer model 250 detector, and a RALS (right angle light scattering, λ = 633 nm) detector (Polymer Laboratories PLgel 2 mixed-C columns, HPLC grade THF as eluent). The sample concentration was less than 1mg/ml. The data was analysed using *Multi* offline GPC software.

9.3.2.2 GPC analysis of PMMA-block-PDEA-block-PMMA triblock samples

Molecular weights and molecular weight distributions of PMMA-*block*-PDEA-*block*-PMMA triblock copolymers were evaluated using gel permeation chromatography (GPC). The system was equipped with a refractive index detector

(mixed "D" columns, HPLC grade THF as eluent, stabilized with BHT at a flow rate of 1.0 mL min^{-1}), and was calibrated with linear poly(methyl methacrylate) calibration standards (Polymer Labs). Triethylamine (50mls per 2500mls) was also added to the eluent to reduce the chances of the polymer sticking to the column.

9.4 SMALL ANGLE X-RAY SCATTERING

9.4.1 Theory of Small angle X-ray scattering (SAXS)

SAXS is an analytical X-ray application technique for the structural analysis of both liquid and solid state materials. The technique is widely used in areas such as polymer science, biology and material science, where it can be harnessed to determine parameters such as particle size, conformation, pore sizes and much more. Scattering is recorded at scattering angles below 3 degrees, and it is therefore ideally suited for probing structures with length scales between 1 - 100nm.

In SAXS, the sample is irradiated with a collimated beam of intense X-rays. Whilst most of the x-rays simply travel straight through the sample, if sufficient electron density contrast is present the sample will undergo scattering. The scattered x-rays are detected by a 2 dimensional detector placed behind the sample, perpendicular to the direction of the incoming light, as shown in figure 9.12.

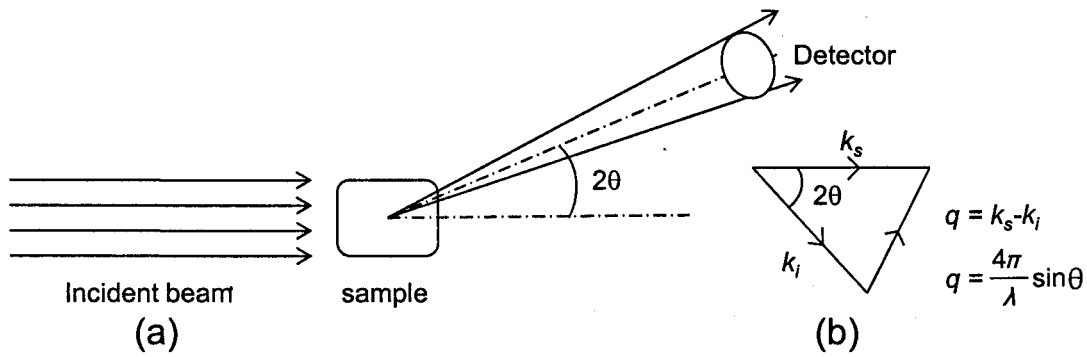

Figure 9.12: (a) Basic geometry of small angle X-ray scattering involving the incident X-ray beam, the sample, scattering wave and detector. (b) scattering vector, elastic scattering only, i.e. $|k_i| = |k_s|$

The intensity of the scattered beam and changes of scattering intensity with scattering angle, 2θ are dependent on the electron density distribution within the sample. In a typical scattering experiment, *I(q)* is measured for different values of the scattering vector *q*.

The origin of this vector quantity is illustrated in figure 9.12b, where k_i and k_s represent the scattering vector of the incident and scattered light respectively. It is defined as the difference between the propagation vectors of the scattered and incident light [21]. The magnitude of *q* quantifies the lengths in the reciprocical space and is expressed in $Å^{-1}$ or nm^{-1}.

The length in reciprocical and direct space are linked together through equation 9.3 [22].

$$d=2\pi/q, \tag{9.3}$$

where d is the domain spacing of the sample. Using Bragg's law shown below,

$$n\lambda= 2d\sin\theta \tag{9.4}$$

where n is an integer, λ is the wavelength of the x-ray beam, d is the distance between scattering planes or d-spacing, and 2θ *is the scattering angle,* equation 9.3 can be re-written in terms of the scattering vector, *q*.

$$q = \frac{4\pi}{\lambda}\sin\theta \tag{9.5}$$

It follows that the intensity of scatter is approximately $\sin\theta / \lambda$

In a two component system of particles, where one phase is immersed in the matrix of another, the scattering intensity can be written as,

$$I(q) = n\Delta p^2 V^2 P(q) S(q) \tag{9.6}$$

where n is the number density of discrete domains, *p* is the electron density difference between the two phases, *V* is the irradiated volume, *P(q)* is the form factor and *S(q)* is the structure factor.

The form factor is a function which describes the scattering from individual domains, it contains information on the shape and dimension of the particles. The structure factor is a function which describes the scattering from the spacial arrangement of domains. It describes the inter-particle interference effects, and as the concentration of the system increases this effect becomes more prominent. In a highly ordered system, such as well ordered block copolymers the structure factor manifests itself as series of peaks in the SAXS profile. From the ratio of the most intensity scattered peak (first order of reflection), q_{max}, to the other peaks it is possible to determine the microphase morphology in the sample.

Examples include:

$q_{max} = 2q_{max} : 3q_{max} : 4q_{max}$	Lamellar structure
$q_{max} = \sqrt{2}q_{max} : \sqrt{3q_{max}} : \sqrt{4q_{max}}$	Body centred cubic (BCC)
$q_{max} = \sqrt{3}q_{max} : \sqrt{4q_{max}} : \sqrt{7q_{max}}$	Hexagonal packed cylinders (HPC)

The intensity of q_{max} is also related to the degree of microphase separation within the sample. In addition, the width gives information on the size distributions of inhomogeneities. A narrower peak indicates a more ordered structure.

9.4.2 SAXS Instrumentation

SAXS data presented in chapters 3 – 7 was collected using two SAXS instruments. Specific details of the two instruments are given in section 9.4.2.1 and 9.4.2.2. Table 1 indicates which instrument was used in each chapter of the thesis for a given set of experiments.

Experiments performed at Synchrotron radiation sources required complex experimental setup such as liquid cells and scanning stages. Details of this setup can be found in section 9.4.3, which is additionally listed in table 9.1 for reference.

9.4.2.1 Bruker AXS NanoStar (Nanostar)

SAXS data was collected using a Bruker AXS NanoStar Laboratory SAXS instrument equipped with a 2D position-sensitive gas detector (Hi-Star, Siemens AXS). A CuK_{α} radiation source was used (1.54 Å). The sample to detector distance was set at 1.045 metres.

9.4.2.2 European Synchrotron Radiation Facility (ESRF), Grenoble, France (BM26)

SAXS data was collected at station BM26 (DUBBLE) using a wavelength of 1.24 Å and sample to detector distance of 6.5 meters.

Table 9.1: Details of the specific SAXS instrument and experimental setup used in each chapter of the thesis

Chapter	SAXS instrument	Special setup, chapter reference
3	Nanostar	
4	BM26	9.4.3.1
5	BM26	9.4.3.1
6	BM26	9.4.3.2
7	BM26	9.4.3.1

9.4.3 Experimental SAXS setup

9.4.3.1 "Static" Small Angle X-ray Scattering Setup

To facilitate a reduction in the amount of time required to scan static SAXS samples a scanning plate was constructed. This is shown in figure 9.13. The scanning plate was constructed from a robust stainless steel plate. 100 holes of equal separation were drilled into the plate in a 10 x 10 configuration, each hole having a diameter of 3mm. Each polymer sample was immersed in 100mls of buffer solution for at least 24hrs. Once it had reached equilibrium it was placed into its respective hole. Kapton tape was added to each face of the plate to seal the hydrogel and stop evaporation of water. The fully loaded sample plate was securely attached to an x-y-z translation stage. Under computer control each sample was scanned in turn and the SAXS data collected.

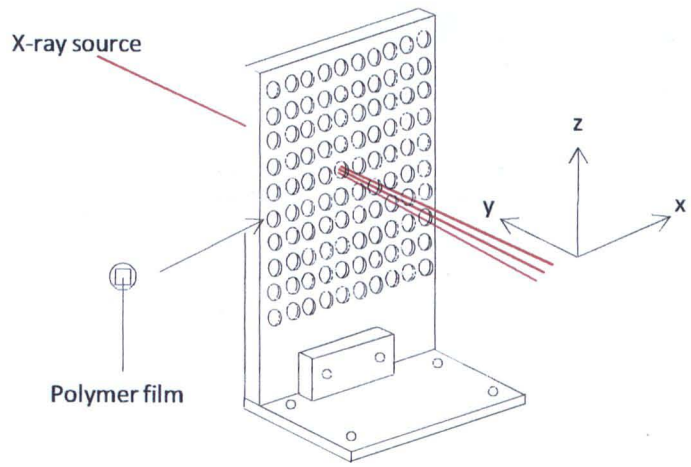

Figure 9.13: Static SAXS experimental setup. A static scanning holder was constructed using stainless steel plate. This consisted of 100 holes (3mm diameter) in a 10 x 10 configuration. Polymer films were sealed into each hole using Kapton tape.

9.4.3.2: "Dynamic" Small Angle X-ray Scattering Setup

Dynamic SAXS data at station BM26 was collected using the experimental setup illustrated in figure 9.14a. A liquid cell was connected into a series consisting of solutions, flow valve, liquid cell and a Watson Marlow 205U peristaltic pump. An expanded view of the cell construction, highlighting the main design elements is shown in figure 9.14b. The cell consisted of two X-ray transparent windows which allowed the polymer sample to be monitored by SAXS. Each X-ray window was constructed from mica, which was mounted onto the end of a hollow brass bolt. The two bolts when fully screwed into the liquid cell had a 4mm gap between them. A 4mm thick PTFE washer was used as a sample holder, and was placed into this gap.

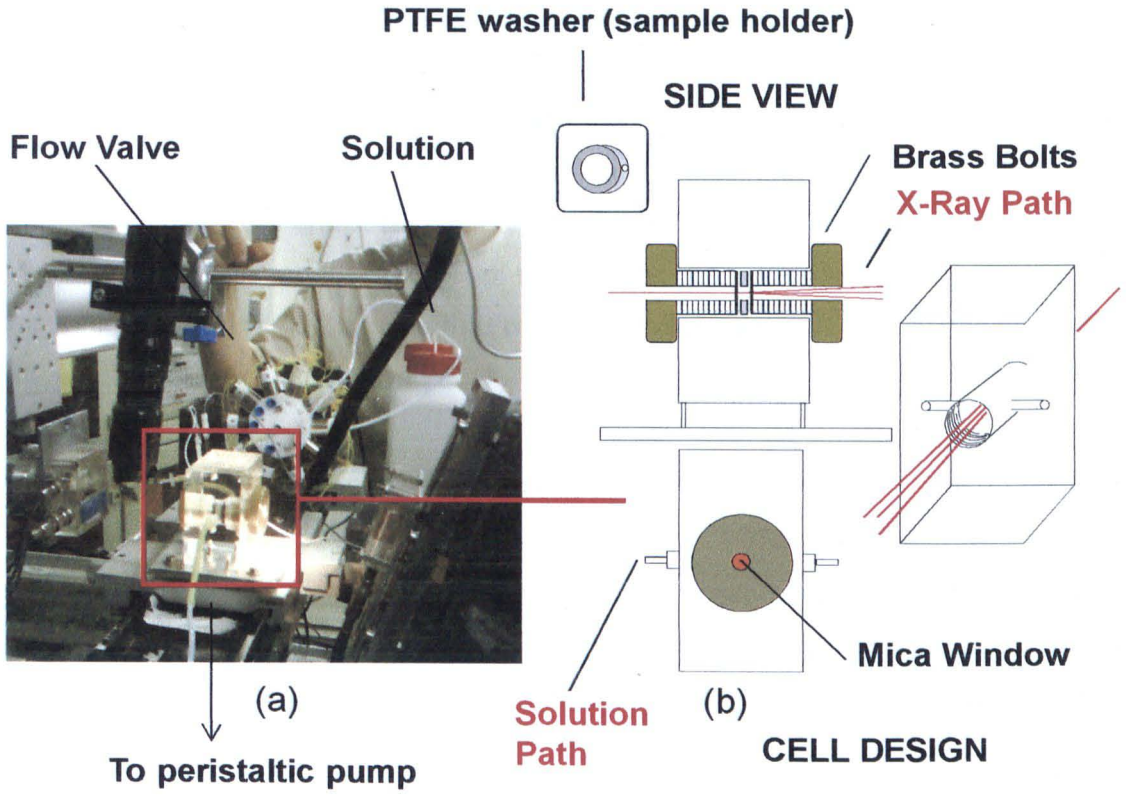

Figure 9.14: Dynamic SAXS experimental setup. (a) Overall SAXS setup, solutions, flow valve, liquid cell and peristaltic pump connected together in series. (b) Illustration of the cell design (approximately 7cms x 4cms x 7cms).

The washer had a small recessed area on one side for attachment of polymer films. It also contained a small liquid channel drilled through the centre. The thickness of the PTFE washer was kept to a minimum to reduce the amount of unwanted solution absorption. A small horizontal channel was also drilled across the liquid cell. This allowed liquid to flow through the cell. When the channel in the liquid cell was in-line with the channel in the sample holder solution could be pumped through creating a liquid environment in the void of the washer.

The flow of the solution entering the cell could be controlled by varying the pump speed. The multi-flow valve could be connected with upto 8 solutions, thus allowing rapid switching between them if needed.

In a typical procedure a cast polymer film (typically 5mmx5mm) was mounted into the PTFE sample holder. This was then placed inside the liquid cell. The two brass bolts were then carefully screwed into the cell ensuring the channel in the washer and cell were aligned. Using a translation stage the liquid cell was moved until the X-ray beam was found to go through the centre of the sample. At this point the solution was introduced into the cell and X-ray scattering was commenced, with a typical resolution of 1 frame every 15 seconds. The pH of the solution was monitored continuously using a microelectrodes Inc 16-702 flow thru reference electrode. This was connected inline between the solution and flow valve.

9.5 ATOMIC FORCE MICROSCOPY

Atomic force microscopy measurements were collected in tapping mode using a multimode Nanoscope IIIa Digital instruments atomic force microscope. Commercial Si tips with a resonant frequency of ~300 kHz and a spring constant of approximately 40 N m^{-1} were used.

9.6 POLYMER CASTING AND ANNEALING

The specially synthesised block copolymers were processed to form nanostructured thin films. This was achieved by polymer casting and solvent annealing. A description of the technique is given below.

The triblock copolymers were first dissolved in a good solvent. The particular solvent depended on the type of material. PMMA-(*block*)-PMAA-(*block*)-PMMA samples were dissolved in an 85/15 methanol/acetone co-solvent or dioxane. PMMA-(*block*)-PDEA-(*block*)-PMMA samples were exclusively dissolved in THF. Thin films were prepared by solvent casting the polymer solution onto a PTFE sheet using a *Precision Gage and Co.* Applicator. "Solvent rich" films were then immediately placed into solvent rich environments, containing the same solvent composition used to cast the film. A small aperture in the solvent environment allowed slow evaporation of solvent. The annealing solvent and annealing time for the respective experiments performed throughout this thesis are listed in table 9.2.

Table 9.2 Annealing conditions used to prepare solvent cast films of PMMA-*block*-PMAA-*block*-PMMA and PMMA-*block*-PDEA-*block*-PMMA. Polymers, with the exception of those used for diffraction experiments in section 7.13 were solvent cast onto PTFE using a *Precision Gage and Co.* Applicator. "Various" indicates a range of annealing times were used of which the specific details are indicated in the relevant chapter.

Chapter	Section	Solvent	Weight Percent	Sample thickness / microns	Annealing time / days
3	3.3.3	THF	40	200	various
		85/15 (v/v)	40	200	
3	3.5.3	THF	40	200	various
3	3.6	THF	40	200	7
3	3.8.1	Dioxane	40	110	30
3	3.8.2	THF	40	110	7
4	4.14 – 4.18	THF	40	80	7
5	5.2	see above	see above	see above	see above
6	6.16 – 6.18	THF	40	80	7
7	7.13– 7.14	THF	40*	80*	7

***Imprinted diffraction grating were prepared at 30 weight percent, cast at a thickness of 30 microns and annealed for one day.**

9.7 GENERAL BUFFER PREPARATION FOR USE IN "STATIC" AND "KINETIC" EXPERIMENTS

9.7.1 Reagents

Formic acid (SDS, purex analytical grade), sodium chloride (SDS, 1380517), sodium phosphate monobasic dihydrate (Acros organics, 99+%, for analysis), citric acid monohydrate (*Riedel* de Haen), sodium bromide (*Riedel* de Haen, puriss), sodium thiocyanate (*Riedel* de Haen), sodium iodide (*Riedel* de Haen, puriss 99-100.5%), sodium nitrate (*Riedel* de Haen, puriss) and ethanol amine (*Riedel* de Haen, 99%) were used as received.

9.7.2 Buffers used to control pH, ionic strength and salt identity.

Citric acid, sodium phosphate and ethanolamine buffers used to measure the "static" and "dynamic" response of the hydrogels, were pH stabilised by relatively small concentrations of buffer species (0.01 M – 0.05 M), and the total ionic strength was controlled by the addition of neutral sodium salts; namely NaCl, NaBr, $NaNO_3$, NaI, NaSCN and NaAce.

9.7.3 Monobasic buffer preparation

The general method used to prepare monobasic buffers is detailed below, an example is included for the preparation of a 0.05 M ethanol amine buffer, at pH 10, using NaCl to fix the overall ionic strength to 0.1 M (prepared at 25°C).

Step 1: The pK_a of ethanol amine (9.50 [23]) was thermodynamically adjusted for temperature and ionic strength using the Debye-Huckel relationship shown in equation 9.7,[24] where pK_a^I is the modified pK_a, z_a is the charge on the conjugate acid, I is the ionic strength of the solution and A is a constant which has a value of 0.5114 at 25 °C.[24]

$$pK_a^{\,I} = pK_a + (2z_a - 1)\cdot\left[\frac{A\sqrt{I}}{1+\sqrt{I}} - 0.1\cdot I\right] \tag{9.7}$$

$$pK_a^{\,I} = 9.5 + ((2\times 0) - 1)\quad \frac{0.5114\sqrt{0.1}}{1+\sqrt{0.1}} - 0.1\times 0.1 \tag{9.8}$$

$$pK_a^{\,I} = 9.61 \tag{9.9}$$

Step 2: The Henderson-Hasselbalch relationship (eq. 9.10) was then used to determine the concentration of base [A^-] and acid [HA] in the buffer at the given pH and the total buffer concentration (i.e. pH 10 at a total buffer concentration of 0.05M).

$$[pH] = pK_a + \log_{10}\frac{[A^-]}{[HA]} \tag{9.10}$$

Equation 4 implies that the acid component of the buffer is neutral, and the basic component has a negative charge. While this is true for many buffers, in the case of ethanol amine for example, the basic component is neutral and the acid component is charged (+1). For clarity the Henderson-Hasselbalch equation may be re-written as shown in equation 9.11, where A^-, defined as a proton acceptor from Bronsted-Lowry theory represents the base.

$$[pH] = pK_a + \log_{10}\frac{[base]}{[acid]} \tag{9.11}$$

The total concentration of acid and base in the buffer is given by equation 9.12.

$$C_{buffer} = [HA] + [A^-] \tag{9.12}$$

The concentration of acid [HA] is related to the concentration of hydrogen ion [H^+] and base [A^-] through the equilibrium constant, K_a, see equation 9.13.

$$[HA] = \frac{[H^+][A^-]}{K_a} \tag{9.13}$$

Rearrangement, followed by substitution of equation 9.13 into 9.12 allows the concentration of base to be determined.

$$C_{buffer} = \frac{[H^+][A^-]}{K_a} + [A^-] \tag{9.14}$$

$$[A^-] = \frac{[C_{buf}]K_a}{K_a + [H^+]} \tag{9.15}$$

$$[A^-] = \frac{[0.05][2.45 \times 10^{-10}]}{[2.45 \times 10^{-10}] + [1 \times 10^{-10}]} \tag{9.16}$$

$$[A^-] = 0.0354\,M \tag{9.17}$$

$$[HA] + [A^-] = 0.05M \tag{9.18}$$

$$[HA] = 0.0146\ M \tag{9.19}$$

Step 3: Using this information the ionic strength of the buffer species can then be determined.

The ionic strength describes the overall ionic properties of the solution. It is a function of the concentration of all individual species dissolved in solution; encompassed in equation 9.20.

$$I = \frac{1}{2}\sum_{i=1}^{n}(c_i z_i^2) \tag{9.20}$$

where c_i is the concentration of the ionic species, i, and z_i is the charge on that ion. The total ionic strength is taken as the sum of all species.

In this example the concentration of [base] and [acid] is 0.0354 M and 0.0146 M, respectively.

In the case of citric acid buffer, the only ions which contribute to the ionic strength are protonated ethanol amine ($HOCH_2NH_3^+$) and chloride anion (Cl^-).

There ionic strength is calculated below,

$$I = \frac{1}{2}(HOCH_2NH_3^+ \times 1^2) + (Cl^- \times -1^2) \tag{9.21}$$

$$I = \frac{1}{2}(0.0146 \times 1^2) + (0.0146 \times -1^2) \tag{9.22}$$

$$I = 0.015\,M \tag{9.23}$$

As, $I_{total} = I_{buffer} + I_{salt}$, (9.24)

where I_{buffer} and I_{salt} are the ionic strength due to the added salt and buffer species acting alone, respectively. This indicates that another 0.085 M of NaCl must be added to maintain an ionic strength of 0.1 M

The final buffer can be prepared in 2 ways, (1) by dissolving the required amount of basic and acidic components in solution to give a final solution at the correct pH, (2) dissolve the required amount of basic or acid component in solution, then titrate it to the required pH using either strong acid or base.

9.7.4 General procedure for preparation of multivalent buffer solutions

The method used to prepare multivalent buffers is more complicated. A full derivation can be found in chapter 5, section 5.2.

Equations (9.26-9.29) describe how the fractional composition of each ionic species (H_3A, H_2A^- and A_3^-) in a trivalent buffer, such as citric acid used in this study, vary with changes in pK_a, (thermodynamically corrected), pH (-log $[H^+]$) and the total buffer concentration [C].

The fractional composition of each species multiplied by the total buffer concentration [C] gives the concentration of each species in solution (mol dm^{-3}). The concentration of each individual species can then be inserted into equation 9.20, to give the ionic strength. Summation of the ionic strength for each species gives I_{buffer} (equation 9.24). From I_{buffer} one can determine the amount of salt that must be added to maintain a fixed ionic strength. Care must be taken to use the correct charge and include all the counterions.

$$K = D^3 + D^2K_{a1} + DK_{a1}K_{a2} + K_{a1}K_{a2}K_{a3} \tag{9.25}$$

$$f(H_3A) = \frac{[H_3A]}{C} = \frac{D^3}{K} \tag{9.26}$$

$$f(H_2A^-) = \frac{[H_2A^-]}{C} = \frac{D^2K_{a1}}{K} \tag{9.27}$$

$$f(HA^{2-}) = \frac{[HA^{2-}]}{C} = \frac{DK_{a1}K_{a2}}{K} \tag{9.28}$$

$$f(A^{3-}) = \frac{[A^{3-}]}{C} = \frac{K_{a1}K_{a2}K_{a3}}{K} \tag{9.29}$$

9.8 DIFFRACTION GRATING EXPERIMENTAL SETUP

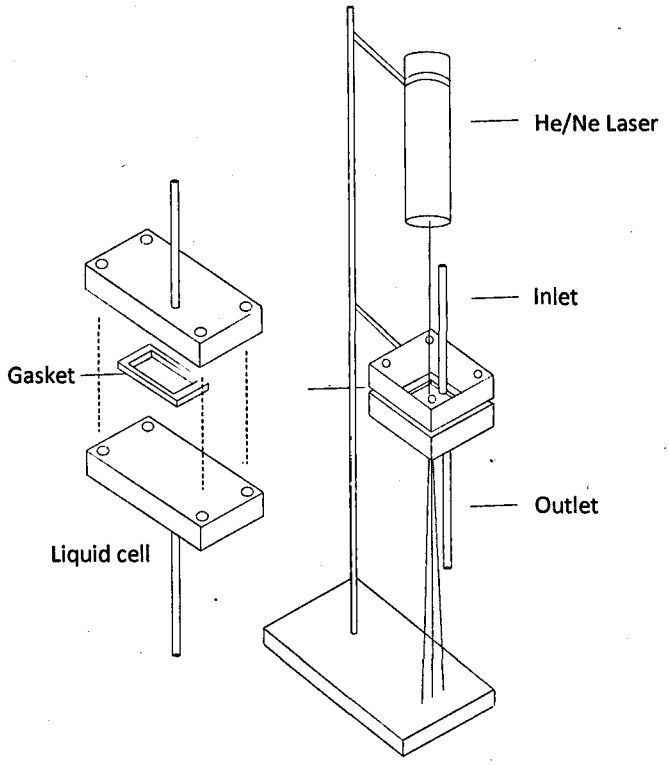

Figure 9.15: Dynamic diffraction grating experimental setup.

9.8.1 Characterisation of the dynamic diffraction grating response

An optically transparent flow cell was constructed out of Perspex (figure 9.15), inside of which a small (5 mm x 5 mm) piece of the imprinted gel was fixed using a polymer based adhesive at one corner of the gel. A rubber gasket was used to define the geometry of the liquid volume inside the cell (10 mm x 30 mm x 1 mm) and the aqueous phase was fed in from one end of the cell and pumped away at the opposing end. The flow geometry was such as to help minimise stress-induced curling of the sample as it changed volume. Initially, distilled water was pumped through the cell at a flow rate of 3.0 mL min^{-1}. After pumping for 20 minutes the solution was alternated between 0.05 M citric acid or 0.05 M ethanol amine at pH 3.6 and 11.5 respectively, the ionic strength was fixed at 0.1 M using NaCl. A low powered 632 nm.Uniphase Helium-Neon gas laser was incident upon the diffraction grating perpendicular to the grating surface. The resulting transmitted diffraction pattern was projected onto a white

surface 229 mm below the polymer sample. The projected diffraction pattern was recorded using a Pixelink PL-A742 colour camera every 10 seconds. The diffraction patterns were vertically integrated to obtain 1D data.

9.8.2 Characterisation of the static diffraction grating response

Pre-cut polymer grating films (5 mm x 5 mm x 30 μm) were equilibrated in buffer solutions for a period of 24 h in a glass Petri dish. In experiments to investigate the effect of counter ion on the expansion ratio, buffers were prepared at pH 3.6 using 0.01 M citric acid. The ionic strength in each case was fixed at 0.1 M using the sodium salts, NaAce, NaCl, NaBr, NaI, $NaNO_3$ and NaSCN. pK_a values (used to determine the concentration of buffer) were thermodynamically adjusted for temperature and ionic strength effects. The effect of pH on the expansion ratio of the hydrogel was also investigated in 0.01 M citric acid (pH 3.6 - 7.1) and 0.01M ethanol amine (pH > 9.5) at a fixed ionic strength of 0.1 M using NaCl. Each solution pH was measured before and after the sample had been removed, using a Thermo Scientific Ross Ultra Glass combination semi-micro pH electrode, calibrated at pH 4, 7 and 10. A HeNe laser (λ = 632 nm) was passed through the sample perpendicular to the surface and the diffraction pattern recorded at a distance of 229 mm from the sample.

9.8.3 Fabrication of pH-sensitive polymeric diffraction gratings

$PMMA_{88}$-*b*-$PDEA_{223}$-*b*-$PMMA_{88}$ copolymer was dissolved in THF (30 % w/w). This solution was poured onto the surface of a prefabricated quartz diffraction grating, which was then immediately added to a THF rich environment. A small aperture was used to allow slow removal of THF over a period of 24 h. Polymer films were removed from the surface of the glass by plasticisation in distilled water.

REFERENCES

1. Hadjichristidis, N., Pispas, S., and Floudas, G., Block Copolymers: Synthetic Strategies, Physical Properties, and Applications, John Wiley & Sons, New Jersey 1, (2003).
2. Szwarc, M., *Nature (London, United Kingdom)*, 1956, **178**, 1168.
3. Hsieh, H. and Quirk, R. P., Anionic polymerization: principles and practical applications, Marcel Dekker, New York 101, (1996).
4. Schreiber, H., *Makromol. Chem*, 1960, **36**, 86.
5. Varshney, S. K., Hautekeer, J. P., Fayt, R., Jerome, R., and Teyssie, P., *Macromolecules*, 1990, **23**, 2618.
6. Fayt, R., Forte, R., Jacobs, C., Jerome, R., Ouhadi, T., Teyssie, P., and Varshney, S. K., *Macromolecules*, 1987, **20**, 1442.
7. Webster, O. W., Hertler, W. R., Sogah, D. Y., Farnham, W. B., and RajanBabu, T. V., *Journal of the American Chemical Society*, 1983, **105**, 5706.
8. Webster, O. W., *Advances in Polymer Science*, 2004, **167**, 1.
9. Quirk, R. P. and Kim, J.-S., *Journal of Physical Organic Chemistry*, 1995, **8**, 242.
10. Steinbrecht, K. and Bandermann, F., *Makromolekulare Chemie*, 1989, **190**, 2183.
11. Hadjichristdis, N., Pispas, S., and Floudas, G., Block copolymers : synthetic strategies, physical properties, and applications, Wiley Interscience, New Jersey 73, (2003).
12. Allen, R. O., Long, T. E., and McGrath, J. E., *Polymer Bulletin*, 1986, **15**, 127.
13. I B. Dicker, G M. Cohen, W B. Farnham, W R. Hertler, E D. Laganis, and D Y. Sogah, *Macromolecules*, 1990, **23**, 4034.
14. Dyakonov, T. A., Huang, B., Hamoudi, A., Burns, D. H., Liu, Y., and Stevenson, W. T. K., *European Polymer Journal* 2000, **36**, 1779
15. D.Topham, P., Howse, J. R., Mykhaylyk, O. O., P.Armes, S., Jones, R. A. L., and Ryan, A. J., *Macromolecules* 2006, **39**, 5573.
16. Ikker, A. and Moller, M., *New Polymeric Materials*, 1993, 35.
17. Ryan, A. J., Crook, C. J., Howse, J. R., Topham, P. D., Jones, R. A. L., Geoghegan, M., Parnell, A. J., rez, L. R.-P., Martin, S. J., Cadby, A., Menelle, A., Webste, J. R. P., Gleesone, A. J., and Bras, W., *Faraday Discussions*, 2004, **128**, 55.
18. Janca, J., Steric Exclusion Liquid Chromatography of Polymers, Marcel Dekker, New York (1984).
19. Benoit, H., Grubisic, Z., Rempp, P., Decker, D., and Zillox, J. G., *J. Chim. Phys*, 1966, **63**, 1507.
20. Cowie, J. M. G., Polymers: Chemistry and Physics of Modern Materials, 2 ed, CRC Press Inc 29, (1991).
21. Glatter, O., The Inverse Scattering Problem in Small-Angle Scattering, in Neutrons, X-rays and Lifht: Scattering Methods Applied to Soft Condensed Matter, Elsevier, Amsterdam 73, (2002).
22. Borsali, R. and Pecora, R., Soft Matter Characterization, 1 ed, Springer 725, (2008).